Defense Threat Reduction Agency
8725 John J. Kingman Road, MS
6201 Fort Belvoir, VA 22060-6201

DTRA-TR-16-57

TECHNICAL REPORT

Mechanistic Studies of Flavivirus Inhibition and Nanoparticle-Catalyzed Decontamination

June 2016

HDTRA1-10-1-0009

Sharon Isern et al.

Prepared by:
Florida Gulf Coast University
10501 FGCU Blvd. South
Fort Myers, FL 33965

DESTRUCTION NOTICE:

Destroy this report when it is no longer needed.
Do not return to sender.

PLEASE NOTIFY THE DEFENSE THREAT REDUCTION AGENCY, ATTN: DTRIAC/ J9STT, 8725 JOHN J. KINGMAN ROAD, MS-6201, FT BELVOIR, VA 22060-6201, IF YOUR ADDRESS IS INCORRECT, IF YOU WISH IT DELETED FROM THE DISTRIBUTION LIST, OR IF THE ADDRESSEE IS NO LONGER EMPLOYED BY YOUR ORGANIZATION.

REPORT DOCUMENTATION PAGE

Form Approved
OMB No. 0704-0188

1. REPORT DATE *(DD-MM-YYYY)*	**2. REPORT TYPE**	**3. DATES COVERED** *(From - To)*
00-06-2016	Technical	January 21, 2010 - August 31, 2012

4. TITLE AND SUBTITLE

Mechanistic Studies of Flavivirus Inhibition and Nanoparticle-Catalyzed Decontamination

5a. CONTRACT NUMBER

5b. GRANT NUMBER
HDTRA1-10-1-0009

5c. PROGRAM ELEMENT NUMBER

6. AUTHOR(S)

Sharon Isern (PI)
Jose C. Barreto (co-PI)
Scott F. Michael (co-PI)

5d. PROJECT NUMBER

5e. TASK NUMBER

5f. WORK UNIT NUMBER

7. PERFORMING ORGANIZATION NAME(S) AND ADDRESS(ES)

Florida Gulf Coast University
10501 FGCU Blvd. South
Fort Myers, FL 33965

8. PERFORMING ORGANIZATION REPORT NUMBER

9. SPONSORING / MONITORING AGENCY NAME(S) AND ADDRESS(ES)

Defense Threat Reduction Agency
8725 John J. Kingman Road, STOP 6201
Fort Belvoir, VA 22060-6201

10. SPONSOR/MONITOR'S ACRONYM(S)

DTRA

11. SPONSOR/MONITOR'S REPORT NUMBER(S)

DTRA-TR-16-57

12. DISTRIBUTION / AVAILABILITY STATEMENT

Distribution Statement A. Approved for public release; distribution is unlimited.

13. SUPPLEMENTARY NOTES

14. ABSTRACT

In this work, we characterized entry inhibitors and human monoclonal antibodies against dengue virus (DENV) and the developed disinfection systems made from titanium oxide nano-materials. For the DENV inhibition aims, we determined that the DN59 peptide functions as an inhibitor by the novel mechanism of causing the RNA genome to be released from the virus particle. We also investigated the mechanism of two other inhibitory peptides and showed that they interfered with virus:cell binding during entry. We also investigated the binding epitope and mechanism of action of broadly neutralizing human monoclonal antibodies against the dengue E protein and found that they recognized the highly conserved fusion loop and blocked fusion between DENV and cell membranes. We extended our decontamination work with catalysts made from titanium oxide nano-materials. We used voltage activation of our TiO2 materials to create a novel germicide, and we described a recyclable, 'self-cleaning sensor' useful for detecting hydrophobic toxins.

15. SUBJECT TERMS

virus, dengue, inhibitor, peptide, human monoclonal antibody, germicides, decontamination, titanium oxide

16. SECURITY CLASSIFICATION OF:			**17. LIMITATION OF ABSTRACT**	**18. NUMBER OF PAGES**	**19a. NAME OF RESPONSIBLE PERSON**
a. REPORT	**b. ABSTRACT**	**c. THIS PAGE**	SAR	147	Heather Meeks
Unclassified	Unclassified	Unclassified			**19b. TELEPHONE NUMBER** *(include area code)* 703-767-3059

UNIT CONVERSION TABLE

U.S. customary units to and from international units of measurement*

U.S. Customary Units	Multiply by → / ← Divide by†		International Units
Length/Area/Volume			
inch (in)	2.54	$\times 10^{-2}$	meter (m)
foot (ft)	3.048	$\times 10^{-1}$	meter (m)
yard (yd)	9.144	$\times 10^{-1}$	meter (m)
mile (mi, international)	1.609 344	$\times 10^{3}$	meter (m)
mile (nmi, nautical, U.S.)	1.852	$\times 10^{3}$	meter (m)
barn (b)	1	$\times 10^{-28}$	square meter (m^2)
gallon (gal, U.S. liquid)	3.785 412	$\times 10^{-3}$	cubic meter (m^3)
cubic foot (ft^3)	2.831 685	$\times 10^{-2}$	cubic meter (m^3)
Mass/Density			
pound (lb)	4.535 924	$\times 10^{-1}$	kilogram (kg)
unified atomic mass unit (amu)	1.660 539	$\times 10^{-27}$	kilogram (kg)
pound-mass per cubic foot (lb ft^{-3})	1.601 846	$\times 10^{1}$	kilogram per cubic meter (kg m^{-3})
pound-force (lbf avoirdupois)	4.448 222		newton (N)
Energy/Work/Power			
electron volt (eV)	1.602 177	$\times 10^{-19}$	joule (J)
erg	1	$\times 10^{-7}$	joule (J)
kiloton (kt) (TNT equivalent)	4.184	$\times 10^{12}$	joule (J)
British thermal unit (Btu) (thermochemical)	1.054 350	$\times 10^{3}$	joule (J)
foot-pound-force (ft lbf)	1.355 818		joule (J)
calorie (cal) (thermochemical)	4.184		joule (J)
Pressure			
atmosphere (atm)	1.013 250	$\times 10^{5}$	pascal (Pa)
pound force per square inch (psi)	6.984 757	$\times 10^{3}$	pascal (Pa)
Temperature			
degree Fahrenheit (^oF)	$[T(^oF) - 32]/1.8$		degree Celsius (^oC)
degree Fahrenheit (^oF)	$[T(^oF) + 459.67]/1.8$		kelvin (K)
Radiation			
curie (Ci) [activity of radionuclides]	3.7	$\times 10^{10}$	per second (s^{-1}) [becquerel (Bq)]
roentgen (R) [air exposure]	2.579 760	$\times 10^{-4}$	coulomb per kilogram (C kg^{-1})
rad [absorbed dose]	1	$\times 10^{-2}$	joule per kilogram (J kg^{-1}) [gray (Gy)]
rem [equivalent and effective dose]	1	$\times 10^{-2}$	joule per kilogram (J kg^{-1}) [sievert (Sv)]

*Specific details regarding the implementation of SI units may be viewed at http://www.bipm.org/en/si/.

†Multiply the U.S. customary unit by the factor to get the international unit. Divide the international unit by the factor to get the U.S. customary unit.

FINAL TECHNICAL REPORT

HDTRA1-10-1-0009

Mechanistic Studies of Flavivirus Inhibition and Nanoparticle-Catalyzed Decontamination

Period of Performance: January 21, 2010 – August 31, 2012

Principal Investigator: Sharon Isern, Ph.D.

Florida Gulf Coast University

10501 FGCU Boulevard South

Fort Myers, FL 33965

Abstract

In this work, we characterized entry inhibitors and human monoclonal antibodies against dengue virus (DENV) and the developed disinfection systems made from titanium oxide nano-materials. For the DENV inhibition aims, we determined that the DN59 peptide functions as an inhibitor by the novel mechanism of causing the RNA genome to be released from the virus particle. We also investigated the mechanism of two other inhibitory peptides and showed that they interfered with virus:cell binding during entry. We also investigated the binding epitope and mechanism of action of broadly neutralizing human monoclonal antibodies against the dengue E protein and found that they recognized the highly conserved fusion loop and blocked fusion between DENV and cell membranes. We extended our decontamination work with catalysts made from titanium oxide nano-materials. We used voltage activation of our TiO_2 materials to create a novel germicide, and we described a recyclable, 'self-cleaning sensor' useful for detecting hydrophobic toxins.

Table of Contents

List of Figures

Executive Summary

The specific aims of this work can be divided into two broad, basic science topic areas: the characterization of entry inhibitors and human monoclonal antibodies against dengue virus (DENV) and the development of disinfection systems made from titanium oxide nano-materials. We have either completed the tasks and specific aims in all project areas, or we have completed alternative experimental approaches and in many cases exceeded the work originally proposed. For the DENV inhibition aims, we have determined that the DN59 peptide functions as an inhibitor by the novel mechanism of causing the RNA genome to be released from the virus particle. We have confirmed physical separation of the genome and the other components of the virus lipoprotein particle, including the virus envelope (E) and capsid (C) proteins, and we have confirmed that the genome is ejected as a double stranded RNA molecule and that no single part of the genome seems to be ejected first. We have also investigated the mechanism of two other inhibitory peptides and shown that they function during the entry process by interfering with virus:cell binding. We have also investigated the binding epitope and mechanism of action of broadly neutralizing human monoclonal antibodies against the dengue E protein and found that they recognize the highly conserved E protein fusion loop and block a late stage during the fusion between the virus and cell lipid membranes. Regarding our basic science investigations related to environmentally benign disinfection systems, we have extended our decontamination work with catalysts made from titanium oxide nano-materials. We used voltage activation of our TiO_2 materials to create a novel germicide, and we describe a recyclable, 'self-cleaning sensor' useful for detecting hydrophobic toxins.

In alphabetical order, following are the personnel that were involved in the research effort:
(position held while involved in the work / current position)

Andreea **Barcan** – undergraduate student / B.S. Biology, P.A., NOVA Southeastern University

Kelli **Barr**, Ph.D. – postdoctoral fellow / postdoctoral fellow, Dept. of Environmental and Global Health, University of Florida

Jose **Barreto**, Ph.D., Co-PI, Professor of Chemistry

Branko **Bulakovski** – undergraduate student / B.S. Bioengineering, Chicago-area engineering job search

Joshua **Costin**, Ph.D. – postdoctoral fellow / Adjunct Faculty, Edison State College

Joseph **Fields** – undergraduate student / B.S. Biology, applying to medical school programs

Marielys **Figueroa-Sierra** – undergraduate student, B.S. Biology, technician / M.D. program, Florida State University College of Medicine

Shane **Finn** – undergraduate student / B.A. Chemistry, Ph.D. Program in Chemistry, Vanderbilt University

Nicholas **Forster** – undergraduate student in Biology

Megan **Fox** – undergraduate student / B.A. Chemistry, Ph.D. Program in Chemistry, University of North Carolina, Chapel Hill

Dawn **Gant** – undergraduate student / B.S. Biology, Ph.D. Program in Biomedical Science, University of Miami

Amanda **Graham** – undergraduate student, B.S. Biotechnology, technician

Greg **Hogancamp** – undergraduate student / B.S. Biotechnology, EMT, Lee County Emergency Medical Services

Sharon **Isern**, Ph.D., PI, Professor of Biological Sciences

Paulo **Leon-Silva** – undergraduate student in Bioengineering

Shane **Lince** – undergraduate student / B.S. Civil Engineering, M.D. Program, Virginia Tech

Maxwell **Lowther** – undergraduate student / B.S. Bioengineering, Design Engineer, Azimuth Technology LLC, Naples, FL

Scott F. **Michael**, Ph.D., Co-PI, Professor of Biological Sciences

Joanne **Mikaiel** – undergraduate student / B.S. Biology, Doctor of Physical Therapy Program, FGCU

Angelina **Montes** – undergraduate student / B.A. Chemistry, Ph.D. Program in Chemistry, University of Buffalo

Cindo **Nicholson** – B.S. Biotechnology, technician / Ph.D. program Department of Molecular Genetics and Microbiology, Duke University

Kirk **Pruitt** – undergraduate student, B.S. Biology, technician / M.D. program, Ross University School of Medicine

Vincent **Rosa** – B.S. Computer Science, technician

Dawne **Rowe** – undergraduate student, B.S. Biology, technician / D.V.M. program, University of Georgia College of Veterinary Medicine

Fernando **Sanchez** – undergraduate student in Civil Engineering

Jonathan **Shute** – undergraduate student / B.S. Bioengineering, graduate student, Clemson University

Jessica **Strnad** – B.S. Biotechnology, technician / Ph.D. Program in Molecular Biology, Vanderbilt University

James **Sweeney**, Ph.D., Professor of Bioengineering

Jorge **Torres**, M.D., Ph.D., Associate Professor of Bioengineering

Carlene **Williams** – undergraduate student / B.S. Biology, USDA Natural Resources Conservation Services

The following peer-reviewed publications stemmed from the research effort:

[Appendix A]
Costin JM, Jenwitheesuk E, Rees CR, Hunsperger E, Conrads K, Fontaine KA, Isern S, Samudrala R, Michael SF. "Structural optimization and de novo design of dengue virus entry inhibitory peptides". ***PLoS Neglected Tropical Diseases*** 4:e721 (2010)

[Appendix B]
Finn ST, Strnad JA, Barreto PD, Fox ME, Torres J, Sweeney JD, Barreto JC. "A screening technique useful for testing the effectiveness of novel 'self-cleaning' photocatalytic surfaces". ***Photochemistry and Photobiology*** 87:1184-1188 (2011)

[Appendix C]
Graham AS, Pruszynski CA, Hribar LJ, DeMay DJ, Tambasco AN, Hartley AE, Fussell EM, Michael SF, Isern S. "Origin of dengue virus from mosquitoes in Key West, Florida, 2010". ***Emerging Infections Diseases*** 17:2074-2075 (2011)

[Appendix D]
Nicholson CO, Costin JM, Rowe DK, Lin L, Jenwitheesuk E, Samudrala R, Isern S, Michael SF. "Viral entry inhibitors block dengue antibody-dependent enhancement in vitro". ***Antiviral Research*** 89:71–74 (2011)

[Appendix E]
Lok S-M, Costin JM, Hrobowski YM, Rowe DK, Kukkaro P, Holdaway H, Chipman P, Fontaine KA, Holbrook MR, Garry RF, Kostyuchenko, V, Isern S, Rossmann MG, Michael SF. "Release of dengue virus genome induced by a peptide inhibitor". ***PLoS ONE*** 7(11): e50995. doi:10.1371/journal.pone.0050995 (2012)

[Appendix F]
Costin JM, Zaitseva E, Kahle KM, Nicholson CO, Rowe DK, Graham AS, Bazzone LE, Hogancamp G, Figueroa Sierra M, Fong RH, Yang S-T, Lin L, Robinson JE, Doranz BJ, Chernomordik LV, Michael SF, Schieffelin JS, Isern S. "Mechanistic study of broadly neutralizing human monoclonal antibodies against dengue virus that target the fusion loop". in press ***Journal of Virology***, (2013, vol. 87, issue 1).

The following patent applications stemmed from the research effort:

Barreto JC "Methods for producing photocatalytic materials and materials and apparatus therewith" Publication no. US2011/0104013A1, Publication date 5/5/2011

Michael SF, Isern S, Costin JM, Samudrala R, Jenwitheesuk E. "Optimized dengue virus entry inhibitory peptide (10AN)" Publication No. US2011/0178003A1, Publication date 7/21/2011

Michael SF, Isern S, Garry RF, Samudrala R, Jenwitheesuk E, Costin JM. "Optimized dengue virus entry inhibitory peptide (DN81)" Publication No. US2011/0112031, Publication date 5/12/2011

Isern S, Michael SF. "Vaccines and methods for creating a vaccine for inducing immunity to all dengue virus serotypes" Application No. 61/550,982, filed 10/25/2011

Specific Aims

Task 1: Investigate the mechanism of peptide-induced flavivirus genome ejection

Introduction

The four serotypes of dengue virus (DENV) are the causative agents of dengue fever and dengue hemorrhagic fever and shock syndrome, globally the most important mosquito transmitted viral disease. The number of cases, the case severity, and the range of dengue appear to be increasing over time. However, there are currently no approved vaccines or specific anti-viral treatments for dengue. Our goal for task 1 of the project specific aims was to characterize the anti-dengue activity of a novel 33 amino acid peptide known as DN59 [Hrobowski et al., 2005]. The amino acid sequence of the DN59 peptide is a portion of the amphipathic pre-anchor or stem domain of the dengue surface E protein. Incubation of DN59 with infectious DENV causes a shard inhibition of infectivity through an poorly understood mechanism. Here we show conclusively that DN59 interacts with the virus particle to irreversibly release the RNA genome and render the virus non-infectious. The RNA genome is released and separated from the virus particle as a predominantly hybridized, double stranded molecule, and no specific portion of the genome appears to be released before any other portion. The internal virus structural capsid protein (C) appears to remain associated with the pelletable lipoprotein particle after the genome has been released. These results improve our understanding of a small peptide dengue inhibitor that may serve as a lead molecule for the development of a novel dengue treatment. These results have been recently published, Costin et al. “Release of Dengue Virus Genome Induced by a Peptide Inhibitor” in the open access journal PLoS One. A second publication, Nicholson, et al. “Viral entry inhibitors block dengue antibody-dependent enhancement in vitro” in the journal Antiviral Research describes how the DN59 and another peptide can inhibit the antibody-dependent infection of cells expressing Fc receptors, which is believed to contribute to progression to severe disease.

Methods, Assumptions, and Procedures

1.1 Determine the genome ejection force (and thus the genome packaging force) using external osmotic pressure

Tartrate density gradient assay. Approximately 10^6 FFU of DENV-2 produced in LLC-MK_2 cells and purified by density gradient ultracentrifugation, was treated with 100 µM DN59 or 1% (v/v) triton X-100 for 30 min at 37°C. Treated virus was loaded onto a 10-35% (w/v) potassium sodium tartrate step gradient and centrifuged at 175,117 x *g* for 2 h. Individual fractions were collected and assayed for virus genome and E protein. Genome quantitation was carried out by qRT-PCR using the 10503F/10599R primer set. E protein detection was carried out using modified ELISA. High bind 96-well plates (Costar, Corning, NY) were coated with concavalin A (Vector Laboratories, Burlingame, CA) at 25 mg/ml in 0.01 M HEPES (for 1 h and washed with PBS containing 0.1% (v/v) Tween-20. Equal aliquots of each gradient fraction were added for 1 h to allow binding of E to the concavalin A and then washed again. Captured E protein was detected using a human anti-E monoclonal antibody, followed by goat anti-human HRP conjugate. After a final wash, color was developed with tetramethylbenzidine-peroxide (TMB)-H_2O_2 stopped by adding 1% (v/v) phosphoric acid. Optical density was measured at 450 nm.

1.2 Determine the effects of temperature on ejection

Infectivity inhibition reversibility assay. Approximately 200 FFU of DENV 2 were incubated with 0 or 10 μM DN59 in a total volume of 100 μl serum-free DMEM for 1 h at room temperature. Immediately before infecting LLC-MK_2 cell monolayers, the virus/peptide mixtures were diluted with serum-free DMEM to 1 ml, reducing the concentration of DN59 to 1 μM.

1.3 Determine if the genome is ejected as single stranded RNA or as hybridized double stranded RNA using specific RNase mapping

Genome degradation assay using different types of nucleases. Approximately 1.4-2.9 x 10^4 FFU of DENV-2 was incubated with DN59 for 1 h at room temperature and then digested with RNase A, RNase T1, or micrococcal nuclease (New England BioLabs, Ipswich, MA) for 1 h at 37°C. RNA was extracted using the Qiagen RNeasy mini kit and qRT-PCR was performed using primers 10503F/10599R.

1.4 Determine the genome order of ejection (what part of the genome comes out first) using hybridization to genome specific probes

Genome degradation assay using micrococcal nuclease. Approximately 1.4-2.9 x 10^4 FFU of DENV-2 was incubated with DN59 for 1 h at room temperature and then digested with micrococcal nuclease (New England BioLabs, Ipswich, MA) for 1 h at 37°C. RNA was extracted using the Qiagen RNeasy mini kit and qRT-PCR was performed using 10503F/10599R, 3M-2F (TCACCAAATCCCACGGTAGAAGCA) / 3M-2R (AGGGCATGTATGGGTTGAGAACCT), M-1F (GAGGCTGGAAGCTAGAAG) / M-1R (GAGATACGGCACCTATGG), 5M-1F (AAGCAGAACCTCCATTCGGAGACA) / 5M-1R (AAACACTCCTCCCAGGGATCCAAA), and 5-1F (AATCCCACCAACAGCAGGGATACT) / 5-1R (CGCCATCACTGTTGGAATCAGCAT) primer sets.

1.5 Determine if the genome is ejected along with any other viral structural proteins using protein specific antibodies

Western blot to determine if DN59 treatment separates the C protein from the pelletable virus particle. Purified DENV-2 (15 μl of 1.4 x 10^8 FFU/ml) was incubated with 0 or 100 μM DN59 in 20 μl total volume for 1h at room temperature, then resuspended in 12 ml NTE buffer. Virus mixtures were centrifuged in an SW41 rotor at 32,000 rpm for 90 min. at 4°C. Supernatants were removed and pellets were soaked overnight on ice in 150 μl NTE and 75 μl 2x non-reducing sample buffer, then subjected to SDS-PAGE using 4-15% (w/v) polyacrylamide preparative gels (Bio-Rad, Hercules CA) under non-reducing conditions in 25 mM Tris, 192 mM glycine, 3.5 mM SDS (Sigma-Aldrich, St. Louis, MO) and loaded in a buffer containing 0.7% (w/v) SDS. Precision Plus protein Kaleidoscope ladder was used as a standard (Bio-Rad, Hercules, CA). Proteins were transferred to Amersham Hybond-LFP PVDF membranes (GE Healthcare, Piscataway NJ) in 25 mM Tris, 192 mM glycine, and 20% (v/v) methanol (Fisher, Pittsburgh PA), and membrane strips were blocked in 3% (w/v) BSA (Sigma-Aldrich, St. Louis, MO), 0.1% (v/v) Tween-20 in PBS and then probed overnight at 4°C with anti-E (4.8A), anti-prM (2H2) or anti-C (D2C2) MAbs, followed by Alexa Fluor 488 conjugated goat anti-human or anti-mouse antibodies (Invitrogen, Carlsbad, CA) diluted in 0.1% (v/v) Tween-20 in PBS for 4 h

at room temperature, and rinsed in 0.1% (v/v) Tween-20 in PBS prior to scanning with a Typhoon TRIO Variable Mode Imager (GE Healthcare, Piscataway NJ).

Results and Discussion

1.1 Determine the genome ejection force (and thus the genome packaging force) using external osmotic pressure

The assay system that we developed to probe genome release involves nuclease digestion of peptide-treated and untreated virus particles to degrade released genomic RNA. We realized that addition of solutes to increase the osmotic pressure would also alter the enzymatic activity of the nuclease, complicating the interpretation of results. In place of this, we performed a gradient density ultracentrifugation assay suggested by the reviewers of our published manuscript. Following peptide treatment, virus particles were run in a density gradient, and the gradient fractions were analyzed by qRT-PCR and ELISA for the presence of virus genome and E protein. We discovered that untreated virus particles remained intact with the E protein and genome in the same fraction, while the E protein and genome separated and were found in different fractions for peptide-treated as well as control detergent-treated virus particles. This assay conclusively demonstrates that DN59 peptide treatment causes a disruption of the virus lipid membrane and physical separation of the RNA genome from the virus lipoprotein particle.

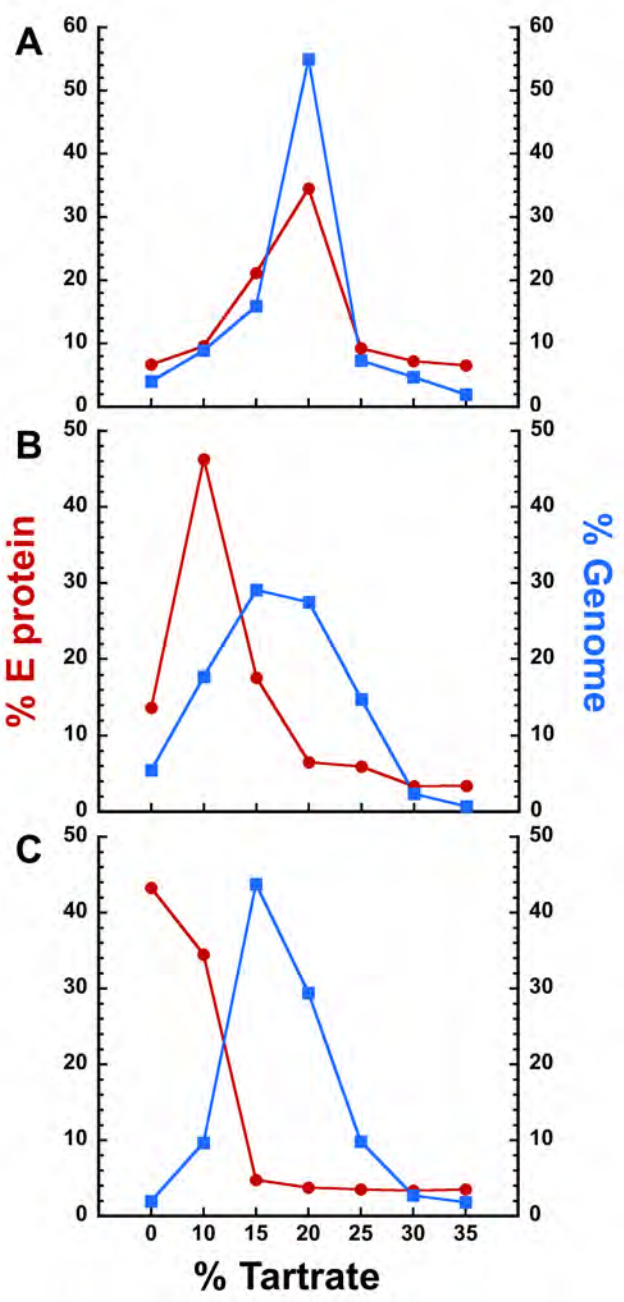

Figure 1: The E protein and genome of virus particles can be separated in a density gradient following treatment with DN59.
DENV-2 was untreated (A), treated with 100 μM DN59 (B), or treated with 1% triton (C), and centrifuged in a tartrate density gradient. Percent total E protein was measured by ELISA (red circles) and % total genome was measured by qRT-PCR (blue squares) in each fraction. Both peptide treatment and triton detergent treatment result in a separation of E protein and genome in the gradients.

1.2 Determine the effects of temperature on ejection

In experiments run at room temperature and 37°C, we observed no difference in the amount of genome sensitivity to nuclease digestion. We hypothesize that there may be a sharp transition occurring and that once the DN59 peptide has begun to disrupt the lipid membrane of the particle in any way, the nuclease contributes to complete genome release by pulling the packaged RNA from the particles in a ratchet-like fashion. To further investigate that the genome is completely separated and released from the virus particles, we conducted an additional reversibility experiment suggested by the reviewers of our published manuscript. This reversibility assay involved treating virus particles with a high enough concentration of DN59 peptide to induce genome release and inhibit infectivity, then diluting the peptide-particle mixture to a point where the peptide concentration was too low to cause genome release and inhibition of infectivity. Prior to and following dilution, the virus-peptide mixture was tested for infectivity by focus forming unit assay. Our results showed that virus particles treated with inhibitory concentrations of DN59 peptide do not recover infectivity after dilution to a non-inhibitory peptide concentration. As controls for the DN59 reversibility experiment, we conducted similar experiments with other peptides (DN57opt and RI57). DN59 irreversibly inhibited the infectivity of treated virus particles, while the inhibitory activity of DN57opt and RI57 were reversible. This is consistent with the mechanism of DN59 disrupting the lipid bilayer of the virus particles and permanently releasing the RNA genome, while DN57opt and RI57 function by reversibly binding to the E protein and altering the surface of the virus particle (see specific aim 2).

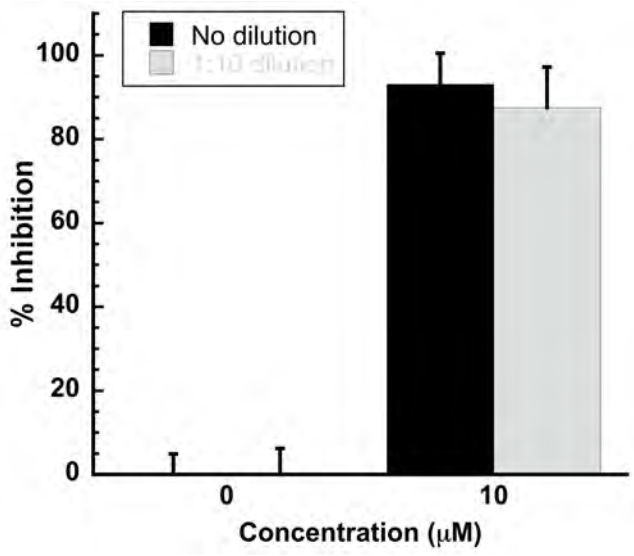

Figure 2: Inhibition of infectivity by DN59 is not reversible.
DENV-2 was incubated with 10 μM DN59, a concentration sufficient to produce approximately 80% inhibition, then either used directly to infect target LLC-MK_2 cells, or diluted 1:10 to 1 μM, a concentration that should produce marginal if any inhibition, then used to infect cells. Virus that was treated with 10 μM DN59, then diluted to 1 μM DN59, showed the same level of inhibition of infectivity as virus that was treated and not diluted.

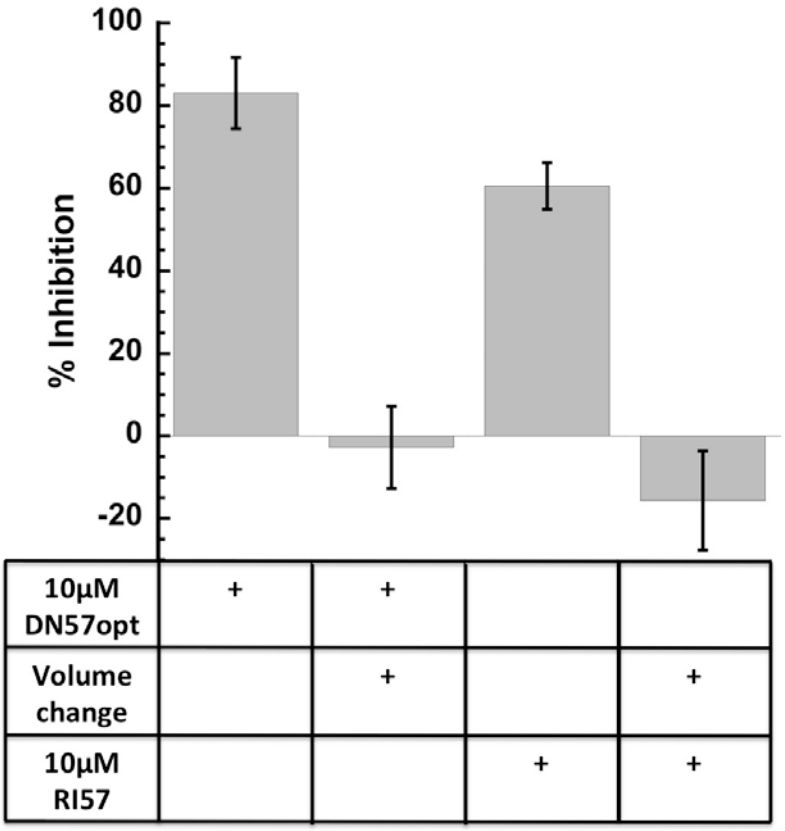

Figure 3: DN57opt and RI57 peptide binding is reversible.
DENV-2 was incubated with 10 µM DN57opt or RI57, a concentration sufficient to produce inhibition, then either used directly to infect target LLC-MK2 cells, or diluted 1:10 to 1 µM, a concentration that should produce marginal if any inhibition, then used to infect cells. Virus that was treated with 10 µM , then diluted to 1 µM, showed no inhibition of infectivity, indicating that the inhibition produced by these peptides is reversible.

1.3 Determine if the genome is ejected as single stranded RNA or as hybridized double stranded RNA using specific RNase mapping

We have found that the 5' untranslated region of the DENV genome is ejected in a form that is not sensitive to degradation with single stranded RNA nucleases (RNase A and/or RNase T1), but is sensitive to nucleases that can degraded double stranded RNA (micrococcal nuclease). This result demonstrates that the 5' end of the genome is released as double stranded RNA, most likely hybridized to sequences located in the 3' untranslated region.

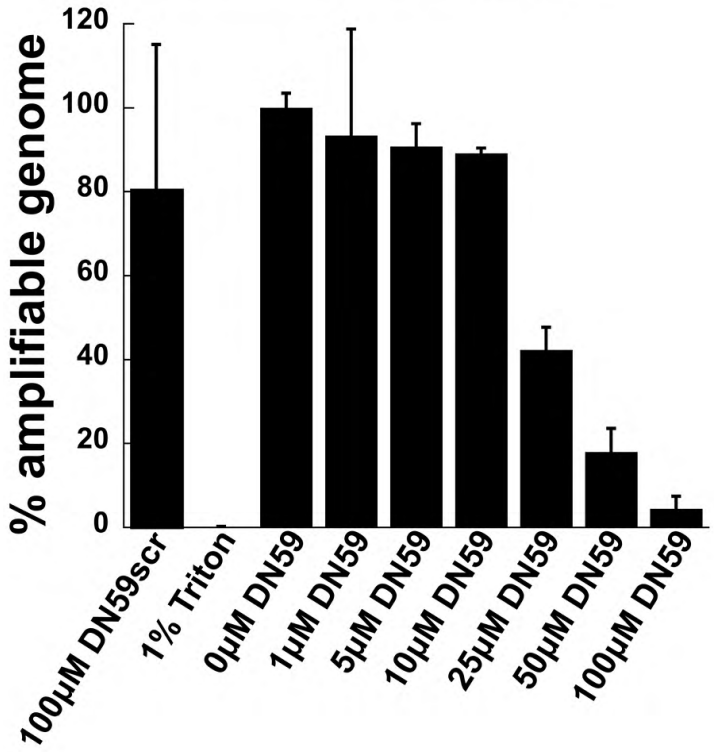

Figure 4: Percent amplifiable genome from micrococcal nuclease digestion in the presence of DN59.
RNase protection assay showing increasing degradation of released viral genome with increasing concentration of DN59. Disruption with detergent (1% triton) resulted in complete degradation. Treatment with a scrambled sequence version of DN59 did not result in significant genome expulsion.

1.4 Determine the genome order of ejection (what part of the genome comes out first) using hybridization to genome specific probes

We used a series of five different qRT-PCR primer sets at spanning different locations in the entire DENV genome to examine if any region of the DENV genome is more or less sensitive to nuclease digestion following peptide-induced ejection than any other. The results show that all primer sets give the same level of sensitivity, indicating that there are no genome regions that are preferentially exposed during the ejection process.

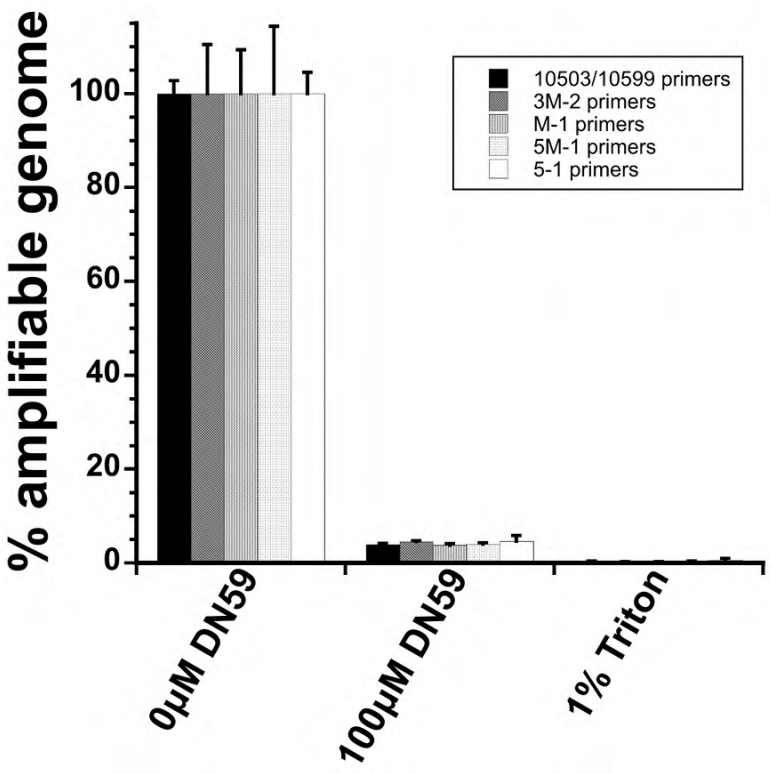

Figure 5: Percent amplifiable genome from micrococcal nuclease digestion using five different qRT-PCR sets at different position of the DENV genome with DN59 peptide. The RNase protection assay is insensitive to the location of the qRT-PCR primers used to detect the viral genome and indicates that there is no part of the genome that has differential sensitivity to degradation. Bars indicate primer sets targeting different locations in the viral genome.

1.5 Determine if the genome is ejected along with any other viral structural proteins using protein specific antibodies

Virus particles were untreated, treated with DN59, or treated with detergent, then spun in an ultracentrifuge under conditions that should pellet virus particles. Following ultracentrifugation, the pelleted material was resuspended, run on an SDS-PAGE gel, and subjected to Western blot analysis with anti-E and anti-C antibodies. Both E and C proteins were detected in the pellets, indicating that the C protein is still associated with the virus particle.

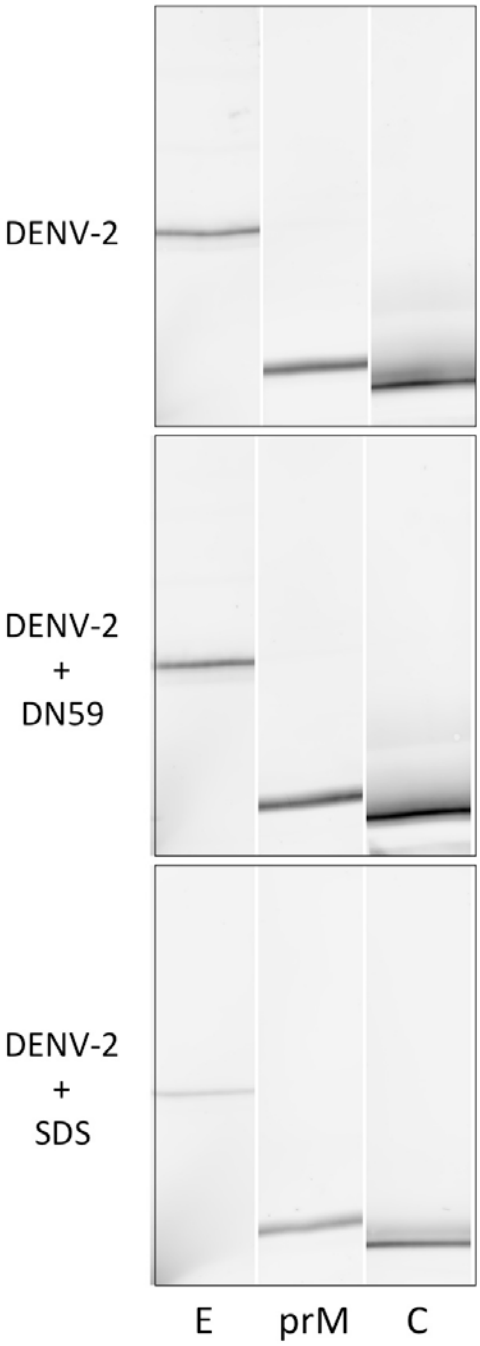

Figure 6: Ultracentrifugation and Western blot analysis of DENV-2 virions in the presence of 100 µM DN59.
DENV-2 E, prM and C proteins remain associated with pelleted virus particles treated with DN59.

Conclusions

The goal of task 1 was to investigate the mechanism of genome ejection caused by a peptide derived from the dengue E protein stem anchor region. We consider that this task has been successfully completed as we have been able to conclusively demonstrate that the DN59 peptide disrupts the virus particle lipid membrane, resulting in the release and separation of the RNA genome from the remainder of the virus lipoprotein shell. This is an entirely novel mechanism of inhibition that has never been previously described. We have also determined that the RNA genome exits the particle in a predominantly hybridized, double stranded form, and that there is no detectable preference for which portion of the approximately 11,000 base genome exits first. Finally, we have also determined that the interior virus C protein does not appear to dissociate from the remainder of the lipoprotein particle after the genome is ejected. This was somewhat unexpected as the C protein is highly positively charged and is thought to associate strongly with the negatively charged RNA genome. The results from task 1 have been published in Costin et al. "Release of Dengue Virus Genome Induced by a Peptide Inhibitor" in the open access journal PLoS One. A second publication, Nicholson, et al. "Viral entry inhibitors block dengue antibody-dependent enhancement in vitro" in the journal Antiviral Research describes how the DN59 and another peptide can inhibit the antibody-dependent infection of cells expressing Fc receptors, which is believed to contribute to progression to severe disease. We expect that these results may direct further research towards the development of membrane disruptive inhibitors for clinical use against enveloped virus infections.

Task 2: Determine the mechanisms of action of other distinct flavivirus peptide inhibitors

Introduction

Since there are no available specific inhibitors against DENV, our goal for task 2 was to characterize the mechanisms of action of other dengue inhibitors, in addition to the DN59 peptide that was the focus of task 1. We found that, unlike the DN59 peptide that caused the RNA genome to be ejected from the virus particle prior to infection, other peptides targeting the viral surface E protein predominantly interfered with virus:cell binding. These results have been published in Costin et al. "Structural Optimization and De Novo Design of Dengue Virus Entry Inhibitory Peptides" in the open access journal PLoS Neglected Tropical Diseases. A second publication, Nicholson, et al. "Viral entry inhibitors block dengue antibody-dependent enhancement in vitro" in the journal Antiviral Research describes how the 1OAN1 peptide can inhibit the antibody-dependent infection of cells expressing Fc receptors, which is believed to contribute to progression to severe disease. Some of the binding and fusion assays developed for this task were also used to characterize human monoclonal antibodies recognizing dengue E protein.

Methods, Assumptions, and Procedures

2.1 Confirm that the inhibition occurs during an entry step in the viral life cycle by exposing the virus to peptide either before or after infection of target cells

Focus forming unit assay. LLC-MK2 target cells were seeded at a density of 1 x10^5 cells in each well of a 6-well plate 24 h prior to infection. Approximately 200 focus forming units (FFU) of virus were incubated with or without peptide in serum-free DMEM for 1 h at room

temperature. Virus/peptide or virus/control mixtures were allowed to infect confluent target cell monolayers for 1 h at 37°C, with rocking every 15 m, after which time the medium was aspirated and overlaid with fresh DMEM/10% (v/v) FBS containing 0.85% (w/v) Sea-Plaque Agarose (Cambrex Bio Science, Rockland, ME) without rinsing. Cells with agar overlays were incubated at 4°C for 20 m to set the agar. Infected cells were then incubated at 37°C with 5% CO_2 for 5 days. Infected cultures were fixed with 10% formalin overnight at 4°C, permeablized with 70% (v/v) ethanol for 20 m, and rinsed with phosphate buffered saline, pH 7.4 (PBS) prior to immunostaining. Virus foci were detected using a specific mouse mAb from hybridoma E60 (obtained from M. Diamond at Washington University), followed by horseradish peroxidase-conjugated goat anti-mouse immunoglobulin (Pierce, Rockford, IL), and developed using AEC chromogen substrate (Dako, Carpinteria, CA). Results are expressed as the average of at least two independent trials with three replicates each. IC_{50} values were determined using variable slope sigmoidal dose-response curve fits with GraphPad Prism 4.0 software (LaJolla, CA).

Post-infection treatment focus forming unit assay. Approximately 200 FFU of DENV-2 without peptide was allowed to bind and enter target cells for 1 h at 37°C as described for the focus forming unit assay. Unbound virus was then removed by rinsing with PBS and peptide was added to the cells for 1 h at 37°C. Cultures were washed again in PBS and agarose overlays, incubation, and immunological detection was conducted as described for the focus forming unit assay.

Analysis. Graphs were generated using KaleidaGraph v.3.6 graphing software (Synergy Software, Reading, PA). Statistical analyses were performed using the GraphPad Prism 4.0 software package (GraphPad Software, San Diego, CA). P values less than 0.05 were considered significant.

2.2 Determine if the peptide inhibits before or after virus/cell binding by adding the peptide after binding, but before fusion

Post-binding treatment focus forming unit assay. Approximately 200 FFU of DENV-2 were allowed to attach to cells for 45 min at 4°C, and then rinsed with cold PBS before peptide was incubated with the target cells for 45 min at 4°C. The cells were rinsed again with cold PBS, and agarose overlays, incubation, and immunological detection were conducted as described for the focus forming unit assay.

2.3 Determine if the peptide directly inhibits fusion using a labeled virus fluorescent dye lipid mixing assay

Virus-liposome fusion assay. Fusogenic activity of dengue virions towards liposomes was characterized using a novel high-throughput plate-reader assay. Viral particles were labeled with fluorescent lipid DiD (Vybrant cell-labeling kit, Molecular Probes, Eugene, OR) in a self-quenching concentration. Large unilamellar liposomes of 100 nm diameter were formed by extrusion technique from the 1:1 (mol/mol) mixture of 1,2-dioleoyl-*sn*-glycero-3-phosphocholine (PC) and 1,2-dioleoyl-sn-glycero-3-phospho-(1'-rac-glycerol) (PG) (Avanti Polar Lipids, Alabaster, AL). DiD-labeled viral particles (~10^5 infectious units) in PBS without calcium and magnesium, pH 7.5 were incubated with different concentrations of the antibodies for 1 h at room temperature in total volume of 50 ml. Virions pre-incubated with antibodies were then mixed in wells of 96-well plates (3 wells for each condition) with acidified liposome-containing

buffer (final concentration of PC and PG 30 mM, pH 5.5). After 10 min co-incubation of virions and liposomes at acidic pH, fluorescence was recorded at excitation and emission wavelengths of 630 and 665 nm. At the end of each recording (10 min incubation at 22^{o}C), Triton X-100 was added to a final concentration of 0.1% (v/v) to fully dequench DiD. The efficiency of fusion is presented as the difference between fluorescence intensities measured after 10 min co-incubation of labeled virions with liposomes at pH 5.5 and at pH 7.5, normalized to the difference between fluorescence intensities measured for fully dequenched DiD and at pH 7.5. In control experiments, we used dengue virions inactivated by an application of a histidine-modifying reagent diethylpyrocarbonate (DEPC) (Sigma, St. Louis, MO) (2 mM, 15 min, room temperature).

2.4 Determine if the peptide directly interferes with virus/cell binding using hemagglutination and quantitative rt-PCR binding assays

Virus:cell binding inhibition assay. LLC-MK2 monolayers were rinsed in 4°C DMEM containing 0.8% BSA and 25mM HEPES, pH7.5. Virus was incubated at 4°C with peptides, control anti-DENV serum, or heparan sulfate in DMEM/BSA/HEPES for one hour before adding to the monolayers for 2 h at 4°C. Monolayers were rinsed 3 times with cold DMEM/BSA/HEPES media prior to RNA extraction using the Qiagen RNeasy mini kit (Valencia, CA) per manufacturer's instructions. Quantitative, real time, reverse transcriptase polymerase chain reaction (qRT-PCR) was conducted utilizing the Roche Lightcycler RNA Master SYBR Green 1 qRT-PCR kit (Basel, Switzerland), using primers Den_F (TTAGAGGAGACCCCTCCC) and Den_R (TCTCCTCTAACCTCTAGTCC) and the following cycling conditions: 1 h at 61°C, 30 s at 95°C, followed by 45 cycles of: 5 s at 95°C, 20 s at 61°C, and 30 s at 72°C. Cp values were used to estimate infectious units according to a standard curve. Independent assays were repeated three times, in duplicate or triplicate.

Virus-intracellular fusion and pre-cellular fusion assays. DENV-2 virions were labeled by DiD as described above. Virus-endosome fusion events were detected as an increase in cell fluorescence upon DiD dilution. MA104 cells (ATCC) (~10^3 cells/well) were grown overnight in the 96-well microtiter plates (Ibidi,Verona, WI). Cells were then incubated for 30 min at 11°C followed by 5 min at 37°C with 10^4 DiD-labeled infectious DENV-2 particles that had been pre-incubated with hMAbs in 100 ml of serum-free ADMEM for 1 h at room temperature. Unbound DENV-2 and hMAbs were removed by washing twice with 400 ml of serum-free ADMEM, and cells were incubated for an additional 25 min at 37°C. For each well, we captured images of 5 randomly chosen fields of view using a Zeiss Observer Z1 (oil immersion objective, 40x) (Carl Zeiss Microscopy, LLC, Thornwood, NY) and generated maximum intensity z-projections based on 15 z-slices of 0.5 mm each for the subsequent analysis. The projections of the cells were analyzed using ImageJ software to subtract the background and threshold using Triangle algorithm. For each condition, we averaged fluorescence intensities in 15 fields (5 fields for each of 3 wells). The data are presented as the mean and the standard deviation of the mean for the averaged intensities (n=3) normalized to the averaged intensities measured for the cells incubated with DENV-2 in the absence of hMAbs. After taking the images for the above analysis, we examined the effects of the hMAbs on the total number of cell-associated virions using a novel assay that measured dequenching of DiD incorporated into unfused viral envelopes. MA104 cells incubated without DENV-2, or with DENV-2 and 10 mg/ml of heparan sulfate, or with DENV-2

and 100 mg/ml of hMAbs 4.8A, D11C or 1.6D were lysed by a 15 min incubation with 0.1% (v/v) triton X-100 at 37°C. The lysates were cleared by a 5 min centrifugation at 14,000xg and 80 ml of each supernatant were mixed with 1920 ml of a 20 mM Hepes, 150 mM NaCl, pH 7.5 buffer. Using a Fluoromax 4 Horiba Jobin Yvon spectrophotometer (Horiba Scientific, Edison, NJ), we measured the emission fluorescence at 665 nm using an excitation wavelength of 600 nm. The data are presented as the mean and the standard deviation of the mean of three independent experiments normalized to the fluorescence intensity measured for DENV-2 infected cells in the absence of hMAbs.

Results and Discussion

2.1 Confirm that the inhibition occurs during an entry step in the viral life cycle by exposing the virus to peptide either before or after infection of target cells

We found that the peptide inhibitors DN57opt and 1OAN1 do not inhibit infectivity when added to previously infected cells. These results indicate that DN57opt and 1OAN1 function during entry. Similarly, DN59 has no inhibitory effect when the peptide is added to cells prior to infection, or when DN59 is added after infection.

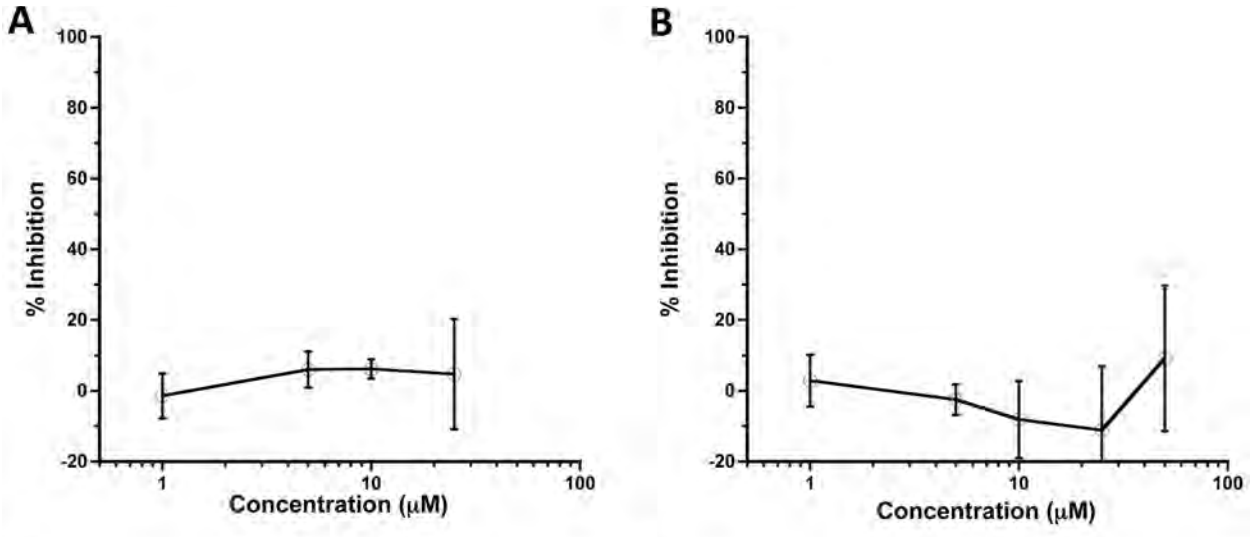

Figure 7: Post-infection peptide treatments.
Treatment of cells with increasing concentrations of (A) DN57opt and (B) 1OAN1 after DENV-2 has infected cells shows no significant inhibition. Error bars are ± sem.

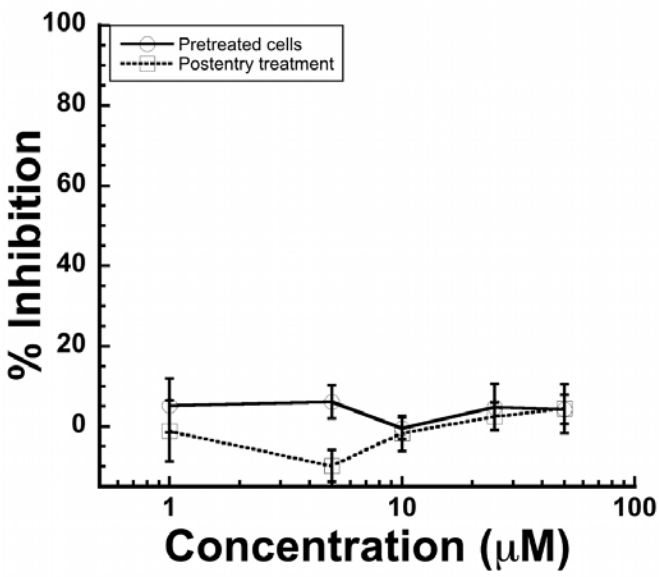

Figure 8: Focus forming unit inhibition results for peptide DN59 when added to target cells before (complete line) or after (dashed line) infection with DENV-2.
Focus-forming unit reduction assay indicates that DN59 has no inhibitory effect on DENV infection when the peptide is added to LLCMK-2 cells and removed prior to the addition of DENV, or when DN59 is added to cells that had already been infected.

2.2 Determine if the peptide inhibits before or after virus/cell binding by adding the peptide after binding, but before fusion

DN57opt and 1OAN1 are both capable of inhibiting infectivity of virus that has been pre-bound to cells and held at 4°C to delay endocytosis and fusion, although the ability to inhibit pre-bound virus is less than the inhibition observed when either peptide is mixed with free virus prior to infection.

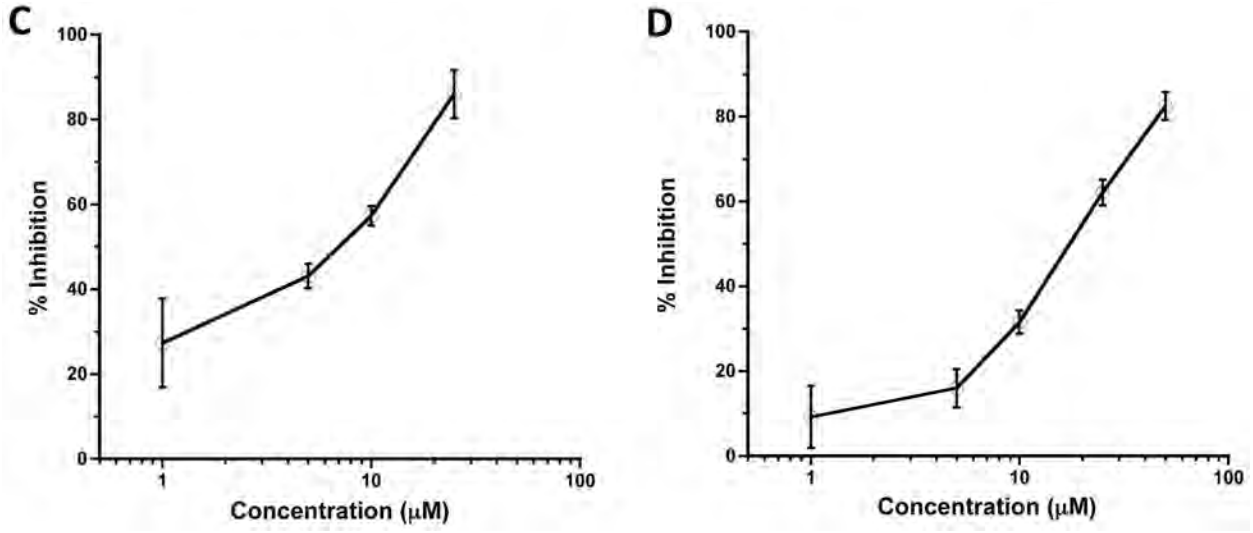

Figure 9: Post-binding peptide treatments.
Treatment with (C) DN57opt or (D) 1OAN1 after DENV-2 has bound to LLCMK-2 cells at 4°C for one hour inhibits infection. Error bars are ± sem.

2.3 Determine if the peptide directly inhibits fusion using a labeled virus fluorescent dye lipid mixing assay

Because both DN57opt and 1OAN1 peptides function primarily by inhibiting virus:cell binding (see below - specific aim 2.4), which occurs before the lipid bilayer fusion step, there was little reason to assay their ability to inhibit fusion.

However, a fluorescent dye mixing assay using liposomes and a fluorescent dye mixing direct cell binding and fusion assay were developed for mechanistic analysis of the anti-dengue monoclonal antibodies that are the subject of specific aim 3. These assays indicated that monoclonal antibodies recognizing the fusion loop of the dengue E protein inhibit infectivity by interfering with the ability of the E protein to catalyze the fusion of the virus and cell membranes.

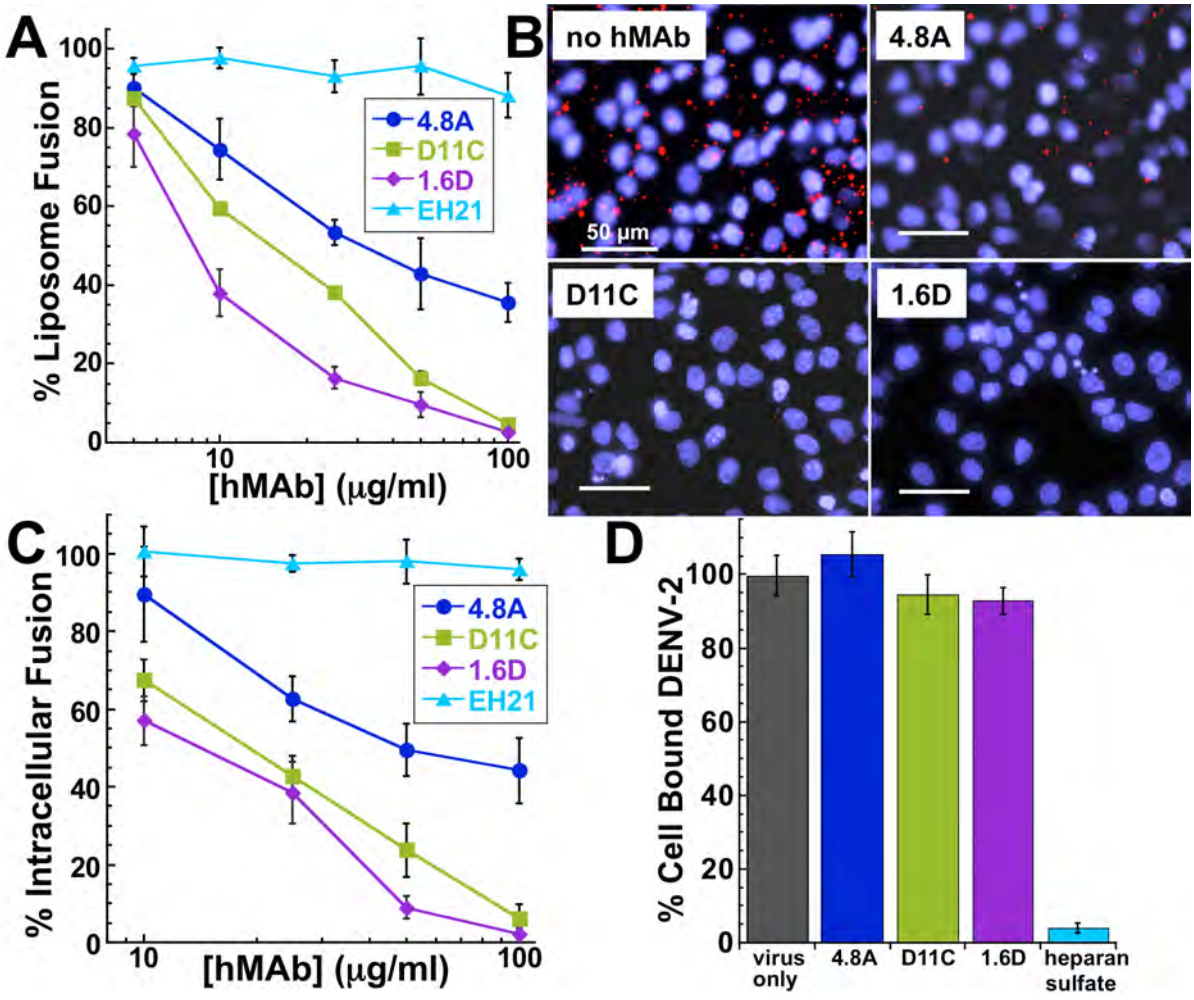

Figure 10: Mechanism of neutralization.
(A) Low pH activated virus-liposome fusion was measured using fluorescently labeled DENV-2 incubated with hMAbs 4.8A, D11C, and 1.6D. Fluorescence signal was normalized to signal generated in the absence of hMAbs to calculate percent liposome fusion. (B) Intracellular fusion of DiD labeled DENV-2 within endosomes leads to dequenching of DiD. Confluent monolayers of MA104 cells were infected with equivalent amounts of DENV-2 pre-incubated with or without 100 mg/ml hMAbs as indicated. Intracellular structures at the site of fusion events fluoresce red. Cells were counterstained with DAPI to visualize nuclei. (C) Intracellular fusion levels were quantified after incubation of DENV-2 with different concentrations of hMAbs. EH21 is an irrelevant anti-HIV hMAb. Fluorescence levels were normalized to virus only controls. (D) Total fluorescence of all bound DENV-2 was quantified by fully dequenching the cells. DENV-2 was incubated with 100 mg/ml of each hMAb. Fluorescence levels were normalized to virus only controls. Heparan sulfate at 10 mg/ml, a known inhibitor of DENV binding, was used as a positive control for binding inhibition. For (A), (C), and (D) each data point is the mean of three replicates. Error bars indicate standard deviation.

Additionally, we tested the DN59 peptide using fluorescent dye mixing assays with liposomes and found that DN59 destabilizes lipid membranes, correlating with genome release.

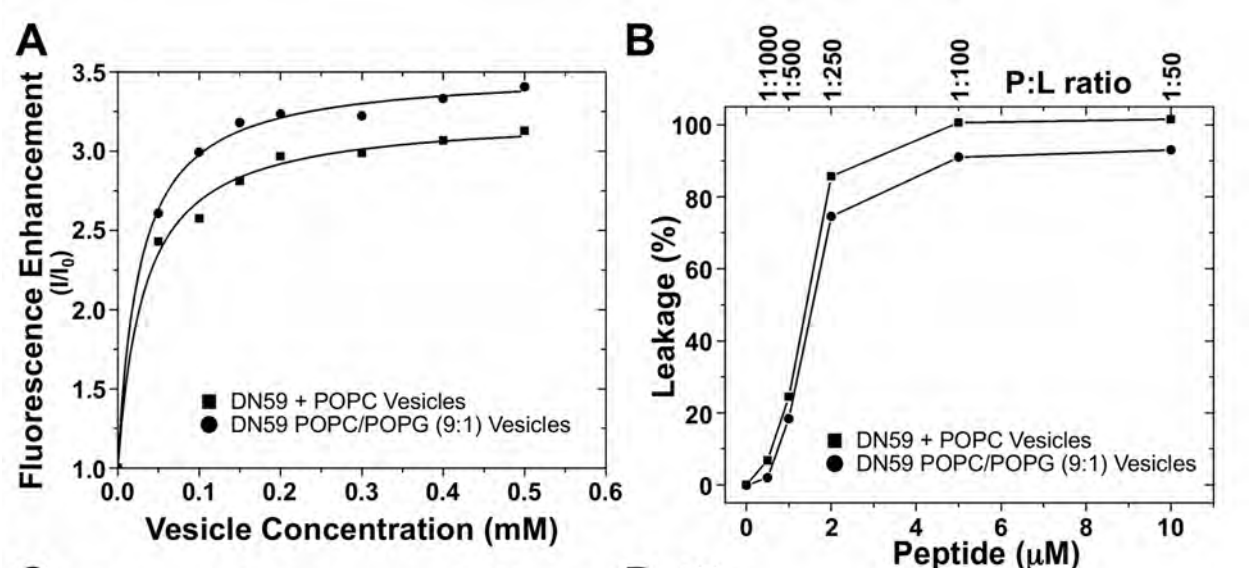

Figure 11: Interaction of DN59 peptide with lipid membranes.
(A) DN59 interacts strongly with liposome vesicles. Tryptophan fluorescence-based binding curves for 1 μM DN59 with additions of zwitterionic vesicles made from POPC and anionic vesicles made from POPC and POPG at a 9:1 ratio. The intensities at 335 nm after each titration are shown and the solid lines are the result of curve fitting with a membrane partitioning equation [White et al., 1998]. (B) DN59 disrupts liposome vesicles. Leakage of the dye/quencher pair ANTS/DPX from 0.5 mM vesicles made from POPC or from POPC/POPG (9:1). Peptide was added to vesicles and the sample was incubated for 1 h prior to the measurement of ANTS intensity. Treatment with 10 μM of the highly lytic bee venom peptide melittin was used to achieve 100% leakage.

2.4 Determine if the peptide directly interferes with virus/cell binding using hemagglutination and quantitative rt-PCR binding assays

Using qRT-PCR to quantitate virus bound to cells, we found that the peptides 1OAN1 and DN57opt inhibit virus:cell binding by greater than 80% and greater than 90%, respectively. This is just slightly less than, and similar to control experiments using heparan sulfate or pooled anti-dengue human serum which also showed high level binding inhibition.

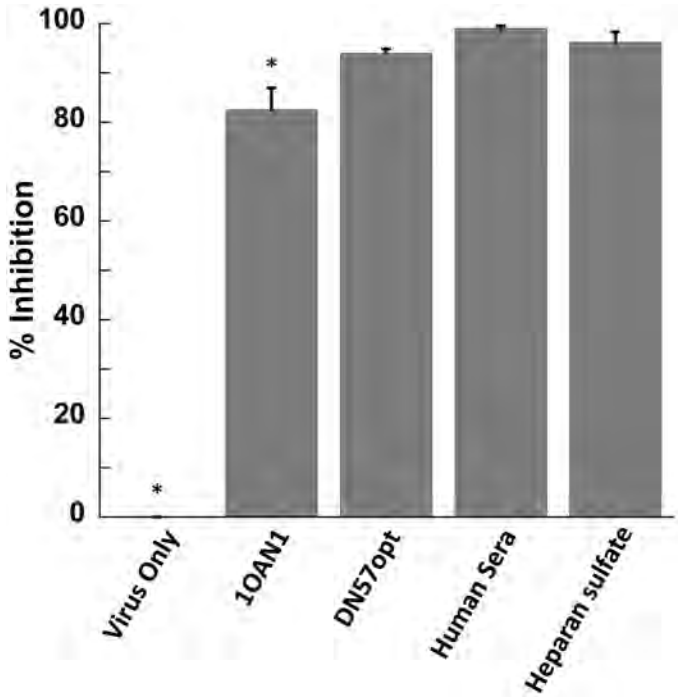

Figure 12: Quantitative reverse transcriptase PCR virus:cell binding.
Virus pre-incubated with either DN57opt or 1OAN1 shows reduced binding to cells compared to control virus without peptide. Pre-incubation of virus with pooled human anti-dengue serum or heparan sulfate similarly shows reduced cell binding. * Indicates a significant difference ($p<0.05$) from all others by 1-way ANOVA followed by Tukey's posthoc test.

Conclusions

The goal of task 2 was to determine the mechanism of action of other distinct flavivirus peptide inhibitors. We consider that this task has been successfully completed as we have been able to demonstrate that two different peptide inhibitors block DENV infectivity by interfering with virus:cell binding, a mechanism distinct from the genome ejection mechainsm of the DN59 peptide in task 1. We had initially anticipated that one or more of the peptide inhibitors would function at a post-cell binding stage, and we had therefore originally planned to use assays to characterize inhibitors that would interfere with the membrane fusion event that occurs post-binding. We found instead that the fusion assays that were developed were perfectly suited for the human monoclonal antibodies that were the subject of task 3. We subsequently made use of the fusion assays to conduct a detailed characterization of the mechanism of neutralization of these monoclonal antibodies. The results from task 2 have been published in Costin et al. "Structural Optimization and De Novo Design of Dengue Virus Entry Inhibitory Peptides" in the open access journal PLoS Neglected Tropical Diseases. A second publication, Nicholson, et al. "Viral entry inhibitors block dengue antibody-dependent enhancement in vitro" in the journal Antiviral Research describes how the 1OAN1 peptide can inhibit the antibody-dependent infection of cells expressing Fc receptors, which is believed to contribute to progression to severe disease. The mechanistic work on the broadly neutralizing human monoclonal antibodies has been published in Costin et al. "Mechanistic study of broadly neutralizing human monoclonal antibodies against dengue virus that target the fusion loop" as an open access article in Journal of Virology. We anticipate that these results will contribute to the development of lead compounds for the clinical treatment of dengue infection.

Task 3: Map the binding epitopes of human anti-dengue virus E protein monoclonal antibodies

Introduction

The severity of dengue infections correlates with the presence of cross-reactive, but incompletely neutralizing antibodies. Previous work has focused on complete or fractionated human serum, which does not allow analysis of the effects of specific antibodies, or on mouse monoclonal antibodies, which do not always recognize the same epitopes, or the same epitopes in the same way as human antibodies. Our group was the first to generate and characterize human monoclonal antibodies against dengue surface proteins and here we provide a detailed characterization of the specific epitopes recognized by a common class of broadly neutralizing human antibody. These antibodies bind to the highly conserved fusion loop in the E protein domain II. Unlike the peptide inhibitors described in the previous task, these antibodies do not substantially interfere with virus:cell binding, but instead prevent fusion of the viral and host cell membranes. This work has been published in Costin et al. "Mechanistic study of broadly neutralizing human monoclonal antibodies against dengue virus that target the fusion loop" as an open access article in Journal of Virology.

Methods, Assumptions, and Procedures

3.1 Protein sequences recognized by individual monoclonal antibodies will be selected using T7 phage display

Western blotting. Purified DENV-2, DENV-2 sE (Hawaii Biotech Inc., Aiea, HI), DENV-2 E sDI/II, and DENV-2 E sDIII (Meridian Life Science, Saco, ME) were subjected to SDS-PAGE using 4-15% (w/v) or 15% (w/v) Tris-HCl polyacrylamide preparative gels, for purified DENV-2 and soluble recombinant proteins, respectively (Bio-Rad, Hercules CA). Unless otherwise specified, samples were electrophoresed under non-reducing conditions in 25 mM Tris, 192 mM glycine, 3.5 mM SDS (Sigma-Aldrich, St. Louis, MO) and loaded in a buffer containing 0.7% (w/v) SDS. Reduced samples were loaded in a buffer containing 0.005% (w/v) SDS and 40 mM DTT. Precision Plus protein Kaleidoscope ladder was used as a standard (Bio-Rad, Hercules, CA). Proteins were transferred to Amersham Hybond-LFP PVDF membranes (GE Healthcare, Piscataway NJ) in 25 mM Tris, 192 mM glycine, and 20% (v/v) methanol (Fisher, Pittsburgh PA), and membrane strips were blocked in 3% (w/v) BSA (Sigma-Aldrich, St. Louis, MO), 0.1% (v/v) Tween-20 in PBS and then probed overnight at 4°C with 5 mg/ml of hMAbs 4.8A, D11C, and 1.6D, mMAbs 3H5.1 (Millipore, Billerica MA) specific for DENV-2 E DIII, 4G2 specific for DENV E DI/II, or 30% (v/v) cell culture supernatant mMAb D2-C2 specific for DENV-2, -4 capsid protein diluted in blocking buffer. Membrane strips were then incubated with Alexa Fluor 488 conjugated goat anti-human or anti-mouse antibodies (Invitrogen, Carlsbad, CA) diluted in 0.1% (v/v) Tween-20 in PBS for 4 h at room temperature, and rinsed in 0.1% (v/v) Tween-20 in PBS prior to scanning with a Typhoon TRIO Variable Mode Imager (GE Healthcare, Piscataway NJ). Photomultiplier tube (PMT) voltage settings used for detecting antibody binding on blot strips ranged from 220 V to 562 V depending on the primary antibody-secondary antibody combination.

3.2 Regions of the E protein recognized by monoclonal antibodies will be identified using antibody/E protein ELISA binding blocking assays with an array of overlapping E protein peptides

E protein peptide binding competition enzyme-linked immunosorbent assay. HMAb D11C was tested for binding competition with a panel of 10-mer peptides spanning the primary sequence of the DENV-2 E protein using an enzyme-linked immunosorbent assay. Solubilized dengue E protein in detergent-treated, serum free culture fluid was immobilized in Con A coated wells. The plates were washed and blocked for 30 min at room temperature. Purified hMAb or dilution buffer was pre-incubated with each of the panel of peptides, then the mixture was incubated in the wells for 30 min at room temperature. Bound hMAb was detected with horseradish peroxidase streptavidin (Vector, Burlingame, CA). After a wash step, color was developed with TMB-H_2O_2 as substrate for peroxidase. The reaction was stopped after 4 min by adding 1% (v/v) phosphoric acid and color was read as optical density (OD) at 450 nm.

3.3 Mutations associated with resistance to binding will be selected by growing virus in the presence of individual antibodies and sequencing the resulting escape mutants

Epitope mapping using prM/E mutants. Mutations were introduced into the prM/E polyprotein of DENV-3 (strain CH53489) by PCR using a Diversity Mutagenesis kit (Clontech Laboratories, Inc., Mountain View, CA), sequenced, and selected to test for hMAb reactivity from a larger library of mutations. Expression plasmids encoding each mutant were transfected

into HEK-293 cells, fixed in 4% (v/v) paraformaldehyde (Electron Microscopy Sciences, Hatfield, PA) 18 h post-transfection, and permeabilized for 45 min with 0.1% (w/v) saponin (Sigma-Aldrich) in PBS plus calcium and magnesium (PBS++). Cells were stained for 1 h with hMAbs 4.8A, D11C, 1.6D (0.11 µg/ml in 10% NGS (Sigma)/0.1% (w/v) saponin), a human polyclonal serum (1:1000), or the anti-DENV E mMAb 1A1D-2, (1:10,000 mouse ascites fluid, kindly provided by John Roehrig, CDC). Cells were washed three times with PBS++/0.1% (w/v) saponin followed by the addition of 0.4 µg/ml HRP-conjugated secondary antibody (Jackson ImmunoResearch Laboratories, West Grove, PA) for 1 h. Following washes, Femto Substrate (Pierce) was added to each well and luminescence values were measured after 5 min (Wallac Victor 2, PerkinElmer, Waltham, MA). All incubations were performed at room temperature. Antibody reactivities against each mutant E protein clone were calculated relative to wild-type E protein reactivity by subtracting the signal from mock-transfected controls and normalizing to the signal from wild-type E-transfected controls. Mutations within critical clones were identified as critical to the hMAb epitope if they did not support reactivity of the test hMAb, but supported reactivity of human polyclonal serum and the conformation-dependent mMAb 1A1D-2. The critical residue within critical clones that contained more than one mutation was identified by assessing other clones containing each of those mutations.

Results and Discussion

3.1 Protein sequences recognized by individual monoclonal antibodies will be selected using T7 phage display

Using denaturing and native Western blots we found that the antibodies are conformationally sensitive to the correctly folded structure of the E protein and do not recognize reduced E protein without disulfide bonds. Since T7 phage can only express small protein sequences that are typically not folded correctly, we did not pursue the T7 system further. See also specific aim 3.2.

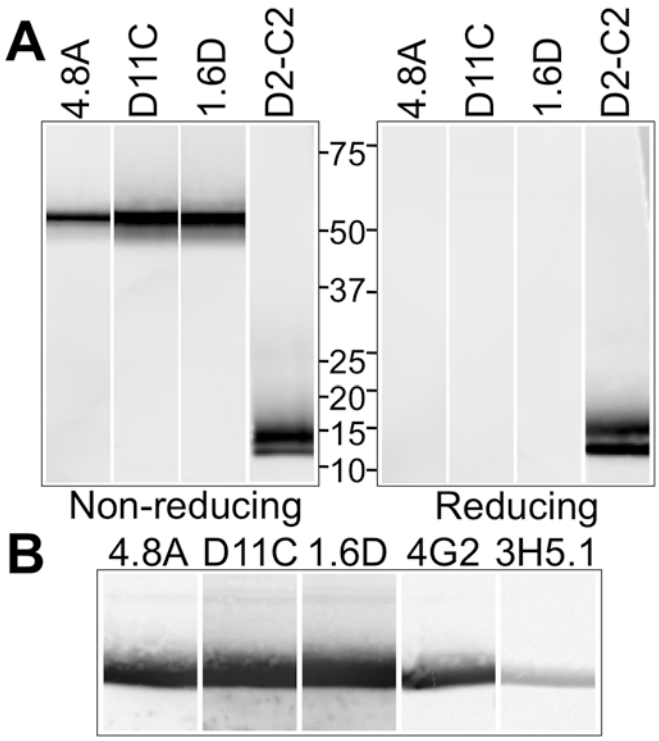

Figure 13: Recognition of the E protein.
(A) Western blots were prepared with gradient purified DENV-2 particles and blot strips were probed with hMAbs 4.8A, D11C, and 1.6D, or anti-DENV capsid mMAb D2-C2 [Puttikhunt et al. 2009] under reducing and non-reducing conditions. Binding of hMAbs to DENV-2 proteins on the blot strips was detected at PMT 400 V. **(B)** Western blots were prepared with DENV-2 sE and blot strips were probed with hMAbs 4.8A, D11C, 1.6D, and control mMAbs 4G2 and 3H5.1 under non-reducing conditions. Binding of hMAbs and mMAbs to DENV-2 sE on the blot strips was detected at PMT 220 V.

3.2 Regions of the E protein recognized by monoclonal antibodies will be identified using antibody/E protein ELISA binding blocking assays with an array of overlapping E protein peptides

Similar to the observation in specific aim 3.1 by Western blot that the monoclonal antibodies did not recognize reduced, unfolded E protein, we found that in an peptide blocking ELISA format the antibodies did not recognize any of a series of overlapping 10-mer peptides spanning the length of the E protein. In this assay, HMAb binding to any of the peptides would interfere with binding to E protein bound to the plate and result in a decrease in ELISA signal. Two peptides did show a slight decrease in ELISA signal, but these two peptides are derived from the transmembrane region and would be completely buried in the virus lipid membrane. The lower ELISA signal for these peptides is likely due to the need to use a low pH buffer to solubilize them for use in the assay.

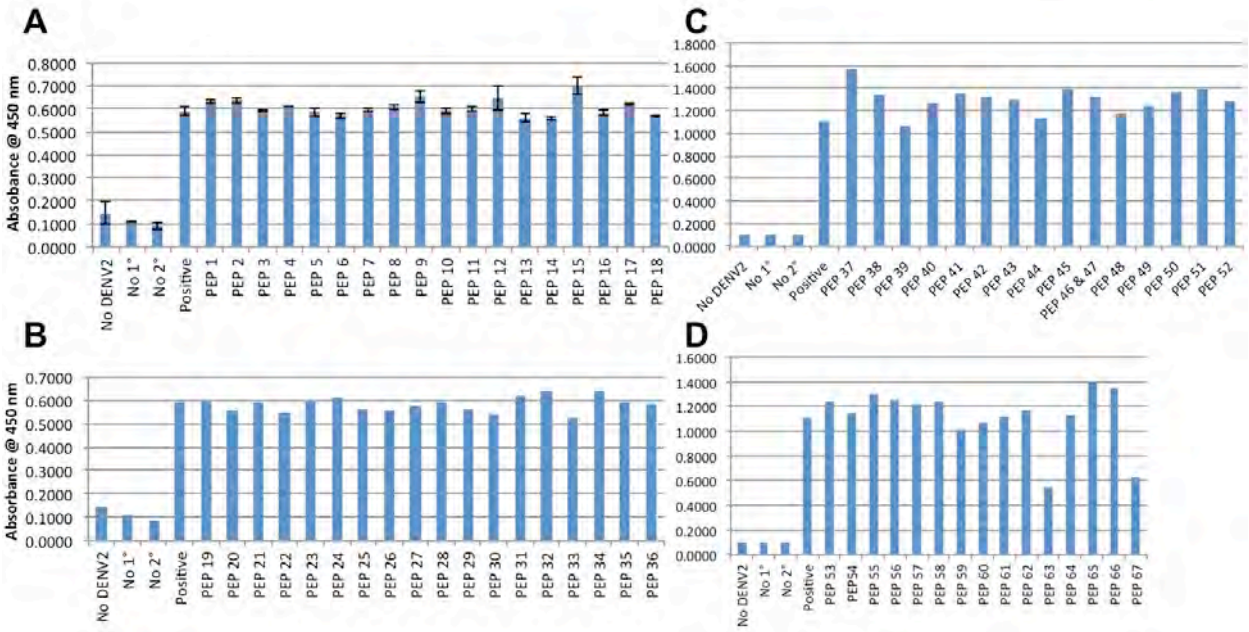

Figure 14: Representative data showing no change in ELISA binding results for antibody D11C with addition of any E protein derived peptide.
(A) Peptides 1-18, **(B)** peptides 19-36, **(C)** peptides 37-52, and **(D)** peptides 53-67.

3.3 Mutations associated with resistance to binding will be selected by growing virus in the presence of individual antibodies and sequencing the resulting escape mutants

We conducted multiple selection experiments where virus was grown in the presence of neutralizing antibodies looking for escape mutants, but were unable to identify convincing mutations that correlated with antibody binding. One possibility is that truly resistant mutants may be very difficult to generate due to the oligomeric function of the DENV E protein. If a resistant mutant was to arise among a population of viruses infecting a single cell, that mutant would have to compete with a large population of wild type virus, and be able to function in a dominant fashion as a monomeric protein subunit when complexed with multiple other wild type viral E proteins.

Instead, we conducted direct binding assays using a library of E protein single site mutants and identified the fusion loop as the site of binding for broadly neutralizing monoclonal antibodies.

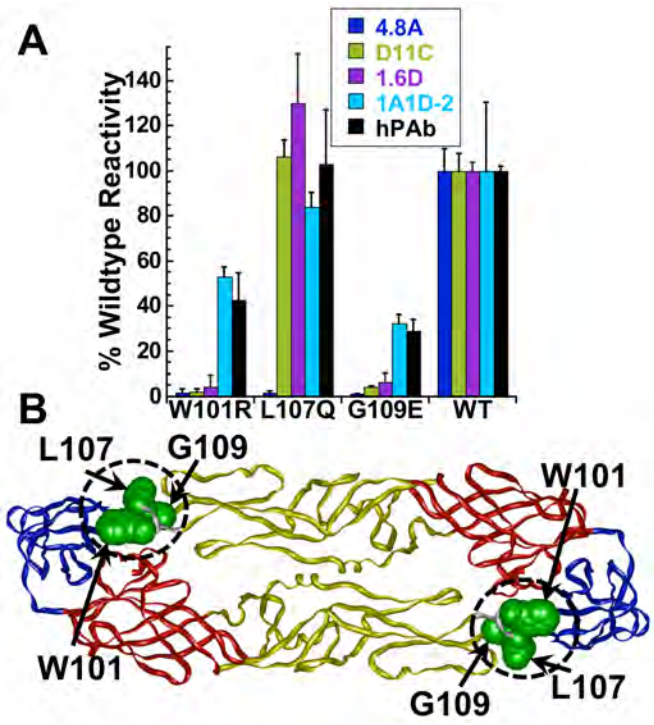

Figure 15: Molecular-level epitope mapping.
(A) Cells expressing DENV E mutants were fixed and immunostained with the indicated antibodies. Clones with reactivity ≤25% relative to WT DENV-3 E were identified as critical for hMAb binding. The reactivities of mutant clones containing each critical residue with hMAbs 4.8A, D11C, 1.6D, and the control mMAb 1A1D-2 and human polyclonal serum (hPAb) are shown. Results were repeated three times and standard deviations of quadruplicate wells are shown. **(B)** Critical residues for hMAbs 4.8A (W101, L107, and G109), D11C (W101 and G109), and 1.6D (W101 and G109) were visualized on a structure of DENV-3 E protein (Protein Data Bank accession code 1uzg; [Modis et al. 2005]). DI, DII, and DIII are depicted in red, yellow, and blue, respectively, and the fusion loop (residues 98-109) is circled.

Conclusions

The goal of task 3 was to map the binding epitopes of human anti-DENV E protein monoclonal antibodies. We consider that this task has been successfully completed as we have been able to identify the precise amino acids recognized by a class of broadly neutralizing monoclonal antibodies that target the dengue E protein fusion loop. We were further able to take advantage of the mechanistic assays for binding and fusion that were developed for the peptide inhibitors in task 2 and apply them to the monoclonal antibodies. The epitope identification and mechanistic work on the broadly neutralizing human monoclonal antibodies has been published in Costin et al. “Mechanistic study of broadly neutralizing human monoclonal antibodies against dengue virus that target the fusion loop” as an open access article in Journal of Virology. We anticipate that these results will lead to novel ideas for a safe and effective vaccine against dengue.

Task 4: Investigate the mechanism of activated nanoparticle-catalyzed decontamination systems

Introduction

Photocatalytic and electrocatalytic molecular destruction can be engendered by electrons ejected from TiO_2 during UV illumination ('UV activation'), or by applying a voltage, ('voltage activation'), or both, which we define as photoelectrochemical destruction (PECD). The ejected electrons are very reactive and can produce destructive radicals, oxidants and reductants (ROR) which can be detected by dosimetry [Barreto et al., 1995]. The ejected electrons can react directly with most molecules, including ambient oxygen (which produces superoxide), or water molecules adsorbed to the TiO_2 surface. 'Activated' TiO_2 will produce odd electron radicals that engender bond breaking, and propagate destructive radical chain reactions [Zhou et al., 2002; Coates et al., 2007]. The ejected electrons also leave behind a positive 'oxidizing hole' in the TiO_2 material which can accept a donated electron, causing further radical production and destruction, (from any molecule that happens to be adsorbed onto the TiO_2 surface) [Fujishima et al., 2000; Wahlstrom et al., 2004; Zhao et al., 2005]. All of the preceding events essentially decontaminate the surface and re-generate the 'clean' TiO_2 catalytic material. In the case of a complex biological toxin, even small changes in the molecular structure can inactivate toxicity (since there is often a tight structure-function relationship involved in bio-toxic mechanisms). For this project we combined voltage activation, UV activation and relative humidity in order to determine whether we could produce enhanced decontamination on the surface of a sensor. We also report further decontamination developments based upon voltage activation alone, using our novel, patented TiO_2 coated foil [Barreto, 2011], to synthesize a germicide.

Methods, Assumptions, and Procedures

4.1 Determine if an applied voltage, along with UV light, will generate enhanced efficiency with regard to chemical destruction

Previously, we hypothesized that voltage and UV activation would increase destruction. In task 4.3 below, we noted that relative humidity enhanced the conductance (and perhaps, destruction) of our titanium oxide catalytic materials. We followed up on our previous findings in sections 4.1 and 4.3 and combined all the variables in order to achieve maximal destruction. We were able to create a 'self-cleaning surface' on a TiO_2 sensor that detects the hydrophobic toxin naphthalene. Our new sensor work therefore builds upon our previously reported data (see relative humidity, and Sudan red destruction data from previous annual reports and our publication, [Finn et al., 2011]. Since our latest sensor experiments combined all modes of destruction, we now report all the new data in this section, instead of separately reporting them in sections 4.1 & 4.3.

We built a titanium oxide - coated interdigitated array electrode (CIDAE) as our sensor, in order to detect the presence of hydrophobic, toxic, naphthalene molecules. The base array electrode, (commercially available from C.H. Instruments), consists of 65 pairs of 5 µm-wide platinum fingers having a gap of 10 µm between them. One member of each pair of fingers was connected to the positive lead of the electrode and the other member of the pair was connected to the negative lead. The total area of the array had dimensions of 2 x 3 mm. The entire array was coated with titanium oxide by spraying (with an airbrush) a methanolic solution of 5 thin layers of P-25 TiO_2 (from Evonik-Degussa) at a concentration of 10 mg/ml. The TiO_2 coating was calcined in a furnace at 600ºC for one hour. The final thin coating covered all the platinum

fingers and the gaps between them. We expected the electrical conductance of the CIDAE sensor to change from a base line reading when the hydrophobic analyte naphthalene was adsorbed onto the coating.

The CIDAE sensor was placed in a sealed 500 mL Erlenmeyer flask with a gas intake glass tube inserted to a point 1 cm above the bottom of the flask, and with the gas exhaust being a lateral side-arm. An ultraviolet pen lamp with a primary emitted wavelength of 365 nm was also placed inside the flask, 1.2 cm from the CIDAE sensor. The intensity of the lamp at that distance was 4 mW/cm^2. Both a humidity sensor and a temperature sensor were placed inside the flask. Ambient air without or with naphthalene vapor was passed through the flask containing the sensor. The air flow maintained at 10 L/min at all times. To introduce naphthalene vapor into the flask, the ambient air was diverted through a chamber containing solid naphthalene flakes (solid naphthalene sublimes to a gas, which was transported by the ambient air flow to the sensor).

A voltage pulse of 1 V was applied to the CIDAE for 5 s and the resulting current was measured. Additional 2 s before and 3 s after the voltage pulse allowed the setting of and the return to a current base line, for a total of 10 s of current data acquisition and recording. The data shown below represents, the peak current, at the onset of the voltage pulse. A voltage pulse was applied and the corresponding current was measured every minute under clean ambient air flow, then air was mixed with naphthalene vapor, and once again, clean ambient air. A total of 5 current measurements were made during each phase. A long cleaning period of 90 to 120 min was subsequently allowed during ambient air flow. The UV lamp was maintained on at all times except for the 10-second period of the current measurement (to eliminate electrical noise from the lamp).

4.2 Determine if an applied voltage alone can generate molecular destruction

Electrocatalytic synthesis of a germicide using voltage alone: In 4.1 above, we hypothesized that UV and voltage activation of our materials would engender improved molecular destruction. In 4.2 we hypothesized that voltage activation alone could create a potentially more useful decontaminating system since it would eliminate the need for inserting an ultraviolet lamp within a 'decontaminating canister' through which air or water would flow. We have now discovered a system wherein voltage activation alone of a proprietary reactant, (herein named R, to protect potential intellectual property) is converted to a potent germicide, which we will name G. Compound G generates a measurable color in a water solution, but the maximum absorbance is in the UV region; by measuring the absorbance of G at its maximum wavelength (λ_{max}), we can determine the production of G over time. The system is safe and simple requiring only that 0.8 V of direct current be applied to an electrolytic cell containing one CT foil electrode (made from our patented titanium coated foil) and a counter electrode of bare titanium foil. The figure below shows the results of our work and the design of the electrolytic cell.

A 0.025 mm thick, 1 cm x 4 cm strip of titanium foil (from Alfa Aesar) was attached from the positive electrode of a DC voltage supply to the side of a 1 cm plastic cuvette with an alligator clip. A similar sized CT foil was attached to the opposite side of the cuvette with the negative electrode. Three milliliters of reagent R were placed into the cuvette along with a stir bar. The cuvette was placed on a stir plate and the voltage was applied at 0.8 volts for 20 min. 200 µl samples were removed to a glass bottom, black 96-well plastic plate every 5 min. After

20 min, the plate was read on an Infinite M1000 TECAN plate reader. The data was plotted over time.

4.3 Determine if there are any differences in destruction produced by PECD under conditions in which oxygen and water vapor are varied.

See 4.1, where all the modes of destruction are combined in our latest experiments.

Results and Discussion

4.1 Determine if an applied voltage, along with UV light, will generate enhanced efficiency with regard to chemical destruction

A self- cleaning' Sensor for hydrophobic toxins: The graph below presents the peak current measurements as a function of time during three phases of the sensing process: The first phase, (P.1) consists of passing ambient air (free of naphthalene) over the sensor, this establishes a baseline current, without an analyte. P.2 is a second phase which now includes naphthalene vapor mixed with the air. The naphthalene signal can be seen as a dramatic drop in conductance as the naphthalene is adsorbed onto the TIO_2 surface of our CIDAE sensor. The third phase, P.3 involves the passage of new, fresh ambient air (which is once again free of the naphthalene analyte). When ambient air is mixed with naphthalene vapors (during P.2), the peak current values dramatically fall from the initial base line of 0.7 µA down to 0.07 µA in 5 min (a ~90% drop) this constitutes a large signal response. With constant UV illumination, and ambient relative humidity, it requires about two hours for the peak current measurements to return to the initial values, indicating that naphthalene is being destroyed by the UV light interacting with the titanium oxide coating of the CIDAE. In separate experiments we have shown that the relative humidity can affect the magnitude of the naphthalene signal, and we are investigating the role of relative humidity during the 'cleaning phase (P.3 in the figure). Our sensor can detect naphthalene in less than one minute and can clean itself in a period of two hours and is ready for re-use. Note that in the figure below, the current did not completely return to the initial P.1 value. We have determined that a return to the original current value requires a return to ambient conditions of temperature and relative humidity. During the cleaning phase, the lamp heats the sensor and appears to lower the relative humidity, and the current. In separate experiments, we have shown that if the ambient conditions are carefully restored, the signal is restored to the original baseline.

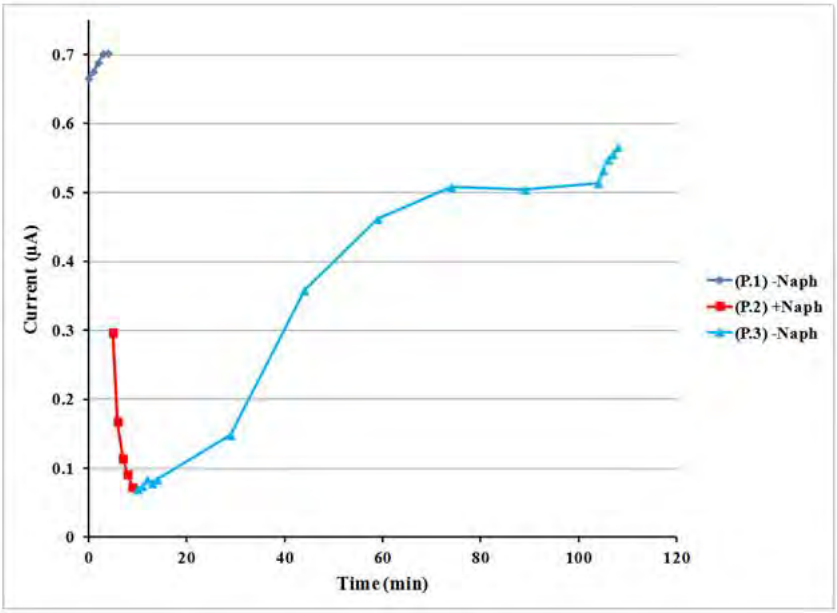

Figure 16: Electrical conductivity of a titanium oxide-coated interdigitated array electrode (CIDAE) when the electrode is exposed to naphthalene vapors.
The CIDAE, constantly exposed to ultraviolet light (4 mW/cm^2), is in a chamber where ambient air flows (10 L/min) with or, without naphthalene vapor. Each point in the figure corresponds to the peak current measured in response to application of a 1 V voltage pulse, applied to the CIDAE for 5 s. Three phases of exposure are shown here: P.1 has ambient air flow with no naphthalene, P.2 is air mixed with naphthalene vapor, and P.3 is a 'cleaning phase' fresh ambient air free of naphthalene. The cleaning phase involves photocatalysis engendered by UV light. Current measurements were made every minute except during the cleaning phase, when the measurements were made every 15 min.

4.2 Determine if an applied voltage alone can generate molecular destruction

The figure below shows that a potent germicide can be generated for the purposes of decontamination using voltage activation alone. G generates a color in aqueous solution so we scanned the compound in order to determine the wavelength of maximum absorbance (λmax) which is in the near UV region, and we used the absorbance at λ_{max} to measure the production of G over time.

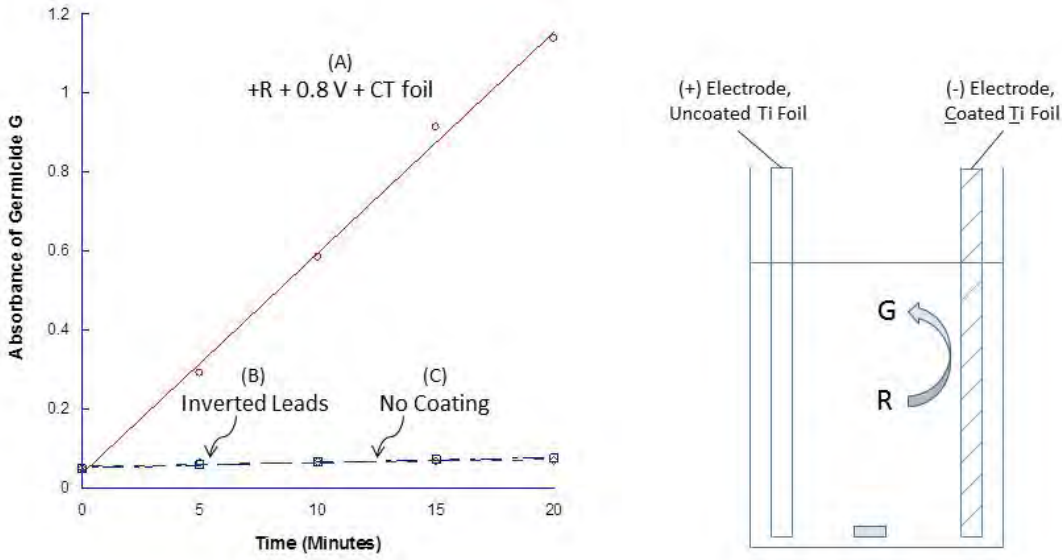

Figure 17: The experimental setup shown above was used to generate germicide 'G'. The uncoated titanium foil on the left was connected to the (+) electrode of a DC power supply and the 'coated titanium foil' on the right was connected to the (-) electrode. Three milliliters of aqueous reactant (R) were placed in the container along with a magnetic stirring bar. The solution was stirred and the voltage set to 0.8 volts. 200 µl samples were removed at 5-minute intervals for 20 min and absorbance was read with a well plate reader. The y-axis in the plot above (left) shows the absorbance of germicide (G) generated when the electrodes were subjected to 0.8 volts for 20 min. Line (A) (with the initial electrode placement shown in the figure) shows that production of G was linear, and very rapid. Note that the final absorbance was very high for line (A), we conclude that substantial amounts of G were produced, with the absorbance being greater than 1.1 units. Line (B) is a control showing that reversal of the leads caused the reaction to cease. Line (C) shows no production of G when both electrodes are uncoated titanium foils. Note that generation of germicide G only occurs when CT foil is connected to the negative electrode and titanium foil is connected to the positive electrode (red line).

4.3 Determine if there are any differences in destruction produced by PECD under conditions in which oxygen and water vapor (relative humidity) are varied

See 4.1, which combine all modes of destruction in a self-cleaning sensor project.

Conclusions

'UV activation' of TiO_2 which caused electron ejection and ROR production (and ensuing molecular destruction) proved to be extremely useful in creating a self-cleaning sensor. The surface of the TiO_2 accumulated a naphthalene toxin analyte that generated a large current signal. The sensor was then 'fouled', and could not be used to detect further accumulations of naphthalene. A cleaning phase, using UV illumination of the photocatalytic surface, restored the sensor's ability to detect naphthalene. 'Voltage activation' alone was used to produce a potent germicide for the purpose of decontaminating water using our proprietary titanium coated foil (Barreto 2011). The germicide can be produced in high concentrations from inexpensive starting

materials. Our germicide generating system has pronounced advantages because no UV lamp is needed; thus simplifying the manufacture of a commercial sterilizing device. We are expanding the results of both projects to include demonstration of germicidal killing and detection of other hydrophobic toxins.

References

Barreto JC, Smith GS, Strobel NH, McQuillin PA, Miller TA. "Terephthalic acid: a dosimeter for the detection of hydroxyl radicals in vitro". *Life Sciences* 56(4):PL89-PL96 (1995).

Barreto JC. "Methods for producing photocatalytic material and apparatus therewith. US Patent application. Publication No. US2011/0104013A1, Publication date 5/5/11.

Coates CM, Caldwell W, Alberte RS, Barreto PD, Barreto JC. "Beta-carotene protects sudan (IV) from photocatalytic oxidation in a micellar model system: Insight into the antioxidant properties of the golden staphylococcus aureus". *World Journal of Microbiology and Biotechnology* 23:1305-1310 (2007).

Costin JM, Jenwitheesuk E, Lok S-M, Hunsperger E, Conrads KA, Fontaine KA, Rees CR, Rossmann MG, Isern S, Samudrala R, Michael SF. "Structural optimization and de novo design of dengue virus entry inhibitory peptides". *PLoS Neglected Tropical Diseases* 4(6): e721 doi: 10.1371/journal.pntd.0000721 (2010).

Costin JM, Zaitseva E, Kahle KM, Nicholson CO, Rowe DK, Graham AS, Bazzone LE, Hogancamp G, Figueroa Sierra M, Fong RH, Yang S-T, Lin L, Robinson JE, Doranz BJ, Chernomordik LV, Michael SF, Schieffelin JS, Isern S. "Mechanistic study of broadly neutralizing human monoclonal antibodies against dengue virus that target the fusion loop". in press *Journal of Virology*, (2013, vol. 87, issue 1).

Finn ST, Strnad JA, Barreto PD, Fox ME, Torres J, Sweeney JD, Barreto JC. "A screening technique useful for testing the effectiveness of novel 'self-cleaning' photocatalytic surfaces". *Photochemistry and Photobiology* 87:1184-1188 (2011).

Fujishima A, Rao T, and Tryk D. "Titanium dioxide photocatalysis". *J. Photochemistry and Photobiology, C* **1**, 1-21 (2000).

Hrobowski YM, Garry RF, Michael SF. "Peptide inhibitors of dengue virus and West Nile virus infectivity". *Virology Journal* 2:49 (2005).

Lok S-M, Costin JM, Hrobowski YM, Rowe DK, Kukkaro P, Holdaway H, Chipman P, Fontaine KA, Holbrook MR, Garry RF, Kostyuchenko, V, Isern S, Rossmann MG, Michael SF. "Release of dengue virus genome induced by a peptide inhibitor". ***PLoS ONE*** 7(11): e50995. doi:10.1371/journal.pone.0050995 (2012)

Modis, Y., S. Ogata, D. Clements, and S. C. Harrison. "Variable surface epitopes in the crystal structure of dengue virus type 3 envelope glycoprotein". *Journal of Virology* 79:1223-1231 (2005).

Nicholson CO, Costin JM, Rowe DK, Lin L, Jenwitheesuk E, Samudrala R, Isern S, Michael SF. "Viral entry inhibitors block dengue antibody-dependent enhancement in vitro", *Antiviral Research* 2011 89:71–74 (2011).

Puttikhunt, C., P. Ong-Ajchaowlerd, T. Prommool, S. Sangiambut, J. Netsawang, T. Limjindaporn, P. Malasit, and W. Kasinrerk. "Production and characterization of anti-dengue capsid antibodies suggesting the N terminus region covering the first 20 amino acids of dengue virus capsid protein is predominantly immunogenic in mice". *Archives of Virology* 154:1211-1221 (2009).

Rees CR, Costin JM, Fink RC, McMichael MM, Fontaine KA, Isern S, Michael SF. "In vitro inhibition of dengue virus entry by p-sulfoxy-cinnamic acid and structurally related combinatorial chemistries". *Antiviral Research* 80:135-142 (2008).

Schieffelin JS, Costin JM, Nicholson CO, Orgeron NM, Fontaine KA, Isern, S, Michael SF, Robinson JE. "Neutralizing and non-neutralizing monoclonal antibodies against dengue virus E protein derived from a naturally infected patient". *Virology Journal* 7:28 (2010).

Wahlstrom E, Vestergaard EV, Schaub R, Rennau A, Vestergaard EL, Laegsgaard E, Stensgaard S, Besenbacher F. "Electron Transfer –Induced Dynamics of Oxygen Molecules on the TiO_2 surface". *Science* 303, 511-513 (2004).

White SH, Wimley WC, Ladokhin AS, Hristova K. "Protein folding in membranes: determining energetics of peptide-bilayer interactions". *Methods Enzymol* 295: 62-87 (1998).

Zhao, J, Chen C, Ma W. "Photocatalytic degradation of organic pollutants under visible light irradiation". *Topics in Catalysis* 35 (3-4) 269-278) (2005).

Zhou, H, Smith DW. "Advanced technologies in water and wastewater treatment". *Journal of Environmental and Engineering Science*: 1 258-264 (2002).

List of Symbols, Abbreviations, and Acronyms

1.6D	anti-dengue virus human monoclonal antibody, neutralizing
1A1D-2	anti-dengue virus mouse monoclonal antibody, recognizes an E protein non domain I epitope
2H2	anti-dengue virus mouse monoclonal antibody, recognizes
3H5.1	anti-dengue virus mouse monoclonal antibody, recognizes E protein domain III
4.8A	anti-dengue virus human monoclonal antibody, neutralizing
4G2	anti-dengue virus mouse monoclonal antibody, recognizes E protein domain II
1OAN1	an E protein first domain I/domain II beta sheet connection region peptide
ADMEM	Advanced Dulbecco's Modified Eagles' Medium
ANOVA	analysis of variance
ANTS	8-aminonapthalene-1,3,6 trisulfonic acid
ATCC	American Type Culture Collection
BSA	bovine serum albumin
^{o}C	degree Celsius
CIDAE	titanium oxide-coated interdigitated array electrode
cm^2	square centimeters
CO_2	carbon dioxide
ConA	Concanavalin A
Cp	value used to estimate infectious units according to a standard curve
C protein	dengue virus capsid protein
CT foil	patented titanium coated foil
D2-C2	mouse monoclonal anti-dengue antibody, recognizes dengue virus 2 and dengue virus 4 capsid protein

D11C	anti-dengue virus human monoclonal antibody, neutralizing
DI	dengue virus E protein domain I
DII	dengue virus E protein domain II
DIII	dengue virus E protein domain III
DAPI	4’,6-diamidino-2-phenylindole, fluorescent stain that binds to nucleic acids
DC	direct current
DENV	dengue virus
DENV-2	dengue virus 2
DENV-3	dengue virus 3
DEPC	Diethylpyrocarbonate
DiD	fluorescent lipid, Vybrant cell-labeling kit
DMEM	Dulbecco’s Modified Eagles’ Medium
DN57opt	an E protein domain II hinge region peptide
DN59	an E protein stem region peptide
DPX	p-xylene-bis-pyridinium bromide
E	glutamic acid, amino acid
E60	anti-dengue virus mouse monoclonal antibody, recognizes E protein domain II
EH21	Anti-HIV-1 human monoclonal antibody
ELISA	enzyme-linked immunosorbent assay
E protein	flavivirus envelope glycoprotein
FBS	fetal bovine serum
FFU	focus-forming units
g	gravitational force

G	glycine, amino acid
G	proprietary germicide
h	hour
H_2O_2	hydrogen peroxide
HEK-293	human embryonic kidney cell line
HEPES	4-(2-hydroxyethyl)-1-piperazineethanesulfonic acid
HIV-1	human immunodeficiency virus 1
HMAb	human monoclonal antibody
HPAb	human polyclonal antibody
HRP	horseradish peroxidase
IC_{50}	fifty percent inhibitory concentration
L	leucine, amino acid
L	liter
LLC-MK-2	rhesus monkey kidney epithelial cell line
λmax	wavelength of maximum absorbance
M	dengue virus membrane protein
M	Molar
MA104	*Macaca mulatta* kidney epithelial cell line
mAb	monoclonal antibody
mg	milligram
min	minute
ml	milliliter
mm	millimeter
mM	millimolar

MMAb	mouse monoclonal antibody
mol	mole
mW	milli Watt
μA	microampere
μl	microliter
μm	micrometer
μM	micromolar
NGS	normal goat serum
nm	nanometer
NTE	buffer 120 mM NaCl, 12 mM Tris, 1 mM EDTA, pH 8.0
P	probability
P.1	first phase
P.2	second phase
P.3	third phase
PBS	phosphate buffered saline
PC	1,2-dioleoyl-*sn*-glycero-3-phosphocholine
PCR	polymerase chain reaction
PECD	photoelectrochemical destruction
PEP	peptide
PG	1,2-dioleoyl-sn-glycero-3-phospho-(1’-rac-glycerol)
pH	corresponds to concentration of hydronium ions in a solution
PMT	photomultiplier tube
POPC	1-palmitoyl-2-oleoyl-sn-glycero-3-phosphocholine
POPG	1-hexadecanoyl-2-(9Z-octadecenoyl)-sn-glycero-3-phospho-(1'-rac-

	glycerol)
prM	dengue virus pre-membrane protein
Q	glutamine, amino acid
qRT-PCR	quantitative real time PCR
R	arginine, amino acid
R	proprietary reagent
RI57	peptide with reverse amino acid sequence and D-amino acids version of an E protein domain II hinge region peptide, DN57opt
RNA	ribonucleic acid
ROR	radicals oxidants and reductants
rpm	revolutions per minute
s	second
sDI	soluble, dengue virus E protein domain I
sDII	soluble, dengue virus E protein domain II
sDIII	soluble, dengue virus E protein domain III
SDS	sodium dodecyl sulfate
SDS-PAGE	sodium dodecyl sulfate polyacrylamide gel electrophoresis
sE	soluble, truncated E protein (missing transmembrane domain)
sem	standard error of the mean
T7 phage	bacteriophage T7, a virus that infects bacteria
TECAN	a particular type of automatic well plate reader
TiO_2	titanium oxide
TMB	3,3’,5,5’-tetramethylbenzidine
UV	ultraviolet light
V	volts

v/v	volume per volume
W	tryptophan, amino acid
wt	wild type
w/v	weight per volume

APPENDIX A

OPEN ACCESS Freely available online

PLoS NEGLECTED TROPICAL DISEASES

Structural Optimization and De Novo Design of Dengue Virus Entry Inhibitory Peptides

Joshua M. Costin[1], Ekachai Jenwitheesuk[2¤a], Shee-Mei Lok[3¤b], Elizabeth Hunsperger[4], Kelly A. Conrads[5], Krystal A. Fontaine[1¤c], Craig R. Rees[1¤d], Michael G. Rossmann[3], Sharon Isern[1], Ram Samudrala[2]*, Scott F. Michael[1]*

1 Department of Biological Sciences, Florida Gulf Coast University, Fort Myers, Florida, United States of America, **2** Department of Microbiology, University of Washington, Seattle, Washington, United States of America, **3** Department of Biological Sciences, Purdue University, West Lafayette, Indiana, United States of America, **4** Dengue Branch, Division of Vector-Borne Infectious Diseases, Centers for Disease Control and Prevention, San Juan, Puerto Rico, **5** FortéBio, Incorporated, Menlo Park, California, United States of America

Abstract

Viral fusogenic envelope proteins are important targets for the development of inhibitors of viral entry. We report an approach for the computational design of peptide inhibitors of the dengue 2 virus (DENV-2) envelope (E) protein using high-resolution structural data from a pre-entry dimeric form of the protein. By using predictive strategies together with computational optimization of binding "pseudoenergies", we were able to design multiple peptide sequences that showed low micromolar viral entry inhibitory activity. The two most active peptides, DN57opt and 1OAN1, were designed to displace regions in the domain II hinge, and the first domain I/domain II beta sheet connection, respectively, and show fifty percent inhibitory concentrations of 8 and 7 μM respectively in a focus forming unit assay. The antiviral peptides were shown to interfere with virus:cell binding, interact directly with the E proteins and also cause changes to the viral surface using biolayer interferometry and cryo-electron microscopy, respectively. These peptides may be useful for characterization of intermediate states in the membrane fusion process, investigation of DENV receptor molecules, and as lead compounds for drug discovery.

Citation: Costin JM, Jenwitheesuk E, Lok S-M, Hunsperger E, Conrads KA, et al. (2010) Structural Optimization and De Novo Design of Dengue Virus Entry Inhibitory Peptides. PLoS Negl Trop Dis 4(6): e721. doi:10.1371/journal.pntd.0000721

Editor: Eva Harris, University of California, Berkeley, United States of America

Received September 11, 2009; **Accepted** April 29, 2010; **Published** June 22, 2010

Funding: Funding for this project was provided by DTRA awards HDTRA1-08-1-0003 and HDTRA1-09-1-0004 and NIH Shannon award 1-56-AI064617-01A2 to SI and SFM, and NSF CAREER award IIS-0448502 to RS. The funders had no role in study design, data collection and analysis, decision to publish, or preparation of the manuscript.

Competing Interests: The authors acknowledge that Florida Gulf Coast University, Tulane University, and the University of Washington have submitted patent applications covering the peptides described in this manuscript.

* E-mail: ram@compbio.washington.edu (RS); smichael@fgcu.edu (SFM)

¤a Current address: National Center for Genetic Engineering and Biotechnology, National Science and Technology Development Agency, Klong Luang, Thailand
¤b Current address: Program in Emerging Infectious Disease, Duke –NUS Graduate Medical School, and Department of Biological Sciences, National University of Singapore, Singapore, Singapore
¤c Current address: Department of Microbiology, University of Washington School of Medicine, Seattle, Washington, United States of America
¤d Current address: School of Public Health, University of Florida, Gainesville, Florida, United States of America

Introduction

Fusogenic viral envelope glycoproteins are multimeric proteins that facilitate the fusion of viral and target cell lipid membranes during the initiation of infection. The membrane fusion process is energetically favorable and essentially irreversible, but has a considerable kinetic energy barrier [1]. These proteins allow rapid membrane fusion by drawing the opposing membranes together and either stabilizing or providing the activation energy to surmount the transition state [1,2]. In this way, they behave in many aspects like a fusion catalyst. Because they effect a macromolecular process that involves large scale conformational changes in the substrate membranes and the proteins themselves, these proteins possess multiple interacting surfaces that could be targeted by inhibitors [3].

There are several distinct types of viral fusion proteins, including the class I, primarily alpha helical proteins (such as HIV TM and influenza HA), the class II, primarily beta sheet proteins (such as the flavivirus E and alphavirus E1), and mixed helix/sheet proteins (including herpes virus gB and rhabdovirus G) [3,4]. To date, most progress with viral fusion protein inhibitors has focused on class I alpha helical proteins. The HIV TM protein provides an excellent example of targeting distinct, interacting surfaces for inhibition. The HIV TM functions as a homotrimer with each monomer contributing two alpha helical regions that interact to form a post-fusion six-helix bundle. Inhibition of the formation of this six-helix bundle can be accomplished by exogenous peptides mimicking either of the two reciprocally interacting helices [5–7].

Only a few examples of viral entry inhibitors with activity against the primarily beta sheet envelope proteins (E) from flaviviruses have been described [8–10]. However, few of these have taken advantage of the available crystal structures of flavivirus E proteins, including both pre-fusion and post-fusion forms [11–22]. The authors of some of these structures have predicted that several regions of these proteins might be targets

Author Summary

Virus surface proteins mediate interactions with target cells during the initial events in the process of infection. Inhibiting these proteins is therefore a major target for the development of antiviral drugs. However, there are a very large number of different viruses, each with their own distinct surface proteins and, with just a few exceptions, it is not clear how to build novel molecules to inhibit them. Here we applied a computational binding optimization strategy to an atomic resolution structure of dengue virus serotype 2 envelope protein to generate peptide sequences that should interact strongly with this protein. We picked dengue virus as a target because it is the causative agent for the most important mosquito transmitted viral disease. Out of a small number of candidates designed and tested, we identified two different highly inhibitory peptides. To verify our results, we showed that these peptides block virus:cell binding, interfere with a step during viral entry, alter the surface structure of dengue viral particles, and that they interact directly with dengue virus envelope protein. We expect that our approach may be generally applicable to other viral surface proteins where a high resolution structure is available.

for inhibition [11,14,15]. Here we report the use of structural data from the pre-fusion dengue virus-2 (DENV-2) E protein as a model for a computational approach to the design of new peptide inhibitors of DENV-2 entry. This approach makes use of a residue-specific all-atom probability discriminatory function (RAPDF) score to identify *in situ* amino acid sequences that are likely to have high structural and binding stability [23,24]. Out of seven computationally designed peptides that were synthesized and tested, two were identified as possessing fifty percent *in vitro* inhibitory activity (IC_{50}) below 10 μM and another with IC_{50} activity below 40 μM. Two of the inhibitors (DN57opt and DN81opt) are binding optimized variants of peptides originally designed from DENV inhibitory peptide sequences located in domain II near the domain I/domain II hinge region [9]. The other (1OAN1) is an entirely novel peptide designed from an extended beta sheet region comprising the first connection between domains I and II. We show that the two peptides with the highest inhibitory activity interfere with virus:cell binding, cause structural changes to the surface of DENV-2 virions, and bind specifically to purified DENV-2 E protein.

The causative agent of dengue fever, dengue hemorrhagic fever and dengue shock syndrome, DENV has emerged in the past several decades as the most important mosquito borne viral disease with an estimated 2.5 billion people living in areas at risk for epidemic transmission and 50–100 million people infected annually [25,26]. Complicating this situation, the four distinct serotypes of DENV generate only low level immunological cross protection, allowing for repeated epidemic outbreaks in the same populations [27,28]. The phenomenon of antibody dependent enhancement has been shown to result in more severe disease in individuals who have been previously infected with a different serotype [29–33]. With no specific treatment or prevention available other than vector control, DENV is an important target for the development of antivirals and vaccines. The results presented here indicate that the DENV E glycoprotein has multiple accessible surfaces that can be targeted by distinct inhibitors and is an amenable target for rational inhibitor design.

Materials and Methods

Computational optimization of hinge region inhibitory peptides

Peptide inhibitors were designed to have improved in situ binding compared to naturally occurring sequences using the residue-specific all-atom probability discriminatory function (RAPDF) [24]. The x-ray diffraction structure of DENV-2 envelope protein (Protein Data Bank identifier 1OAN) was used as a template for creating mutant structures from which the peptides were derived [14]. For each peptide, we randomly selected a residue side chain and substituted it with a new side chain. The substitution was performed using a backbone-dependent side chain rotamer library and a linear repulsive steric energy term provided by SCWRL version 3.0 [34]. The resulting all-atom models were energy minimized for 200 steps using the Energy Calculation and Dynamics (ENCAD) program [35–37]. RAPDF scores were then calculated to estimate the structural stability of a given E protein structure derivative. For a selected residue, side chain substitution was carried out ten times. The amino acid that produced the best RAPDF score was selected and used as a template for further mutation. The entire mutation process was repeated 100,000 times to enable a rigorous search for peptides that produced the best RAPDF score (i.e., highest predicted stability).

Computational design of novel inhibitory peptides

A 20 residue acid sliding window that moved from the N to the C terminus of the E protein in 10 residue acid increments was evaluated by a structural stability (pseudoenergy) optimization protocol using the RAPDF. A Metropolis Monte Carlo search algorithm [38] was used to change each amino acid in the 20 residue window to one of the other 19 naturally occurring amino acids, and the stability of corresponding peptide in the context of the entire E protein structure was evaluated. This process was iterated 100,000 times using RAPDF as the target scoring function. The Metropolis criterion was used to select a particular change in the simulation: if a particular change resulted in a better RAPDF score (lower pseudoenergy), then it was retained. If a particular change resulted in a worse RAPDF score (higher pseudoenergy), then a random choice, based on the score difference between the previous change and the current one, was made to retain the corresponding change. This procedure enables not only enables design of peptides that will result in high structural and binding stability (i.e., the best RAPDF scores/pseudoenergies), but also enables surmounting local minima encountered during the search. Computational optimization was performed on the four regions corresponding to the best RAPDF score, and therefore the highest binding potential, within the E protein as described above to generate variant peptides sequences.

Viruses and cells

DENV-2 strain NG-C was obtained from R. Tesh at the University of Texas at Galveston. Virus was propagated in the *Macaca mulatta* kidney epithelial cell line, LLC-MK2 (ATCC catalog number CCL-7). Cells were grown in Dulbecco's modified eagle medium (DMEM) with 10% (v/v) fetal bovine serum (FBS), 2 mM Glutamax, 100 U/ml penicillin G, 100 μg/ml streptomycin and 0.25 μg/ml amphotericin B, at 37°C with 5% (v/v) CO_2.

Peptides

Peptides were synthesized by solid-phase N-α-9-flurenylmethyloxycarbonyl chemistry, purified by reverse-phase high performance liquid chromatography and confirmed by amino acid analysis and electrospray mass spectrometry (Genemed Synthesis,

San Antonio, TX). Peptide stock solutions were prepared in 20% (v/v) dimethyl sulfoxide (DMSO): 80% (v/v) H_2O, and concentrations determined by absorbance of aromatic side chains at 280 nm.

Focus forming unit assay

LLC-MK2 target cells were seeded at a density of 1×10^5 cells in each well of a 6-well plate 24 h prior to infection. Approximately 200 focus forming units (FFU) of virus were incubated with or without peptide in serum-free DMEM for 1 h at rt. Virus/peptide or virus/control mixtures were allowed to infect confluent target cell monolayers for 1 h at 37°C, with rocking every 15 m, after which time the medium was aspirated and overlaid with fresh DMEM/10% (v/v) FBS containing 0.85% (w/v) Sea-Plaque Agarose (Cambrex Bio Science, Rockland, ME) without rinsing. Cells with agar overlays were incubated at 4°C for 20 m to set the agar. Infected cells were then incubated at 37°C with 5% CO_2 for 5 days. Infected cultures were fixed with 10% formalin overnight at 4°C, permeablized with 70% (v/v) ethanol for 20 m, and rinsed with phosphate buffered saline, pH 7.4 (PBS) prior to immunostaining. Virus foci were detected using a specific mouse mAb from hybridoma E60 (obtained from M. Diamond at Washington University), followed by horseradish peroxidase-conjugated goat anti-mouse immunoglobulin (Pierce, Rockford, IL), and developed using AEC chromogen substrate (Dako, Carpinteria, CA). Results are expressed as the average of at least two independent trials with three replicates each. IC_{50} values were determined using variable slope sigmoidal dose-response curve fits with GraphPad Prism 4.0 software (LaJolla, CA), except for DN81opt, which was determined graphically due to a lack of data points to produce a reasonable curve fit.

Toxicity assay

Cytotoxicity of peptides was measured by monitoring mitochondrial reductase activity using the TACS^{TM} MTT cell proliferation assay (R&D Systems, Inc., Minneapolis, MN) according to the manufacturer's instructions. Dilutions of peptides in serum-free DMEM were added to confluent monolayers of LLC-MK2 cells in 96-well plates for 1 h at 37°C, similar to the focus forming inhibition assays, and incubated at 37°C with 5% (v/v) CO_2 for 24 h. Absorbance at 560 nm was measured using a Tecan GeniosPro plate reader (Tecan US, Durham, NC).

Cryoelectron microscopy

DENV-2 NGC strain used for the cryoEM reconstructions was propagated in mosquito C6/36 cells. Virus was purified by precipitation with 40% PEG 8000 and then ultracentrifugation onto a 25% sucrose cushion. Virus was further purified by banding on a 10%–30% potassium tartrate gradient. The virus band was removed and dialyzed against 12 mM Tris pH 8.0, 120 mM NaCl, 1 mM EDTA, and concentrated using a Millipore Centricon filter. Purified virus was mixed with 1OAN or DN57opt at a concentration of 1 molecule of peptide for every E protein on the surface of the virus. The complex was incubated for half an hour at 37°C followed by half an hour at 4°C and then flash frozen on holey carbon grids in liquid ethane. Images of the frozen complex were taken with a Philips CM200 FEG transmission electron microscope (Philips, Eindhoven, The Netherlands) at a magnification 51,040 using an electron dose of approximately, 25e-/Å 2 using a Charge-Couple device.

Peptide:E protein biolayer interferometry binding assay

Real time binding assays between peptides and purified DENV-2 S1 E protein were performed using biolayer interferometry on an Octet QK system (Fortebio, Menlo Park, CA). This system monitors interference of light reflected from the surface of a fiber optic sensor to measure the thickness of molecules bound to the sensor surface. Purified, recombinant, 80% truncated DENV-2 S1 E protein was obtained from Hawaii Biotechnology (Honolulu, HI). Peptides were N-terminally biotinylated with a 5:1 molar ratio of NHS-LC-LC-Biotin (Pierce/ThermoFisher, Rockford, IL) in PBS pH 6.5 at 4°C. Excess biotinylation reagent was removed using Pepclean C-18 spin columns (Pierce/ThermoFisher, Rockford, IL). Biotinylated peptides were coupled to kinetics grade streptavidin high binding biosensors (Fortebio, Menlo Park, CA) at several different concentrations. Sensors coated with peptides were allowed to bind to E protein in PBS with 0.02% (v/v) Tween-20 and 1 mg/ml BSA at several different E protein concentrations. Binding kinetics were calculated using the Octet QK software package, which fit the observed binding curves to a 1:1 binding model to calculate the association rate constants. E protein was allowed to dissociate by incubation of the sensors in PBS. Dissociation curves were fit to a 1:1 model to calculate the dissociation rate constants. Binding affinities were calculated as the kinetic dissociation rate constant divided by the kinetic association rate constant.

Post-infection treatment focus forming unit assay

Approximately 200 FFU of DENV-2 without peptide was allowed to bind and enter target cells for 1 h at 37°C as described for the focus forming unit assay. Unbound virus was then removed by rinsing with PBS and peptide was added to the cells for 1 h at 37°C. Cultures were washed again in PBS and agarose overlays, incubation, and immunological detection was conducted as described for the focus forming unit assay.

Post-binding treatment focus forming unit assay

Approximately 200 FFU of DENV-2 were allowed to attach to cells for 45 min at 4°C, and then rinsed with cold PBS before peptide was incubated with the target cells for 45 min at 4°C. The cells were rinsed again with cold PBS, and agarose overlays, incubation, and immunological detection were conducted as described for the focus forming unit assay.

Hemagglutination inhibition assay

Hemagglutination inhibition (HI) was performed according to [39] adapted to microtiter plates.

Virus:cell binding inhibition assay

Binding inhibition assays were modified from Thaisomboonsuk, et al [40].}. Briefly, LLC-MK2 monolayers were rinsed in 4°C DMEM containing 0.8% BSA and 25 mM HEPES, pH 7.5. Virus was incubated at 4°C with peptides, control anti-dengue serum, or heparan sulfate in DMEM/BSA/HEPES for one hour before adding to the monolayers for 2 hours at 4°C. Monolayers were rinsed 3 times with cold DMEM/BSA/HEPES media prior to RNA extraction using the Qiagen RNeasy mini kit (Valencia, CA) per manufacturers instructions. Quantitative, real time, reverse transcriptase polymerase chain reaction (qRT-PCR) was conducted utilizing the Roche Lightcycler RNA Master SYBR Green 1 qRT-PCR kit (Basel, Switzerland), using primers Den_F (TTAGAGGAGACCCCTCCC) and Den_R (TCTCCTCTAACCTCTAGTCC) from Chutinimitkul et al [41].}. and the following cycling conditions: 1 h at 61°C, 30 s at 95°C, followed by 45 cycles of: 5 s at 95°C, 20 s at 61°C, and 30 s at 72°C. Cp values were used to estimate infectious units according to a standard curve. Independent assays were repeated three times, in duplicate or triplicate.

Analysis

Graphs were generated using KaleidaGraph v.3.6 graphing software (Synergy Software, Reading, PA). Statistical analyses were performed using the GraphPad Prism 4.0 software package (GraphPad Software, San Diego, CA). P values less than 0.05 were considered significant.

Results

Computational optimization of hinge region peptide inhibitors

We had previously identified several E protein regions where peptides mimicking the E protein sequence might function as inhibitors. Several of these mimic peptides did not show substantial DENV inhibitory activity [9]. These included a peptide derived from the domain II fusion sequence (DN80, corresponding to amino acids 96–114 in the DENV-2 E protein) and two overlapping peptides derived from the domain II hinge region (DN57 and DN81, corresponding to amino acids 205–223 and 205–232, respectively). Predictions from crystal structures [11,14,15], as well as the previously confirmed inhibitory activity of an analogous WNV domain II hinge region peptide [9] lent support to the idea that the domain II hinge region was an attractive target for inhibition. Energy minimized peptides with sequences computationally optimized for structural stability and binding to the target regions, as evaluated by our residue-specific all-atom probability discriminatory function (RAPDF), were selected for further characterization and evaluation. These sequences generally had the best RAPDF scores (or "pseudoenergies") for structural stability and binding, much better (lower) than the original wild type sequences (see Table 1 for original and optimized sequences.). These sequences, DN57opt, DN80opt and DN81opt, were selected for synthesis and evaluated for antiviral activity.

Computational design and optimization of novel peptide inhibitors

To identify additional novel peptide inhibitors and their corresponding targets, a 20 residue sliding window that moved from the N to the C terminus of the DENV-2 strain S1 E protein (PDB ID 1OAN) in 10 residue acid increments was evaluated by a structural stability (pseudoenergy) optimization protocol using the RAPDF. A Metropolis Monte Carlo search algorithm [38] was used to change each amino acid in the 20 residue window to one of the 19 other naturally occurring amino acids, and the stability of each corresponding peptide in the context of the entire E protein structure was evaluated. Our approach identified four E protein regions with the potential for the highest *in situ* binding affinities. These correspond to DENV-2 strain S1 E protein amino acids 41–60, 131–150, 251–270, and 351–370 (see Figure 1) that were selected for synthesis and antiviral testing (1OAN1, 1OAN2, 1OAN3, and 1OAN4).

Inhibition of DENV-2

In order to verify the effectiveness of the binding optimization process and peptide design, synthesized peptides were tested for antiviral activity against DENV-2 strain NG-C in a focus forming unit (FFU) reduction assay. DENV-2 strains S1 (GenBank accession number M19197.1) and NG-C (GenBank accession number AF038403.1) share 98% amino acid sequence identity in the E protein and the majority of differences are conservative. Dose response curves generated for the optimized peptides DN57opt, DN80opt, and DN81opt are shown in Figure 2A. The domain II region peptides, DN57opt and DN81opt displayed IC_{50} values of 8 ± 1 μM and 36 ± 6 μM (mean ± sem) respectively, while no inhibition of infection was observed with the fusion region peptide, DN80opt. Correspondingly, maximum inhibition of 97% and 57% was achieved at 20 μM and 50 μM for DN57opt and

Table 1. Sequences and IC_{50} values of peptides.

Name	LOCATION	Sequence	IC_{50} (μM)
DN57wt	205–232	AWLVHTQWFLDLPLPWLPGADTQGSNWI	--*
DN57opt		RWMVWRHWFHRLRLPYNPGKNKQNQQWP	8±1
DN57opt-scram		RWRHLKKMQRLQPRNPNWPGQFWVHYNW	--
DN80wt	96–114	MVDRGWGNHAGLFGKGSIV	--*
DN80opt		MVIVQHQWMQIMRWPWQPE	--
DN81wt	205–223	AWLVHRQWFLDLPLPWLPG	--*
DN81opt		RQMRAWGQDYQHGGMGYSC	36±6
1OAN1wt	41–60	LDFELIKTEAKQPATLRKYC	ND
1OAN1		FWFTLIKTQAKQPARYRRFC	7±4
1OAN1-scram		QQCFRFPALRKKATYTRFWI	--
1OAN2wt	131–150	QPENLEYTVVITPHSGEEHA	ND
1OAN2		YPENLEYRVYITPHPGEEHH	--
1OAN3wt	251–270	VVLGSQEGAMHTALTGATEI	ND
1OAN3		EWSKHREGRWHTALTGATEI	--
1OAN4wt	351–370	LITVNPIVTEKDSPVNIEAE	ND
1OAN4		WHTVEPIVTEKDRPVNYEWE	--

Names and sequences for previously tested wild type peptides are denoted with an asterisk [9], computationally designed peptides, wild type sequence peptides, and scrambled control peptides are shown. 50% inhibitory concentrations (IC_{50} values ± sem) determined from sigmoidal curve fits to the dose response curves in Figure 2 are given for DN57opt, DN81opt, and 1OAN1. Tested peptides that did not achieve 50% inhibition are noted with a dashed line. Peptides that were not tested for antiviral activity are noted ND (no data).

doi:10.1371/journal.pntd.0000721.t001

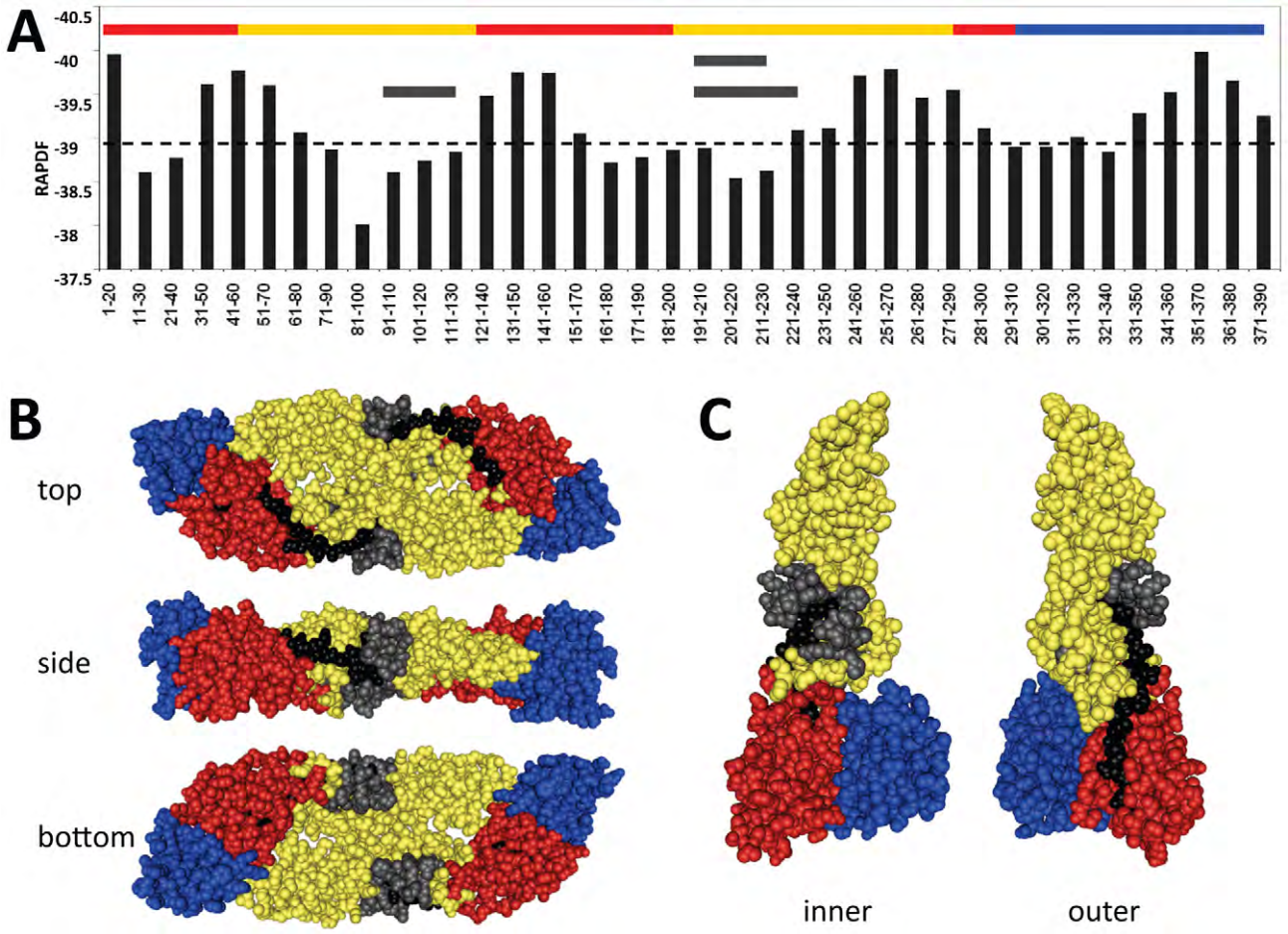

Figure 1. Locations of predicted peptides on the DENV-2 E protein primary sequence. (A) The DENV-2 E protein is shown linearly from N to C terminus. The three domains are color coded above, domain I is shown in red, domain II is yellow, and domain III is in blue according to [46]. The calculated RAPDF scores of a sliding window of 20 amino acid peptide sequences are shown graphically by vertical black lines. Four major high binding regions are predicted, from amino acids 31–70, 121–160, 241–270, and 341–380, respectively, corresponding to the locations of peptides 1OAN1, 1OAN2, 1OAN3, and 1OAN4. The locations of the other optimized peptides are indicated by three horizontal black lines, amino acids 96–114 is DN80opt, 205–223 is DN81opt, and 205–232 is DN57opt. (B) Structure of dimeric dengue E protein in the pre-fusion conformation showing locations of inhibitory peptides. Top, side, and bottom views are shown. Structures are color coded as above. Black and grey residues show the positions of the 1OAN1 and DN57opt peptides respectively. (C) Structure of monomeric dengue E protein in the low pH post-fusion conformation. Inner (interacting) and outer surfaces are shown.
doi:10.1371/journal.pntd.0000721.g001

DN81opt. Both DN57opt and DN81opt showed improved inhibition of DENV-2 compared to their non-optimized counterparts, with DN57opt and DN81opt showing a nearly 14 fold and a 2 fold increase, respectively, in inhibition of DENV-2 at equivalent concentrations [9]. The most active inhibitor, DN57opt was chosen for further study. A scrambled version of DN57opt (DN57optscr) did not display inhibition at any concentration tested (Figure 2B). Four *de novo* designed peptides, 1OAN1, 1OAN2, 1OAN3, and 1OAN4 were also tested for inhibitory activity using the same FFU reduction assay (Figure 2C). 1OAN1 was found to be an effective inhibitor of DENV-2 infection with an IC_{50} of 7 ± 4 μM and a maximum inhibition of 99% at 50 μM. A scrambled version of 1OAN1 (1OAN1scr) did not inhibit infection by DENV-2 at any concentration tested (Figure 2D). In addition to these full dose response inhibition experiments using approximately 100 infectious units of virus, both the DN57opt and 1OAN1 peptides were also capable of inhibiting 4,000 infectious units of virus (data not shown).

Peptide toxicity

Because toxicity could result in a decrease in focus formation and be interpreted as evidence of antiviral activity, the inhibitory peptides and their scrambled versions were assessed for cellular toxicity. Confluent monolayers of LLC-MK2 cells used in FFU reduction assays were exposed to increasing concentrations of peptide before measuring mitochondrial reductase activity using an MTT mitochondrial reductase activity assay (Figure 3). When we initially performed these assays to exactly mimic the focus forming unit assay by waiting five days after peptide exposure, we saw no evidence of toxicity at any concentration of any peptide (data not shown). However, we found that a shorter post-exposure incubation time revealed a subtle toxicity on the part of one of the peptides. Apparently, waiting more than 24 h post-exposure gives the cells a chance to recover and conceals this effect. At 24 h post-exposure, DN57opt was found to be mildly toxic to cells at 40 μM (one-way ANOVA with Dunnet's *post hoc* test, $P = 0.0004$, $N = 18$), so only inhibitory data using lower, nontoxic concentrations was considered. Peptides DN57optscr,

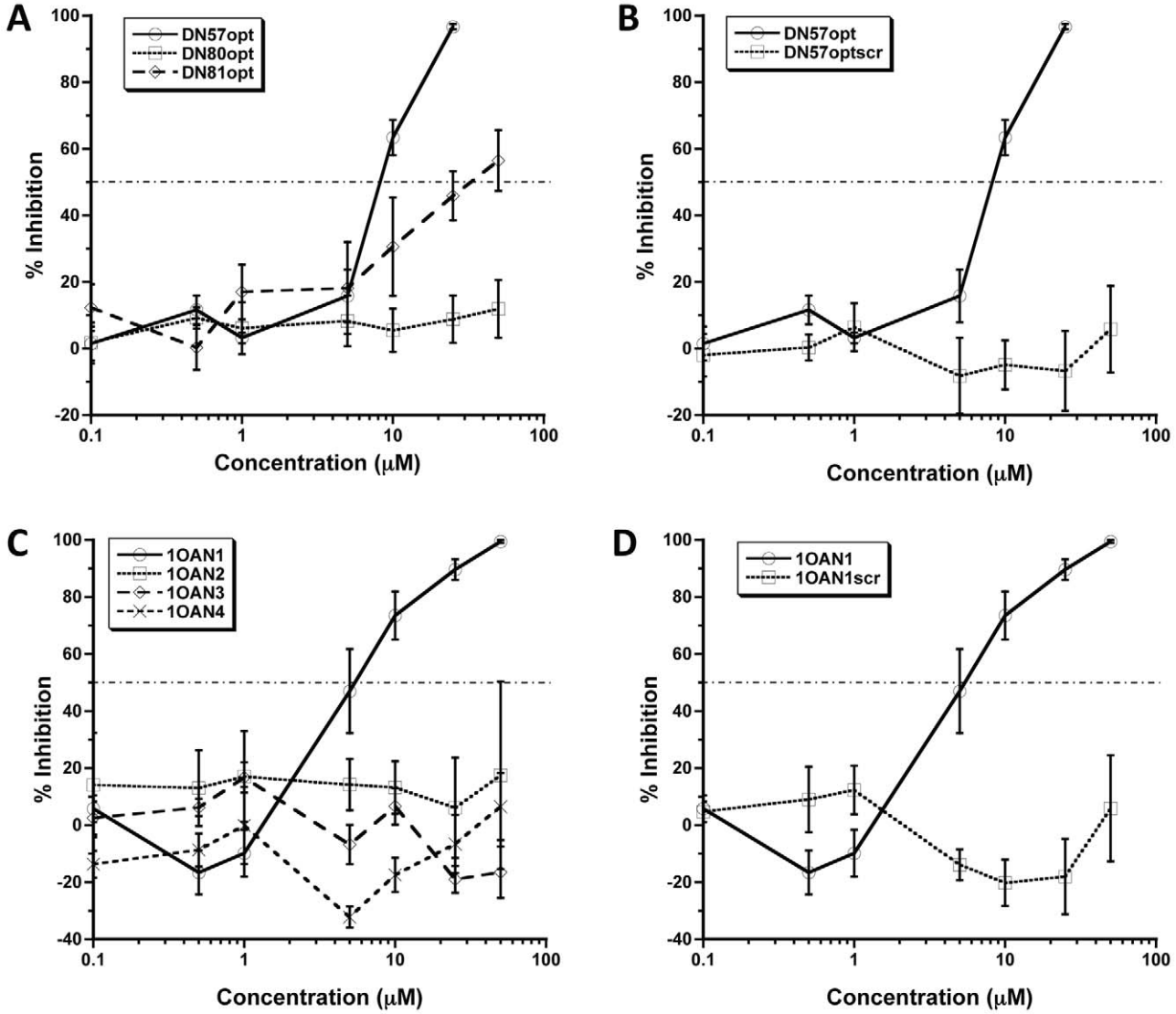

Figure 2. Inhibition of DENV-2 *in vitro*. Increasing concentrations of optimized inhibitor peptides and corresponding scrambled peptides of identical composition were tested against DENV-2 in a focus forming unit reduction assay. (A) Optimized peptides (B) DN57opt and corresponding scrambled peptide of identical composition (C) Novel peptides (D) 1OAN1 and corresponding scrambled peptide of identical composition. Error bars are ±sem.
doi:10.1371/journal.pntd.0000721.g002

1OAN1, and 1OAN1scr were not toxic at any concentration tested (one-way ANOVA, $P>0.05$).

DN57opt and 1OAN1 cause changes to the surface of DENV-2 virus

Cryoelectron microscopy (cryoEM) was used to visualize the effect of the DN57opt and 1OAN1 peptides on DENV-2 viral particles. Control dengue virions exhibited the normal, nearly smooth outer surface typical of mature flaviviruses [42]. The surfaces of the virus particles werebecome followingrough after treatment with peptides, implying a possible rearrangement of the envelope glycoproteins (Figure 4). The treated virions no longer showed icosohedral symmetry, Attempts to reconstruct the structure of virus complexed with DN57opt and 1OAN1 structures by imposing icosahedral symmetry failed, indicating the viruses are no longer icosahedral. Control treatments with equivalent DMSO alone did not produce this morphological alteration.

DN57opt and 1OAN1 bind to soluble DENV-2 E protein

Biolayer interferometry was performed to examine binding of the peptides to purified, truncated DENV-2 E protein. Amino terminally biotinylated peptides were immobilized onto streptavidin biosensors and then the association and dissociation of truncated E protein with the immobilized peptides was monitored. The interactions of three different concentrations of truncated E protein to peptides DN57opt and 1OAN1 are shown (Figure 5). A buffer blank containing no E protein was run for each peptide. The affinities of the peptides for the truncated E protein were calculated with a 1:1 binding model: DN57opt $K_D = 1.2\times10^{-6}\pm0.6\times10^{-6}$ M (mean±sd), 1OAN1 $K_D = 4.5\times10^{-7}\pm2.0\times10^{-7}$ M. While the data for the 1OAN1 peptide show a lower K_D, these numbers are not statistically different (unpaired student's T-test, $P = 0.16$, $N = 3$). The association rate constants were: DN57opt $k_a = 8.0\times10^{2}\pm 5.0\times10^{2}$ $M^{-1}s^{-1}$, 1OAN1 $k_a = 3.9\times10^{3}\pm1.5\times10^{3}$ $M^{-1}s^{-1}$.

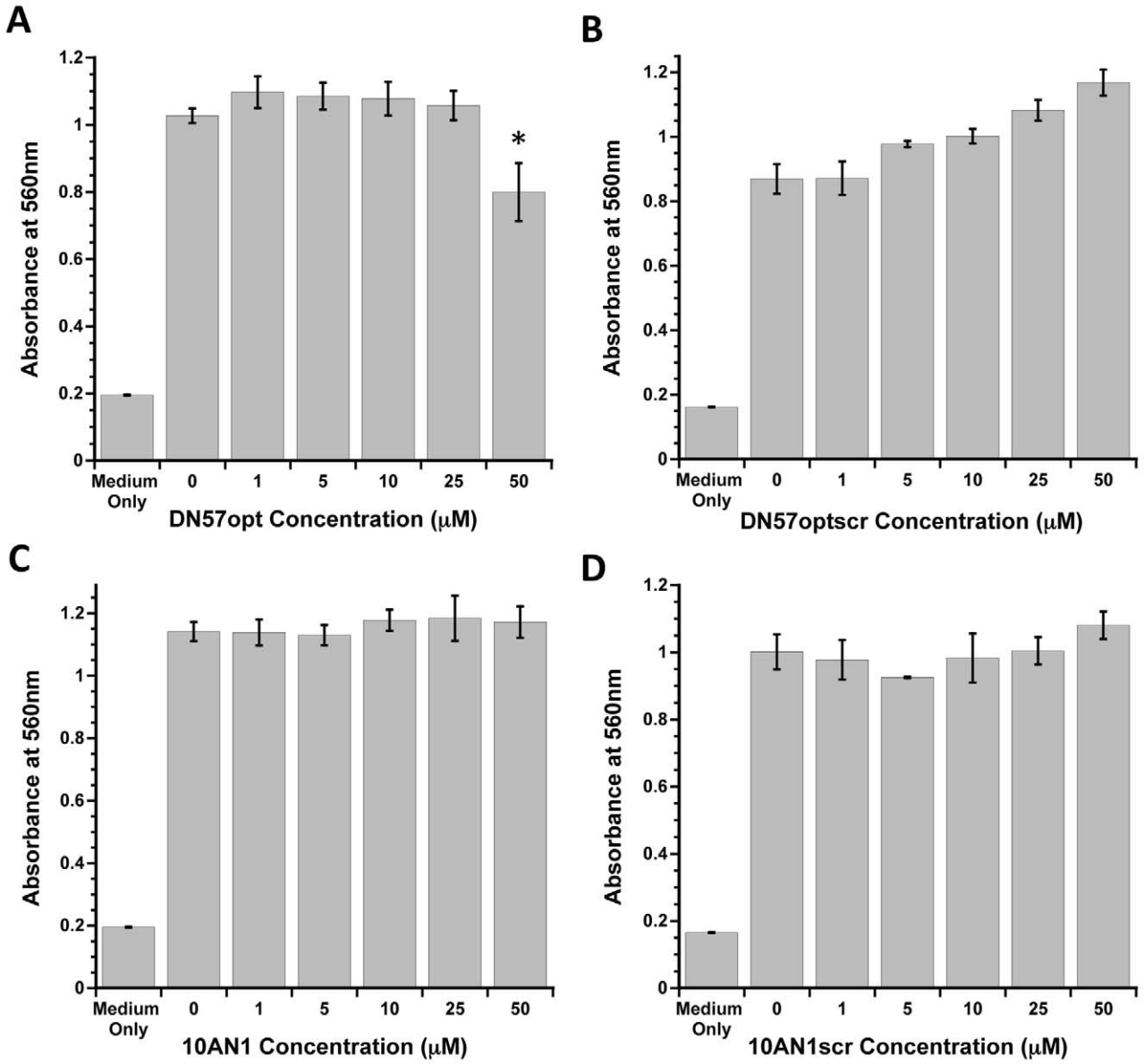

Figure 3. Inhibitory peptide toxicity *in vitro*. Increasing concentrations of peptides were tested in an MTT mitochondrial reductase activity assay. Error bars are ± sd. (A) DN57opt (B) Scrambled version of DN57opt (C) 1OAN1 (D) Scrambled version of 1OAN1. * denotes a statistically significant difference from the no peptide control.
doi:10.1371/journal.pntd.0000721.g003

The dissociation rate constants were: DN57opt $k_d = 7.7\times10^{-4}\pm1.7\times10^{-4}$ s^{-1}, 1OAN1 $k_d = 1.6\times10^{-3}\pm0.2\times10^{-3}$ s^{-1}. We have previously used this system to characterize the binding affinities of several human monoclonal antibodies for DENV E proteins [43].

Treatment of cells with DN57opt and 1OAN1 post-infection does not inhibit replication of DENV-2

In order to determine if the peptides were exerting their effects on post-entry steps in the virus replication cycle, DENV-2 was allowed to infect LLC-MK2 cells before peptide was added to the cells (Figure 6). No inhibition of viral replication was observed at any concentration of DN57opt (Figure 6A) or 1OAN1 in these assays (Figure 6B), indicating that the peptides are not acting at a post-infection step.

Treatment of cells with DN57opt and 1OAN1 after virus binding to cells but before entry inhibits DENV-2 infection

Since we had determined that inhibition with both peptides occurs at a viral entry step, we asked if infection could still be inhibited after virus had bound to the surface of target cells. We bound virus to cells at 4°C, then treated with increasing concentrations of DN57opt or 1OAN1 before warming the cells back to 37°C and allowing the infections to progress (Figure 6C and D). Inhibition of viral entry was observed for both peptides when added to the virus after it was bound to target cells.

DN57opt and 1OAN1 block virus binding to target cells

To determine if the peptides interefere with virus:cell interactions, we conducted two different experiments. We first performed

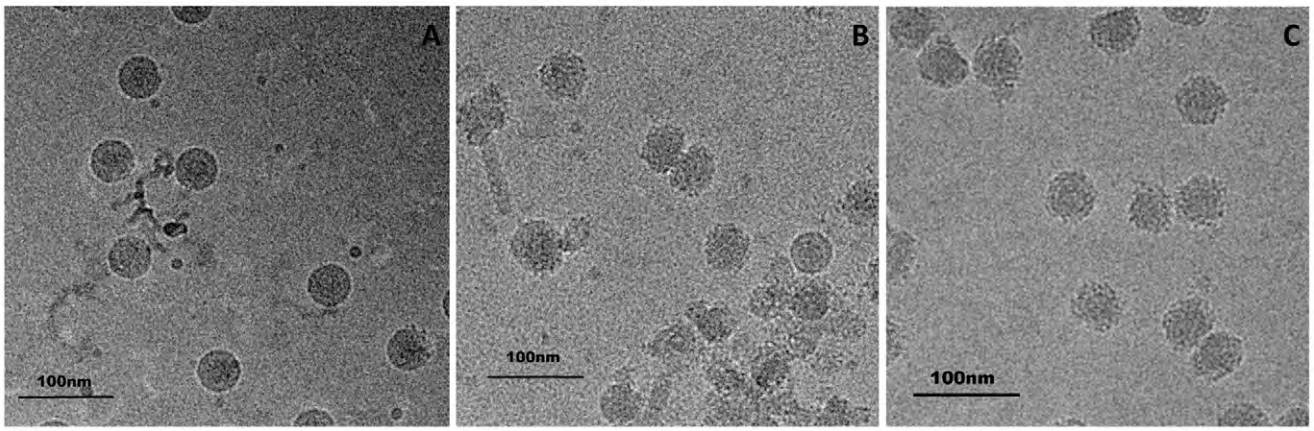

Figure 4. Cryoelectron microscopy. Purified and concentrated virus was prepared with or without incubation with peptides and then flash frozen for imaging. Panels show (A) virus only, (B) virus incubated with DN57opt, (C) virus incubated with 1OAN1. Scale bars indicate 100 nm.
doi:10.1371/journal.pntd.0000721.g004

hemagglutination inhibition assays, but were unable to detect any inhibition of the ability of viral antigen to agglutinate red blood cells (data not shown). To further investigate virus:cell binding in a more relevant system, we treated virus with DN57opt or 1OAN1, bound the virus to cells, and washed the cells repeatedly at 4°C before measuring the amount of virus remaining on the cells by quantitative rt-PCR. Both peptides showed evidence of ability to block virus:cell binding compared to control virus without peptide (Figure 7). Treatment of virus with pooled human anti-dengue serum or heparan sulfate similarly showed reduced cell binding.

Discussion

We have used computational methods to design multiple peptide inhibitors of the DENV E glycoprotein. Importantly, out of seven peptides synthesized and tested, two peptides with high activity and one peptide with intermediate activity were identified. A high resolution crystal structure of the pre-fusion conformation of the DENV-2 E [14] was used as the starting point to generate *in situ* energy minimized peptides. Two distinct approaches were used for the design of these peptides. First, we built upon previous work targeting DENV fusion peptide and domain II hinge regions with naturally occurring E protein sequences from these regions [9]. No inhibitory activity was found for the optimized fusion peptide region sequence (DN80opt), indicating that this region may not be a promising target mechanistically for DENV peptide inhibitors. Since an analogous, naturally occurring WNV domain II hinge region peptide was shown to be inhibitory against WNV [9], we reasoned that a more tightly binding analog of this region in the DENV E protein could be designed and might have

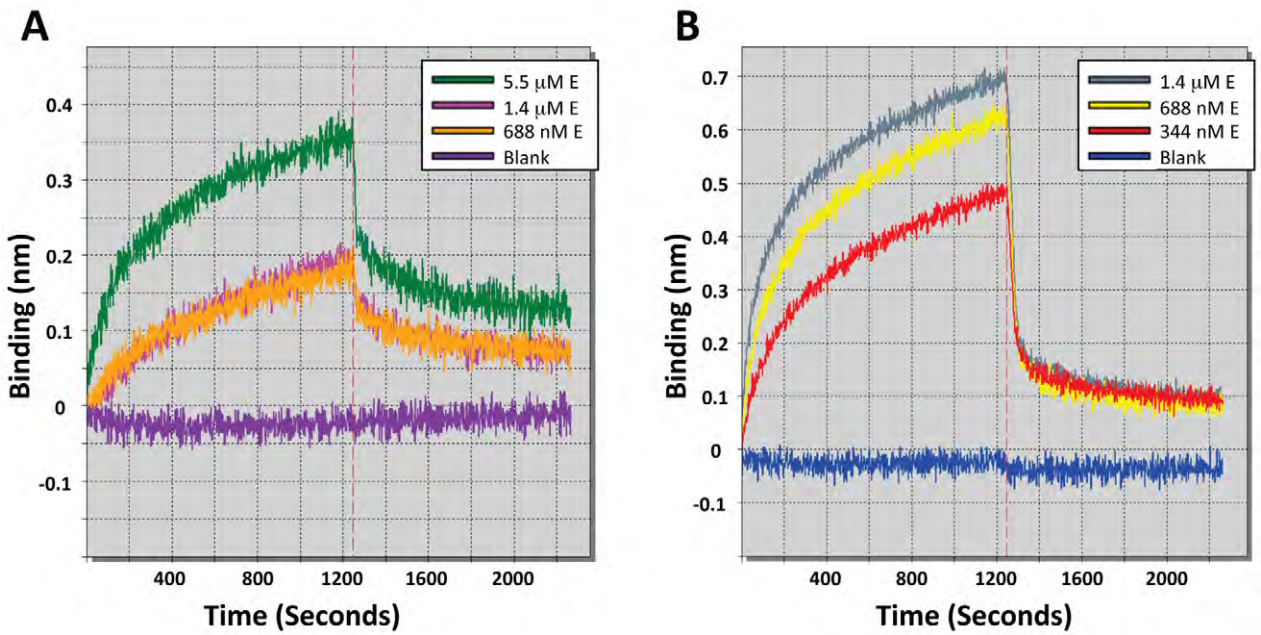

Figure 5. Peptide:E protein binding assay. Biolayer interferometry was used to assay the binding of the peptides to truncated E Protein. The association and dissociation of increasing concentrations of truncated E protein to peptides DN57opt (A) and 1OAN1 (B) are shown. A buffer blank (PBS, 0.02% Tween-20, 0.1% BSA) containing no E protein was run for each peptide. The affinity of the peptides for the truncated E protein was calculated (DN57opt $K_D = 1.2\times10^{-6}\pm0.6\times10^{-6}$ M (mean±sd), 1OAN1 $K_D = 4.5\times10^{-7}\pm2.0\times10^{-7}$ M).
doi:10.1371/journal.pntd.0000721.g005

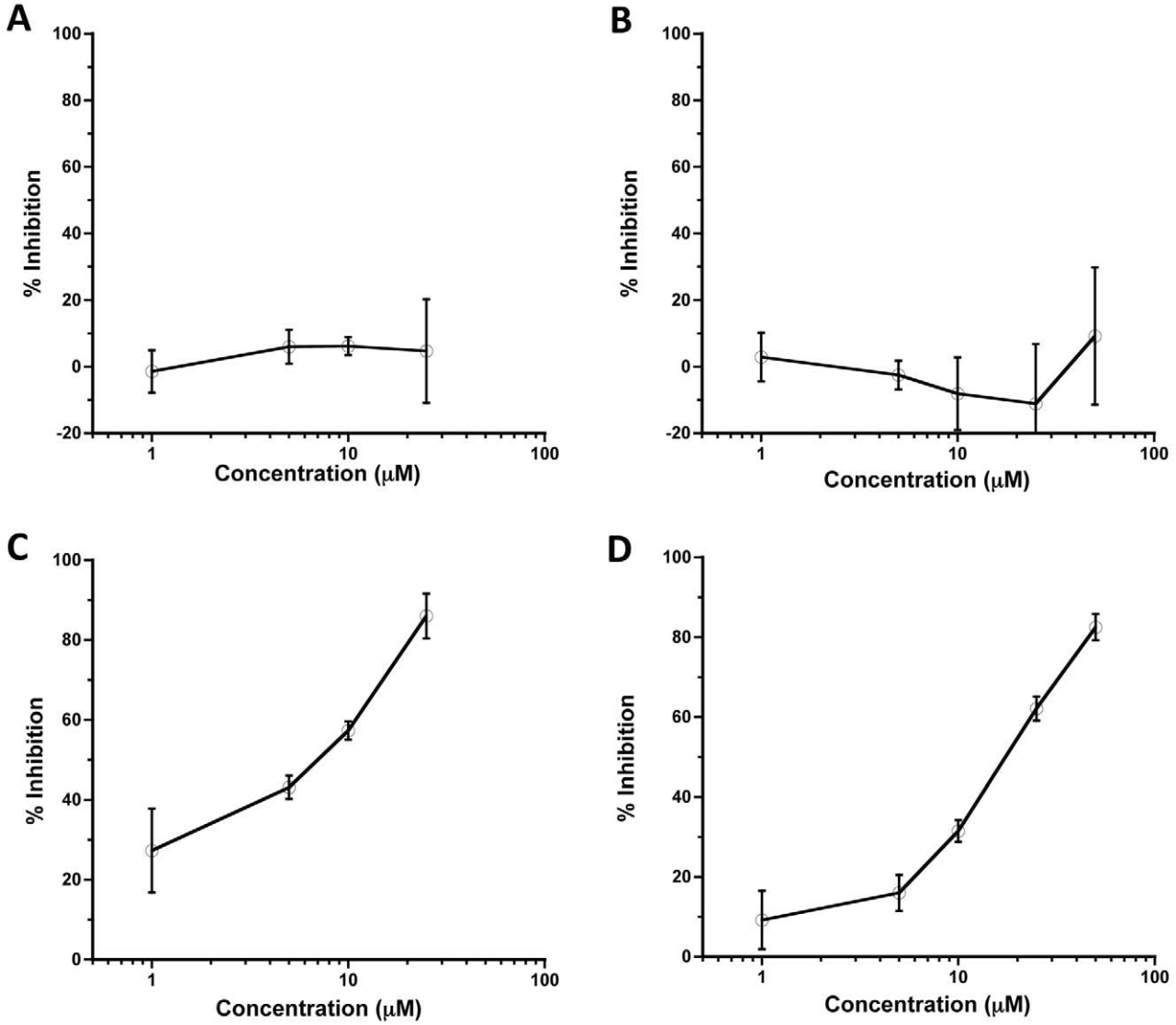

Figure 6. Post-infection and post-binding peptide treatments. Treatment of cells with increasing concentrations of (A) DN57opt and (B) 1OAN1 after DENV-2 has infected cells shows no significant inhibition. Treatment with (C) DN57opt or (D) 1OAN1 after DENV-2 has bound to LLCMK-2 cells at 4°C for one hour inhibits infection. Error bars are ±sem.
doi:10.1371/journal.pntd.0000721.g006

improved inhibitory activity. This turned out to be correct, and we identified two distinct binding-optimized peptide sequences to this region with antiviral activity, DN57opt and DN81opt. This supports previous predictions of hinge region inhibitors and the proposed mechanism of fusion based on hinge region movements [11,14,15]. The second approach to designing peptide inhibitors was to identify peptides with non-native sequences derived from E protein regions that are highly stable in terms of structure and binding as evaluated by an all-atom scoring function (RAPDF). This identified four regions that were used to derive additional optimized peptides (Figure 1). Of the four resulting peptides tested, one, 1OAN1, was identified as having antiviral activity. This confirms the use of the sliding window RAPDF minimization approach for finding tightly binding protein ligands [23,24]. It is perhaps not surprising that computational binding optimization increased the activity of previously inactive peptides that were based on naturally occurring E protein sequences. Naturally occurring sequences have multiple balancing selection pressures that may limit their binding stability *in vivo*. The combined use of primary sequence prediction tools [9] and structural optimization tools [23,24] should be a valuable approach for finding binding partners and inhibitors for other protein targets.

Neither peptide showed inhibitory activity when added directly to cells after infection had already occurred, indicating that the peptides were acting during an entry step in the virus life cycle, and sequence scrambled versions of the two most active peptides were inactive, confirming sequence specific activity. Both peptides also block virus:cell binding, but are still capable of inhibiting infection even when added after virions have already bound to the surface of target cells.

CryoEM was used to visualize the effect of the peptides on DENV-2 virions. The surface of virions appeared to change from smooth to rough after incubation with the antiviral peptides. This suggests that there may be an alteration of the arrangement of the surface envelope protein (Figure 4). Biolayer interferometry was used to measure the kinetics of binding between the peptides and

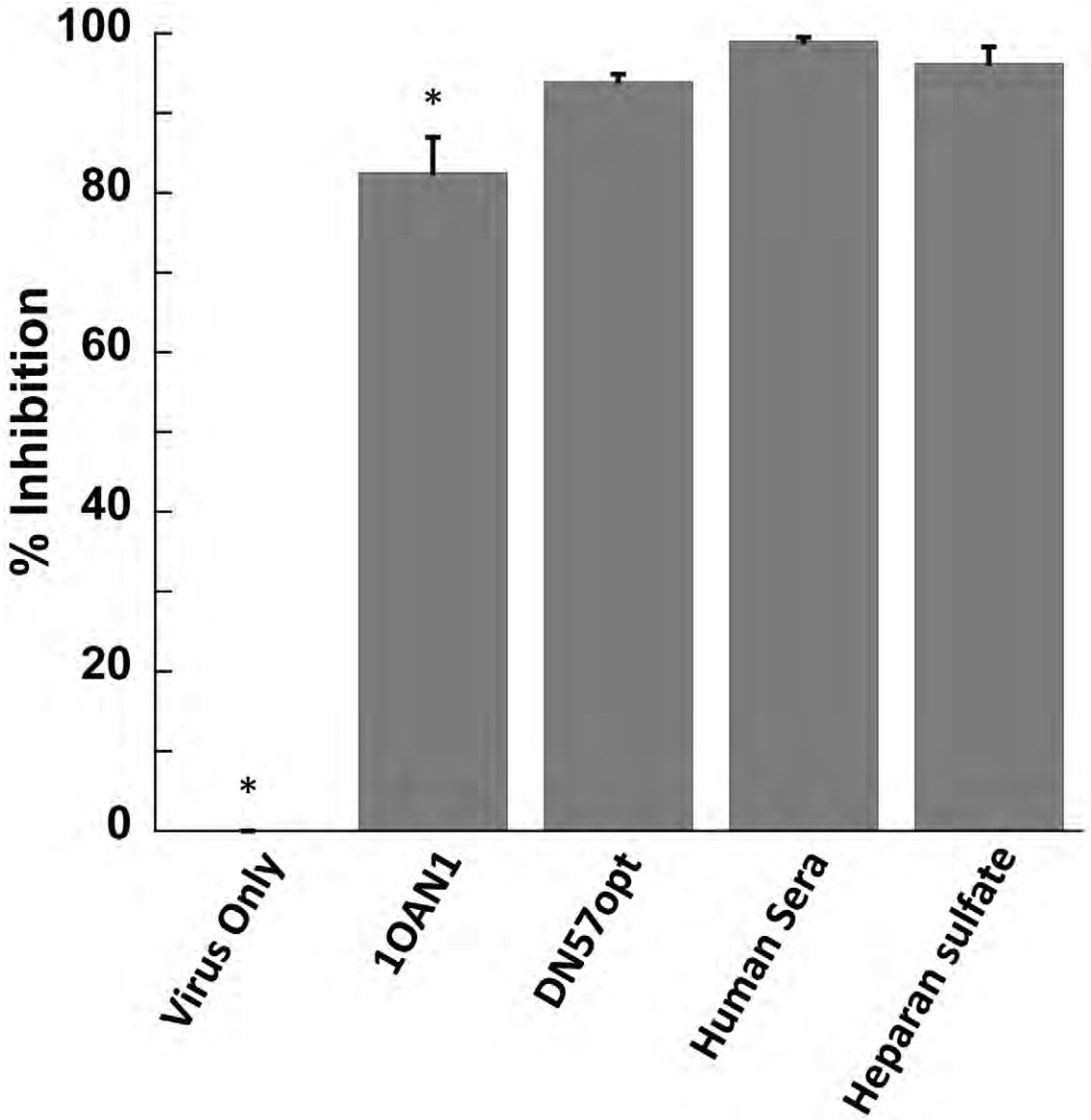

Figure 7. Quantitative reverse transcriptase PCR virus:cell binding. Virus pre-incubated with either DN57opt or 1OAN1 shows reduced binding to cells compared to control virus without peptide. Pre-incubation of virus with pooled human anti-dengue serum or heparan sulfate similarly shows reduced cell binding. * Indicates a significant difference ($p<0.05$) from all others by 1-way ANOVA followed by Tukey's posthoc test.
doi:10.1371/journal.pntd.0000721.g007

soluble, truncated E protein (Figure 5). These binding studies showed a direct interaction between the peptides and DENV-2 E protein with affinities in the 1 μM range and relatively fast on/off rates. The cryoEM images demonstrate that these inhibitory peptides probably cause structural deformations in intact viral particles, but do not provide information about the kinetics of these changes. It is possible that the peptides trap the viral E proteins in some conformation that is part of the normal breathing of the viral particles, and that this interferes with cell binding and entry.

The DN57opt and 1OAN1 peptides were designed for optimized binding to the pre-fusion E structure and we show direct evidence for this interaction, both with the purified, monomeric E protein, and with virion particles. These peptides likely function by displacing portions of the E protein and interfering with normal cell binding or the structural changes during entry. Although separate in the primary protein sequence, the regions targeted in the design the DN57 and 1OAN1 peptides are partially adjacent to each other in the crystal structure, with the C terminus of the 1OAN1 region occupying a pocket surrounded by the DN57 region (See Figure 1). We stress that we do not know the structures of the bound and inhibited peptide/E protein complexes, but these structures may shed light on the mechanistic details of cell binding and fusion. Taken together, our results support the hypothesis that both of these peptides interact directly with DENV-2 E proteins and are entry inhibitors.

Despite difficulties with oral administration and degradation in the digestive tract, peptides may make useful antiviral agents when targeted against viral envelope proteins. Directing inhibitors to viral surface proteins avoids the major difficulty of crossing cellular membranes in order to reach the target. For example, peptide inhibitors of intercellular viral targets, such as proteases or polymerases, would need to cross the cell plasma membrane, and in the case of flaviviruses, possibly internal membrane bound

replication and assembly compartments. The HIV entry inhibitor T-20 (Fuzeon) is a peptide, and in the context of a chronic infection, repeated life-long injections are problematic. DENV is an acute infection and most severe DENV infections require intravenous fluid support, facilitating delivery of anti-DENV peptides by this route.

We have established the existence of multiple, distinct inhibitory peptides targeting the DENV E glycoprotein and confirmed the utility of rational design using structural data for developing DENV E protein inhibitors. Applications of this strategy should also be possible for the generation and refinement of lead compounds for other viral envelope fusion proteins. It would be optimistic to propose that any single antiviral would provide an effective treatment for DENV given the enormous genetic variability of the four serotypes and multiple substrains. Different classes of inhibitors targeting the E protein and other DENV targets [44,45], could form the basis for the development of a combination treatment plan to combat this disease.

Supporting Information

Alternative Language Abstract S1 Translation of the abstract into Thai by Ekachai Jenwitheesuk.
Found at: doi:10.1371/journal.pntd.0000721.s001 (0.03 MB DOC)

Alternative Language Abstract S2 Translation of the abstract into Spanish by Sharon Isern.
Found at: doi:10.1371/journal.pntd.0000721.s002 (0.04 MB DOC)

Author Contributions

Conceived and designed the experiments: JMC EJ SI RS SFM. Performed the experiments: JMC EJ SML EH KAC KAF CRR. Analyzed the data: JMC EJ SML KAF MGR SI RS SFM. Contributed reagents/materials/analysis tools: JMC EJ SML MGR SI RS SFM. Wrote the paper: JMC SFM.

References

1. Chernomordik LV, Kozlov MM (2008) Mechanics of membrane fusion. Nat Struct Mol Biol 15: 675–683.
2. Sainz B, Jr., Rausch JM, Gallaher WR, Garry RF, Wimley WC (2005) The aromatic domain of the coronavirus class I viral fusion protein induces membrane permeabilization: putative role during viral entry. Biochemistry 44: 947–958.
3. Harrison SC (2008) Viral membrane fusion. Nat Struct Mol Biol 15: 690–698.
4. Garry RF, Dash S (2003) Proteomics computational analyses suggest that hepatitis C virus E1 and pestivirus E2 envelope glycoproteins are truncated class II fusion proteins. Virology 307: 255–265.
5. Qureshi NM, Coy DH, Garry RF, Henderson LA (1990) Characterization of a putative cellular receptor for HIV-1 transmembrane glycoprotein using synthetic peptides. Aids 4: 553–558.
6. Wild C, Dubay JW, Greenwell T, Baird T, Jr., Oas TG, et al. (1994) Propensity for a leucine zipper-like domain of human immunodeficiency virus type 1 gp41 to form oligomers correlates with a role in virus-induced fusion rather than assembly of the glycoprotein complex. Proc Natl Acad Sci U S A 91: 12676–12680.
7. Wild C, Greenwell T, Matthews T (1993) A synthetic peptide from HIV-1 gp41 is a potent inhibitor of virus-mediated cell-cell fusion. AIDS Res Hum Retroviruses 9: 1051–1053.
8. Bai F, Town T, Pradhan D, Cox J, Ashish, et al. (2007) Antiviral peptides targeting the west nile virus envelope protein. J Virol 81: 2047–2055.
9. Hrobowski YM, Garry RF, Michael SF (2005) Peptide inhibitors of dengue virus and West Nile virus infectivity. Virol J 2: 49.
10. Rees CR, Costin JM, Fink RC, McMichael M, Fontaine KA, et al. (2008) In vitro inhibition of dengue virus entry by p-sulfoxy-cinnamic acid and structurally related combinatorial chemistries. Antiviral Res.
11. Bressanelli S, Stiasny K, Allison SL, Stura EA, Duquerroy S, et al. (2004) Structure of a flavivirus envelope glycoprotein in its low-pH-induced membrane fusion conformation. Embo J 23: 728–738.
12. Heinz FX, Mandl CW, Holzmann H, Kunz C, Harris BA, et al. (1991) The flavivirus envelope protein E: isolation of a soluble form from tick-borne encephalitis virus and its crystallization. J Virol 65: 5579–5583.
13. Kanai R, Kar K, Anthony K, Gould LH, Ledizet M, et al. (2006) Crystal structure of west nile virus envelope glycoprotein reveals viral surface epitopes. J Virol 80: 11000–11008.
14. Modis Y, Ogata S, Clements D, Harrison SC (2003) A ligand-binding pocket in the dengue virus envelope glycoprotein. Proc Natl Acad Sci U S A 100: 6986–6991.
15. Modis Y, Ogata S, Clements D, Harrison SC (2004) Structure of the dengue virus envelope protein after membrane fusion. Nature 427: 313–319.
16. Modis Y, Ogata S, Clements D, Harrison SC (2005) Variable surface epitopes in the crystal structure of dengue virus type 3 envelope glycoprotein. J Virol 79: 1223–1231.
17. Huang KC, Lee MC, Wu CW, Huang KJ, Lei HY, et al. (2008) Solution structure and neutralizing antibody binding studies of domain III of the dengue-2 virus envelope protein. Proteins 70: 1116–1119.
18. Nybakken GE, Nelson CA, Chen BR, Diamond MS, Fremont DH (2006) Crystal structure of the West Nile virus envelope glycoprotein. J Virol 80: 11467–11474.
19. Rey FA, Heinz FX, Mandl C, Kunz C, Harrison SC (1995) The envelope glycoprotein from tick-borne encephalitis virus at 2 A resolution. Nature 375: 291–298.
20. Volk DE, Lee YC, Li X, Thiviyanathan V, Gromowski GD, et al. (2007) Solution structure of the envelope protein domain III of dengue-4 virus. Virology 364: 147–154.
21. Yu S, Wuu A, Basu R, Holbrook MR, Barrett AD, et al. (2004) Solution structure and structural dynamics of envelope protein domain III of mosquito- and tick-borne flaviviruses. Biochemistry 43: 9168–9176.
22. Zhang Y, Zhang W, Ogata S, Clements D, Strauss JH, et al. (2004) Conformational changes of the flavivirus E glycoprotein. Structure 12: 1607–1618.
23. Huang E, Samudrala R, Park B (2000) Scoring functions for ab initio folding. In: Walker J WD, ed. Predicting Protein Structure: Methods and Protocols: Humana Press.
24. Samudrala R, Moult J (1998) An all-atom distance-dependent conditional probability discriminatory function for protein structure prediction. J Mol Biol 275: 895–916.
25. CDCDVBID (2008) Dengue Fever http://www.cdc.gov/ncidod/dvbid/dengue/index.htm. Centers for Disease Control Division of Vector-Borne Infectious Disease.
26. WHO (2008) Dengue http://www.who.int/topics/dengue/en/. World Health Organization (WHO).
27. Halstead SB (1988) Pathogenesis of dengue: challenges to molecular biology. Science 239: 476–481.
28. Mackenzie JS, Gubler DJ, Petersen LR (2004) Emerging flaviviruses: the spread and resurgence of Japanese encephalitis, West Nile and dengue viruses. Nat Med 10: S98–109.
29. Halstead SB (2003) Neutralization and antibody-dependent enhancement of dengue viruses. In: Chambers TJ, Monath T P, eds. The flaviviruses: pathogenesis and immunity.
30. Kliks SC, Nisalak A, Brandt WE, Wahl L, Burke DS (1989) Antibody-dependent enhancement of dengue virus growth in human monocytes as a risk factor for dengue hemorrhagic fever. Am J Trop Med Hyg 40: 444–451.
31. Halstead SB, O'Rourke EJ (1977) Antibody-enhanced dengue virus infection in primate leukocytes. Nature 265: 739–741.
32. Morens DM, Halstead SB (1990) Measurement of antibody-dependent infection enhancement of four dengue virus serotypes by monoclonal and polyclonal antibodies. J Gen Virol 71 (Pt 12): 2909–2914.
33. Burke DS, Kliks S (2006) Antibody-dependent enhancement in dengue virus infections. J Infect Dis 193: 601–603; author reply 603-604.
34. Bower MJ, Cohen FE, Dunbrack RL, Jr. (1997) Prediction of protein side-chain rotamers from a backbone-dependent rotamer library: a new homology modeling tool. J Mol Biol 267: 1268–1282.
35. Levitt M (1974) Energy refinement of hen egg-white lysozyme. J Mol Biol 82: 393–420.
36. Levitt M (1983) Molecular dynamics of native protein. I. Computer simulation of trajectories. J Mol Biol 168: 595–617.
37. Levitt M, Lifson S (1969) Refinement of protein conformations using a macromolecular energy minimization procedure. J Mol Biol 46: 269–279.
38. Metropolis N, Rosenbluth AW, Rosenbluth MN, Teller AH (1953) Equation of state calculations by fast computing machine. Journal of Chemical Physics 21: 1087–1092.
39. Clarke DH, Casals J (1958) Techniques for hemagglutination and hemagglutination-inhibition with arthropod-borne viruses. Am J Trop Med Hyg 7: 561–573.
40. Thaisomboonsuk BK, Clayson ET, Pantuwatana S, Vaughn DW, Endy TP (2005) Characterization of dengue-2 virus binding to surfaces of mammalian and insect cells. Am J Trop Med Hyg 72: 375–383.
41. Chutinimitkul S, Payungporn S, Theamboonlers A, Poovorawan Y (2005) Dengue typing assay based on real-time PCR using SYBR Green I. J Virol Methods 129: 8–15.

42. Lok SM, Kostyuchenko V, Nybakken GE, Holdaway HA, Battisti AJ, et al. (2008) Binding of a neutralizing antibody to dengue virus alters the arrangement of surface glycoproteins. Nat Struct Mol Biol 15: 312–317.
43. Schieffelin JS, Costin JM, Nicholson CO, Orgeron NM, Fontaine KA, et al. Neutralizing and non-neutralizing monoclonal antibodies against dengue virus E protein derived from a naturally infected patient. Virol J 7: 28.
44. Whitby K, Pierson TC, Geiss B, Lane K, Engle M, et al. (2005) Castanospermine, a potent inhibitor of dengue virus infection in vitro and in vivo. J Virol 79: 8698–8706.
45. Ganesh VK, Muller N, Judge K, Luan CH, Padmanabhan R, et al. (2005) Identification and characterization of nonsubstrate based inhibitors of the essential dengue and West Nile virus proteases. Bioorg Med Chem 13: 257–264.
46. Stiasny K, Kossl C, Heinz FX (2005) Differences in the postfusion conformations of full-length and truncated class II fusion protein E of tick-borne encephalitis virus. J Virol 79: 6511–6515.

APPENDIX B

Photochemistry and Photobiology, 2011, 87: 1184–1188

Research Note

A Screening Technique Useful for Testing the Effectiveness of Novel ''Self-Cleaning'' Photocatalytic Surfaces

Shane T. Finn[1,2], Jessica A. Strnad[1,2], Patricia D. Barreto[1,2], Megan E. Fox[1,2], Jorge Torres[2,3], James D. Sweeney[2,3] and José C. Barreto*[1,2]

[1]Department of Chemistry, Florida Gulf Coast University, Fort Myers, FL
[2]Green Technology Research Group, Florida Gulf Coast University, Fort Myers, FL
[3]Department of Bioengineering, Florida Gulf Coast University, Fort Myers, FL

Received 1 April 2011, accepted 30 May 2011, DOI: 10.1111/j.1751-1097.2011.00953.x

ABSTRACT

We describe a screening methodology that can be used to quickly determine the effectiveness of newly synthesized photocatalysts. We were particularly interested in measuring the destruction of organic molecules painted onto a photocatalytic surface by spraying, with destruction proceeding in ambient air (as a model for airborne toxin destruction). Our method can utilize photocatalysts that are synthesized as powders (such as doped and undoped titanium oxide) and which are then calcined onto a glass substrate disk at 600°C. Herein, we used UV illumination of Aeroxide P-25 TiO_2, but the method is general and can accommodate any region of the light spectrum.

INTRODUCTION

Upon illumination with UV light, photocatalytic surfaces generate destructive radicals, oxidants and reductants (ROR) that are useful for molecular destruction and decontamination processes. A UV photon contains sufficient energy to promote an electron into the conduction band of titanium oxide (TiO_2), a process which generates an oxidizing positive ''hole'' on the surface of the material, while the ejected electrons create radicals and reductants. Recent reviews are available which describe the photocatalytic process in detail (1,2). Given the destructive mechanism just described, UV illuminated TiO_2 constitutes a ''self-cleaning surface'' that can destroy organic molecular targets adsorbed onto the TiO_2 surface in ambient air. There is great interest in developing new photocatalytic materials that are more effective in producing ROR because these novel materials have broad application for germicidal and decontaminating technologies (see, for example, [3]). Adsorption to the surface occurs with both hydrophobic and hydrophilic organic molecules because UV activated TiO_2 is amphiphilic; wherein discreet hydrophobic and hydrophilic sites are scattered on the photocatalytic surface (4). Certain other metal oxides and sulfides such as ZnO (5) and CdS (6) also possess photocatalytic activity. ''Doped'' TiO_2 with carbon, nitrogen and metal dopants have been reported, all with claims for improved activity in the UV (and sometimes, in the visible region of the electromagnetic spectrum [7]). Our group is then one of many engaged in developing new and more effective self-cleaning photocatalytic materials.

Herein, we report a rapid, high throughput, screening process for studying the effectiveness of novel photocatalytic materials and ranking their effectiveness as decontaminating surfaces, specifically in the context of destroying model toxin molecules which might be adsorbed onto the surface in ambient air. This method consists of depositing a uniform layer of TiO_2 powder onto a 12 mm glass disk (a readily available, inexpensive, glass microscope cover slip) by spraying the photocatalytic powder in a methanolic suspension onto the disk with a small pneumatic airbrush. The powder is then calcined onto the disk by heating it in a muffle furnace, a process that helps adhere the powdered photocatalyst to the glass substrate. We have a particular interest in hydrophobic toxin destruction, so we have airbrushed hydrophobic Sudan, dissolved in toluene, onto bright white photocatalyst disks to produce then bright red disks. Placing a red disk under a UV lamp causes photocatalytic bleaching of the dye, whereas the Sudan red IV (hereafter referred to as Sudan) alone is otherwise very impervious to UV illumination. We have measured the reflectance of such surface coatings before and after photocatalytic bleaching in order to obtain the rate of dye destruction. Using our system, we then rank given compositions of photocatalysts with regard to effectiveness in destroying a particular surface target. Notably, the procedure we describe herein is not limited to any particular dye so a multitude of dyes constituting different hydrophobic and hydrophilic targets can be sprayed and photocatalytically bleached, in order to obtain an overall picture of photocatalytic effectiveness. For the sake of brevity, this report has been limited to one case, a description of Sudan photocatalytic bleaching using Aeroxide P-25 TiO_2.

Dyes are colored due to conjugation of a continuous single-double-single pi bond system, (R—C=C—C=C—R). Breaking the conjugation of a dye at any point with a redox reaction, regardless of the oxidant or reductant, typically decreases the extent of conjugation, and usually shifts the wavelength of

*Corresponding author email: jbarreto@fgcu.edu (José C. Barreto)

maximum absorbance into the UV region. This effectively bleaches the dye; one recent demonstration is carotenoid dye bleaching caused by peroxidation of pi bonds (8). Dye destruction is therefore achieved upon the breaking of any bond in the pi system of conjugation. There are a multitude of reports which use dyes and photocatalysts in aqueous solutions (9,10), but our technique is directed toward surface destruction of dyes at an air interface (not in solution) and uses key modifications to existing approaches, resulting in a high-throughput system for both sample and substrate production as well as testing and characterization: glass disks as substrates, sprayed coatings and dyes, with consistent UV illumination of many samples. The resulting data can be used to quickly screen the effectiveness of photocatalysts, and investigate photocatalytic mechanisms as new material compositions are proposed and synthesized.

MATERIALS AND METHODS

Procedure. Coating the photocatalyst onto the glass disk surface: A suspension of 10 mg mL^{-1} TiO_2 (Evonik Aeroxide P-25) in methanol was vortexed for several minutes and the homogenous TiO_2/methanol suspension was placed in an airbrush sprayer (Central Pneumatic Model 93657). Ten, 12 mm glass disks (Fisher) were taped down to a plastic substrate and the TiO_2/methanol suspension was sprayed onto the disks using 40 psi air pressure (with constant airbrush agitation). The airbrush tip was held *ca* 6 inches from the surface of the disks which were then coated with *ca* 10 passes of the airbrush, with 1 min drying interval between spray passes, until a thin, uniform TiO_2 coating was visible. The disks were then placed in a glass Petri dish and calcined in a muffle furnace (Barnstead/Thermolyne Model 47900) at 600°C for 1 h.

Spraying the dye: 3.0 mg mL^{-1} Sudan (Fisher) dissolved in toluene was sprayed (using one pass of the air brush @ ~50 psi) to paint the TiO_2 surface until a red color intensity was achieved which results in a reflectance ratio of *ca* 0.25–0.45 (unpainted disks have ratios of *ca* 0.8).

Uncoated glass fiber control disks: Glass fiber disks (Fisher) have been used as uncoated control surfaces (*i.e.* no TiO_2 coatings applied) for experiments demonstrating the lack of UV bleaching of Sudan painted onto a nonphotocatalytic surface.

Conducting photocatalysis: The photocatalytic painted (and non-photocatalytic painted control) disks were placed in a 24 well plate and illuminated directly under a 48 inch long UV Lamp (Eliminator® Lighting Model E124 T8 UV Tube 40 W) emitting 1.9 mW cm^{-2} intensity on a sample placed 1.7 cm from the lamp face. Nonilluminated controls were also run for comparison.

Reading the reflectance: Reflectance measurements were made using a Shimadzu UV-2450 UV–Vis spectrophotometer with a specular reflectance attachment. Both reference and sample stages were fitted with a 9.525 mm aperture. Surfaces to be scanned were centered, face-down, over the sample stage aperture. Percent reflectance (%*R*) of each disk was scanned from 800 to 400 nm using a "medium" scan speed, 1.0 nm sampling interval and 2.0 nm slit width.

RESULTS AND DISCUSSION

High-throughput production of test disks

Initially, we attempted a "dripping" method for coating TiO_2 onto glass disks, but this approach led to nonuniform coatings of the glass disks producing ridges and variations in TiO_2 coating thickness (Fig. 1). The dripping method thus resulted in artifacts in photocatalytic kinetics and reflectance measurements and was abandoned. "Dipping" the whole disk for coating constituted an improvement, but coatings made this way were also not sufficiently uniform (data not shown). Both "dripping" and "dipping" are time consuming methods and require significant practice in order to generate many disks of similar appearance and coating thickness. By comparison, we discovered that spraying with a small pneumatic airbrush produced coatings of better uniformity and thickness (also shown in Fig. 1) and was more amenable to high-throughput production of many similar coated disks. Uniform coating with TiO_2 and painting of a dye coating are highly desirable because nonuniformity of the coating produces light scattering. Variability in coloration causes differential light absorption in different locations on each disk.

Photocatalysis of Sudan

Figure 2 shows the self-cleaning properties of a sample photocatalytic surface. When the Sudan dye was painted by airbrushing onto a TiO_2 coating, a red uniform color was achieved. Illuminating these red disks with UV light from a medium pressure mercury arc lamp (emitting primarily at 365 nm with some shorter wavelengths present as a minor emission) engendered destruction of the Sudan with greater fading of the red color with increased UV illumination time. Prolonged illumination (2 h) engendered almost complete photocatalytic destruction and the color of the illuminated red disks returned to almost pure white (the slight blue tint of the coated and unpainted disks, and the UV bleached coated and painted disks, in Fig. 2 is an optical artifact due to the necessity of photographing the translucent coated surfaces on a dark background). Notably, glass fiber (nonphotocatalytic

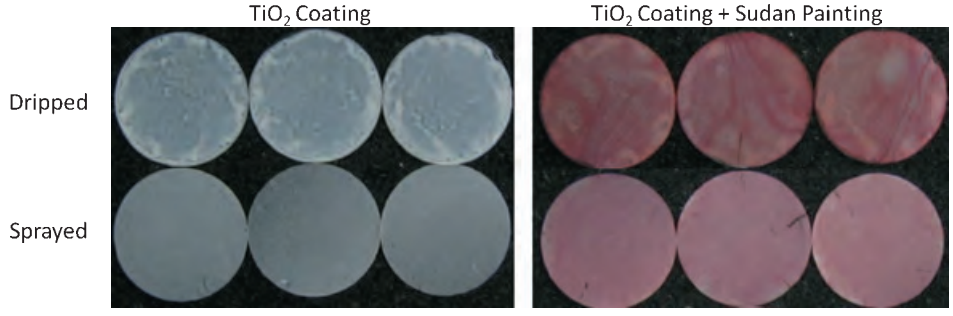

Figure 1. The top left row of disks were coated by dripping and evaporating a methanolic TiO_2 suspension onto the disk and the bottom left row of disks were coated by spraying the TiO_2 suspension with an airbrush; spraying clearly yields better uniformity when making TiO_2 coatings. The top right row shows drip-coated, drip-painted disks which are much less uniform in coating and coloration than spray-coated, spray-painted disks (bottom row).

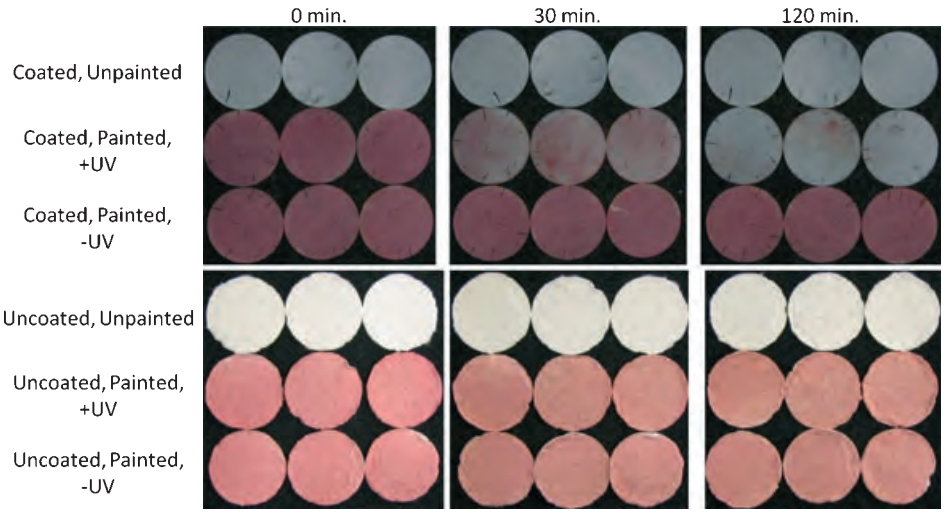

Figure 2. The effect of illuminating Sudan IV with UV atop TiO_2 (coated) and glass fiber (uncoated) surfaces. Unpainted disks are shown in the first and fourth rows as controls. The second and fifth rows show Sudan-painted disks exposed to UV: significant bleaching is observed on painted and coated disks after 30 min and is nearly complete after 2 h. The third and sixth rows show dark controls (−UV); note that painted disks do not bleach in ambient laboratory conditions and uncoated, painted disks do not bleach under UV light.

controls) appear white in Fig. 2 because they are not translucent. To the naked eye all these disks appear white. Note also from Fig. 2 that when we painted Sudan onto white glass fiber disks as a control (*i.e.* these disks contained no photocatalytic coating), no significant fading of the Sudan was noted under these conditions at the relevant times, thus confirming that a photocatalytic substrate is needed in order to generate ROR for destruction of the dye coating. To clarify, the Sudan dye is very resistant to UV photolysis both as a solid on a surface, and in a micellar detergent solution (data not shown). This makes it an excellent model target for the investigation of photocatalysis since no confounding UV photobleaching event is engendered by UV illumination alone.

Reflectance measurements. Figure 3 shows a surface scan of the Sudan dye which has been painted onto a photocatalytic surface by airbrushing. The painted red surface clearly has an optical reflectance spectrum that is very different from the unpainted surface. We investigated the possibility that surface scans of the red surface could be used to rapidly quantify dye destruction and obtain the kinetics of the destruction. Figure 4 shows the kinetics of Sudan destruction painted onto TiO_2 coated disks, as well as the expected lack of dye destruction on control uncoated glass fiber disks both with and without UV exposure. In our approach, we have used the ratio of absorbance at two different wavelengths in order to remove any artifacts in the "reflectance baseline" from otherwise identical coatings. The reflectance baseline of different coatings varies slightly, probably due to small differences in roughness (even with the smoother airbrushed coatings), slight scratches of the surface and/or minor position adjustment between readings. It is also important for users of our methodology to practice the techniques for disk coating, and for dye painting, in order to insure sufficient uniformity between samples. Figure 4 clearly shows how useful our procedure is for quickly screening the self-cleaning effectiveness of different photocatalytic coatings. The standard deviation bars seen in the figure constitute an acceptable variation

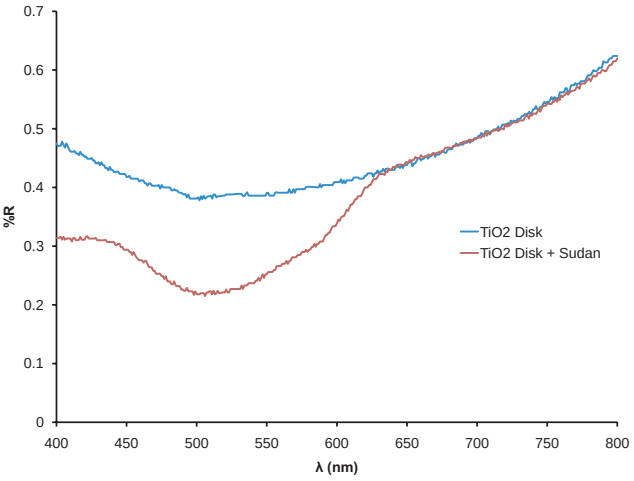

Figure 3. This plot shows percent reflectance (%R) *vs* wavelength for one typical TiO_2-coated disk before and after painting with Sudan. The %R spectrum of the Sudan-painted disk deviates from that of the unpainted disk from 400 to 630 nm, but is roughly the same from 630 to 800 nm. The minimum %R value of the painted disk was measured at 512 nm, which is near the λ_{max} of Sudan.

between identical trials. While using our procedures in an air-conditioned laboratory environment should stablilize well-known variables for photocatalytic effect on TiO_2 surfaces, such as ambient humidity, UV exposure of samples could if desired be carried out in a humidity-controlled chamber.

One final important approach we have incorporated into our system is the use of a very long, standard, inexpensive 48 inch mercury lamp. We have measured the intensity of this lamp along its length and confirmed that it was extremely uniform except within 6 inches of each end. Use of this lamp allows us to illuminate 42 disks at one time. We place the disks in a 24 well plate which established a uniform distance between the disks as well as a uniform distance from the lamp to each disk. The results are then very reproducible (*e.g.* see the standard deviation bars for the data in Fig. 4).

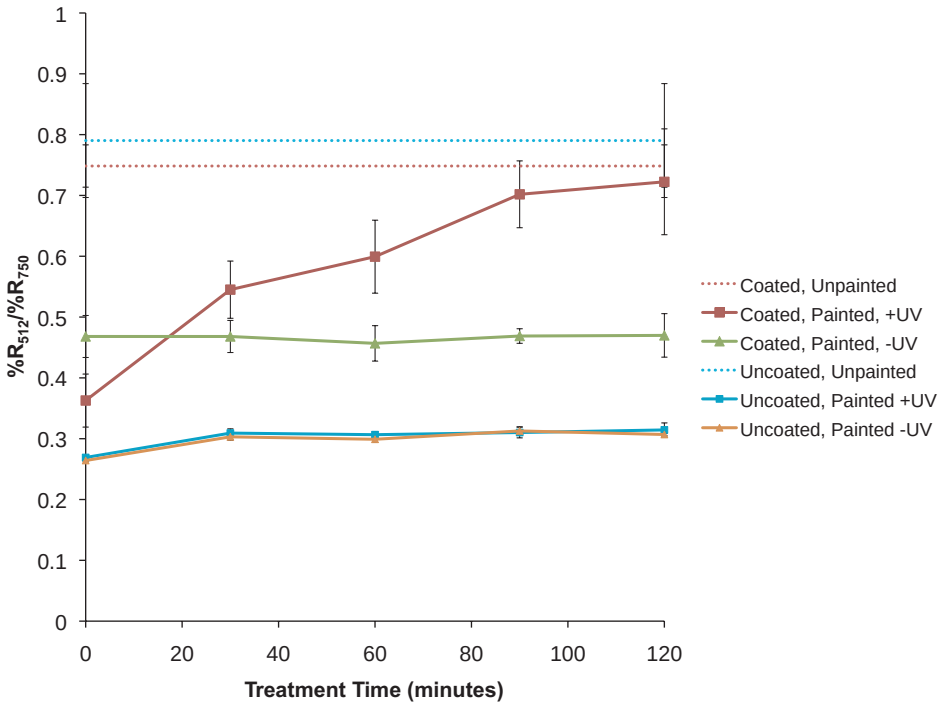

Figure 4. For each disk, the $\%R$ value at 512 nm was divided by $\%R$ at 750 nm ($\%R_{512nm}/\%R_{750nm}$); this is a normalization step that eliminates errors resulting from baseline variation in the reflectance scans. Our plot of $\%R_{512nm}/\%R_{750nm}$ *vs* treatment time shows the kinetics of photocatalytic bleaching with appropriate controls (unpainted and painted, coated and uncoated disks, +UV and −UV groups). The dotted lines show the ratio value of the coated and uncoated treatment groups before painting and the red squares show that the ratio values of the Sudan-painted disks increase during UV illumination (+UV) from the "Painted" value toward the "Unpainted" value. The +UV treatment group is expected to achieve its "Unpainted" value when photocatalytic bleaching is 100% complete. Standard deviations (N = 3 trials) show good reproducibility for the method.

SUMMARY OF OVERALL ADVANTAGES OF APPROACH

Taken as a whole, our methodology for investigating molecular destruction on photocatalytic surfaces in ambient air contains a series of important advantages: The glass cover slips we used were an excellent inert substrate for supporting a photocatalytic coating. These glass disks are inexpensive, easily procured and impervious to the high heat needed to calcine photocatalytic coatings onto the glass. While we have found that calcining helps to adhere the photocatalytic powder to the glass, our coatings do remain somewhat susceptible to scratching but much less so when compared to TiO_2 surfaces that have not been calcined. The "long lamp" illumination method we used enabled us to photocatalyze many samples at once with the same UV intensity under identical ambient conditions. Sudan dye bleaching does not occur in the absence of photocatalyst, so during the time intervals described no interference from UV photolysis alone was encountered.

Figure 1 illustrates the effectiveness of airbrushing in creating smooth, uniform TiO_2 coatings on 12 mm glass cover slips. Spraying the coating and dye has proven to be a quick and superior method for uniformly coating and painting the surfaces, and has enabled high-throughput production of many identical disks. Optical artifacts are also minimized when using the spraying technique. By comparison, scanning the disk surfaces has revealed significant differences between painted and unpainted disks (Fig. 3). Lastly, our quantitative reflectance "ratio" method for determining the extent and kinetics of photobleaching has proven to be successful in measuring the degree and kinetics of Sudan (a model hydrophobic toxin) destruction. We recommend that a standard photocatalytic control surface, such as Evonik Aeroxide P-25, be carried into experiments using our screening method so that novel photocatalysts can be compared against a known reference.

Acknowledgements—This work has been supported in part by defense grants from DOD as a subproject in the Florida Biodefense Research consortium (Grant 6415-1012-66-A) and (Grant HDTRA1-10-1-0009). Aeroxide P-25 TiO_2 was a generous gift from Evonik.

REFERENCES

1. Lu, S. Y., D. Wu, Q. L. Wang, J. H. Yan, A. G. Buekens and K. F. Cen (2011) Photocatalytic decomposition on nano-TiO2: Destruction of chloroaromatic compounds. *Chemosphere* **82**, 1215–1224.
2. Ravelli, D., D. Dondi, M. Fagnoni and A. Albini (2009) Photocatalysis. A multi-faceted concept for green chemistry. *Chem. Soc. Rev.* **38**, 1999–2011.
3. Ayoub, K., E. D. van Hullebusch, M. Cassir and A. Bermond (2010) Application of advanced oxidation processes for TNT removal: A review. *J. Hazard. Mater.* **178**, 10–28.
4. Watanabe, T. and N. Yoshida (2008) Wettability control of a solid surface by utilizing photocatalysis. *Chem. Rec.* **8**, 279–290.
5. Hayat, K., M. A. Gondal, M. M. Khaled and S. Ahmed (2010) Kinetic study of laser-induced photocatalytic degradation of dye (alizarin yellow) from wastewater using nanostructured ZnO. *J. Environ. Sci. Health A Tox. Hazard. Subst. Environ. Eng.* **45**, 1413–1420.

6. Gartner, M., J. Ballmann, C. Damm, F. W. Heinemann and H. Kisch (2007) Support-controlled chemoselective olefin-imine addition photocatalyzed by cadmium sulfide on a zinc sulfide carrier. *Photochem. Photobiol. Sci.* **6**, 159–164.
7. Rehman, S., R. Ullah, A. M. Butt and N. D. Gohar (2009) Strategies of making TiO2 and ZnO visible light active. *J. Hazard. Mater*. **170**, 560–569.
8. Montenegro, M. A., M. A. Nazareno, E. N. Durantini and C. D. Borsarelli (2002) Singlet molecular oxygen quenching ability of carotenoids in a reverse-micelle membrane mimetic system. *Photochem. Photobiol.* **75**, 353–361.
9. Tayade, R. J., P. K. Surolia, R. G. Kulkarni and R. V. Jasra (2007) Photocatalytic degradation of dyes and organic contaminants in water using nanocrystalline anatase and rutile TiO2. *Sci. Tech. Adv. Mat*. **8**, 455–462.
10. Xiao, Q., J. Zhang, C. Xiao, Z. C. Si and X. O. Tan (2008) Solar photocatalytic degradation of methylene blue in carbon-doped TiO2 nanoparticles suspension. *Sol. Energy* **82**, 706–713.

3. Shimosako J, Onaka T, Yamanouchi M, Yokota M, Nakamura T, Fujji F, et al. An outbreak of extended-spectrum beta-lactamase (ESBL)–producing *Shigella sonnei* at a day care nursery in Sakai City, 2006. Jpn J Infect Dis. 2007;60:408–9.
4. Muller L, Jensen T, Petersen RF, Molbak K, Ethelberg S. Imported fresh sugar peas as suspected source of an outbreak of *Shigella sonnei* in Denmark, April–May 2009. Euro Surveill. 2009;14:pii:19241.
5. Alcoba-Flórez J, Pérz-Roth E, González-Linares S, Méndez-Alvarez S. Outbreak of *Shigella sonnei* in a rural hotel in La Gomera, Canary Island, Spain. Int Microbiol. 2005;8:133–6.
6. von Seidlein L, Kim DR, Ali M, Lee H, Wang X, Thiem VD, et al. A multicentre study of *Shigella* diarrhoea in six Asian countries: disease burden, clinical manifestations, and microbiology. PLoS Med. 2006;3:e353. doi:10.1371/journal.pmed.0030353
7. Vinh H, Nhu NTK, Nga TVT, Duy PT, Campbell JI, Hoang NVM, et al. A changing picture of shigellosis in southern Vietnam: shifting species dominance, antimicrobial susceptibility and clinical presentation. BMC Infect Dis. 2009;9:204. doi:10.1186/1471-2334-9-204
8. Pichel M, Gonzalez Fraga S, Terragno R, Mulki J, Gentile A, Kremer C, et al. Short report: analysis of clonal relationship among *Shigella sonnei* isolates circulating in Argentina. Epidemiol Infect. 2007;135:681–7. doi:10.1017/S0950268806007230
9. Nandy S, Mitra U, Rajendran K, Dutta P, Dutta S. Subtype prevalence, plasmid profiles and growing fluoroquinolone resistance in *Shigella* from Kolkata, India (2001–2007): a hospital-based study. Trop Med Int Health. 2010;15:1499–507. doi:10.1111/j.1365-3156.2010.02656.x
10. Bhattacharya SK, Sarkar K, Nair GB. Multidrug-resistant *Shigella dysentery* type 1 in south Asia. Lancet Infect Dis. 2003;3:755. doi:10.1016/S1473-3099(03)00829-6

Address for correspondence: Shanta Dutta, Bacteriology Division, National Institute of Cholera and Enteric Diseases, P-33, CIT Rd, Scheme XM, Beliaghata, Kolkata 700010, India; email: shanta1232001@yahoo.co.in

Mosquito-associated Dengue Virus, Key West, Florida, USA, 2010

To the Editor: Except for sporadic cases along the Texas–Mexico border, local transmission of dengue virus (DENV) has not occurred in the contiguous United States since 1946. In 2009, DENV was diagnosed in a vacationer to Key West, Florida (*1*). Subsequently, 25 other cases were reported that year, transmission was confirmed by detection of DENV serotype 1 (DENV-1) in local mosquitoes, and a random serosurvey showed evidence of recent DENV infection in 5.4% of Key West residents (*1*). Transmission continued in 2010, and an additional 63 cases were confirmed (*2*). We used PCR amplification and sequence analysis of virus identified from mosquito collections during 2010 to identify the closest relatives, probable geographic origin, and divergence time of the Key West DENV.

A total of 1,178 pools of *Aedes aegypti* mosquitoes were collected in Monroe County, Florida, during January 27–December 17, 2010 (online Appendix Figure, panel A, wwwnc.cdc.gov/EID/article/17/11/11-0419-FA1.htm), by using BG-Sentinel (Biogents, Regensburg, Germany) or CDC (Clarke, Roselle, IL, USA) light traps, and stored at −80°C. Reverse transcription PCR was conducted on each pool by using primers designed to amplify all 4 DENV serotypes, followed by seminested PCR with serotype-specific primers (*3*). Results from 2 Key West mosquito pools collected on June 25 and 30 showed a positive first-round reverse transcription PCR and a positive second-round PCR specific for DENV-1. A third Key West pool collected on August 27 showed only a positive second-round PCR specific for DENV-1. No other DENV serotypes were detected.

DENV-1–specific primers (5′-GGGCCTTGAGACACCCAGG-3′ and 5′-CCTCCCATGCCTTCCCAATGGC-3′) were used to amplify products encompassing the envelope (E) gene region and parts of the premembrane and nonstructural 1 genes from the pools collected on June 25 and 30. PCR products were sequenced by using amplification and internal primers to provide double or triple coverage (Functional Biosciences, Madison, WI, USA). The sequences from these 2 pools were identical (GenBank accession no. JF519855). We used ClustalX (*4*) to align the Key West sequences with 175 nonredundant American DENV-1 sequences from the National Center for Biotechnology Information Virus Variation database (*5*) and 9 additional DENV-1 subgenomic E sequences from GenBank, which provided a comprehensive set of American DENV-1 sequences, including several isolates from Hawaii (USA) and Easter Island (Chile) that grouped with Asian DENV-1 clades as an outgroup. Maximum-likelihood phylogenetic analysis of the 1,484-nt E gene region was conducted by using SeaView software (*6*).

The analysis showed that American DENV-1 strains clustered by geography and by year of collection (online Appendix Figure, panel B). This clustering might be the result of lineage replacement that has been described in DENV-1 (*7*). Additionally, clustering might be influenced by serotype prevalence or sampling bias. For example, the sequence database contains few Caribbean isolates from after 2000 and few Central or South American isolates from before 2000. The Key West sequence grouped as a member of a large clade of recent viruses from Central America that was separated from Caribbean and South American viruses with a well-supported bootstrap value (86%) and relatively long branch length. The closest relatives were 2 strains isolated

in Nicaragua in 2006 and 2008. The bootstrap support for this grouping was 100%. Phylogenetic analyses with neighbor-joining, maximum-parsimony, and Bayesian methods gave trees with similar topologies, including clear separation of most recent Central American isolates into 1 clade, as well as grouping of the Key West sequence with the same 2 isolates from Nicaragua (data not shown). No protein coding changes between these strains were identified, which suggests purifying selection for an optimum phenotype. There were 8 synonymous differences over the 1,708-nt amplified region between the Key West and Nicaragua 2008 sequences. Previous molecular clock determinations for DENV-1 provided a range of 2.5–7.0 × 10^{-4} substitutions per nucleotide per year (*8*). This calculation produced an estimate of a 6.7–18.7-year divergence time between the Key West virus and the most closely related Nicaragua strain. When during this time the ancestor of Key West DENV was introduced to Florida is unknown.

Analysis of the entire Key West DENV-1 genome may help pinpoint the origin and address the possibility of selective pressure on other genes or recombination events (*9*). Given the recent reports of DENV in residents of other Florida counties who had no travel histories (*2*), monitoring of Key West and other nearby urban areas for evidence of local DENV transmission should continue.

Acknowledgments

We thank the staff of the Florida Keys Mosquito Control District for assistance with mosquito collection, Chris Geiger for use of laboratory space, and Michael Shannon and Ram Samudrala for computing assistance.

This work was supported in part by Defense Threat Reduction Agency awards HDTRA1-09-1-0004 and HDTRA1-10-1-0009 to S.F.M. and S.I.

Amanda S. Graham, Catherine A. Pruszynski, Lawrence J. Hribar, David J. DeMay, Adriane N. Tambasco, Anne E. Hartley, Edsel M. Fussell, Scott F. Michael, and Sharon Isern

Author affiliations: Florida Gulf Coast University, Fort Myers, Florida, USA (A.S. Graham, A.E. Hartley, S.F. Michael, S. Isern); and Florida Keys Mosquito Control District, Key West, Florida, USA (C.A. Pruszynski, L.J. Hribar, D.J. DeMay, A.N. Tambasco, E.M. Fussell)

DOI: http://dx.doi.org/10.3201/eid1711.110419

References

1. Centers for Disease Control and Prevention. Locally acquired dengue—Key West, Florida, 2009–2010. MMWR Morb Mortal Wkly Rep. 2010;59:577–81.
2. Anil L, Stanek D, Blackmore C, Stark L, Mock V. Florida arbovirus surveillance week 52: December 26–January 1, 2011 [cited 2011 Mar 18]. http://www.doh.state.fl.us/Environment/medicine/arboviral/pdfs/2010/2010Week52ArbovirusReport_1_1_2011.pdf
3. Lanciotti RS, Calisher CH, Gubler DJ, Chang GJ, Vorndam AV. Rapid detection and typing of dengue viruses from clinical samples by using reverse transcriptase–polymerase chain reaction. J Clin Microbiol. 1992;30:545–51.
4. Thompson JD, Gibson TJ, Plewniak F, Jeanmougin F, Higgins DG. The ClustalX windows interface: flexible strategies for multiple sequence alignment aided by quality analysis tools. Nucleic Acids Res. 1997;24:4876–82. doi:10.1093/nar/25.24.4876
5. Resch W, Zaslavsky L, Kiryutin B, Rozanov M, Bao Y, Tatusova TA. Virus variation resources at the National Center for Biotechnology Information: dengue virus. BMC Microbiol. 2009;9:65. doi:10.1186/1471-2180-9-65
6. Gouy M, Guindon S, Gascuel O. SeaView version 4: a multiplatform graphical user interface for sequence alignment and phylogenetic tree building. Mol Biol Evol. 2010;27:221–4. doi:10.1093/molbev/msp259
7. Zhang C, Mammen MP Jr, Chinnawirotpisan P, Klungthong C, Rodpradit P, Monkongdee P, et al. Clade replacements in dengue virus serotypes 1 and 3 are associated with changing serotype prevalence. J Virol. 2005;79:15123–30. doi:10.1128/JVI.79.24.15123-15130.2005
8. Twiddy SS, Holmes EC, Rambaut A. Inferring the rate and time-scale of dengue virus evolution. Mol Biol Evol. 2003;20:122–9. doi:10.1093/molbev/msg010
9. Carvalho SES, Martin DP, Oliveira LM, Ribeiro BM, Nagata T. Comparative analysis of American dengue virus type 1 full-genome sequences. Virus Genes. 2010;40:60–6. doi:10.1007/s11262-009-0428-0

Address for correspondence: Sharon Isern, Department of Biological Sciences, College of Arts and Sciences, AB7 304, Florida Gulf Coast University, 10501 FGCU Blvd South, Fort Myers, FL 33965-6565, USA; email: sisern@fgcu.edu

Mycobacterium doricum Osteomyelitis and Soft Tissue Infection

To the Editor: Infections with nontuberculous mycobacteria (NTM) are being increasingly identified. Several factors may contribute to this finding, including increased awareness of these organisms as pathogens, improved ability of laboratories to isolate and identify these organisms, and increasing prevalence (*1*). We describe a case of osteomyelitis and soft tissue infection with *Mycobacterium doricum* after trauma in a previously healthy adult.

A 21-year-old man sustained an open right femur fracture with gross contamination of the wound with dirt and gravel. The wound was irrigated and debrided, the fracture was fixed by intramedullary nailing, and the wound was closed.

Sixteen weeks later, pain, swelling, and erythema developed in the right thigh of the patient.

Antiviral Research 89 (2011) 71–74

Contents lists available at ScienceDirect

Antiviral Research

journal homepage: www.elsevier.com/locate/antiviral

Viral entry inhibitors block dengue antibody-dependent enhancement *in vitro*

Cindo O. Nicholson[a], Joshua M. Costin[a], Dawne K. Rowe[a], Li Lin[b], Ekachai Jenwitheesuk[c], Ram Samudrala[d], Sharon Isern[a], Scott F. Michael[a,*]

[a] *Department of Biological Sciences, Florida Gulf Coast University, Fort Myers, FL 33965, USA*
[b] *Communicable Disease Center, Tan Tock Seng Hospital, Singapore 308433, Singapore*
[c] *National Center for Genetic Engineering and Biotechnology, National Science and Technology Development Agency, Klong Luang, Pathumthani 12120, Thailand*
[d] *Department of Microbiology, University of Washington, Seattle, WA 91895, USA*

ARTICLE INFO

Article history:
Received 6 October 2010
Received in revised form 2 November 2010
Accepted 10 November 2010

Keywords:
Dengue
Antibody
Enhancement
Peptide
Entry
Inhibitor

ABSTRACT

Severe dengue virus (DENV) disease symptoms, including dengue hemorrhagic fever and dengue shock syndrome, have been correlated with the presence of pre-existing antibodies that enhance rather than neutralize infections in Fc receptor bearing cells. These antibodies can originate from previous infection with a different serotype of dengue, or from waning antibody titers that occur in infants and young children as they are weaned from breast milk that contains protective dengue-specific antibodies. Despite the apparent importance of this antibody dependent enhancement (ADE) effect, there has been no description of any specific inhibitors of this process. We explored DENV entry inhibitors as a potential strategy to block ADE. Two different peptide entry inhibitors were tested for the ability to block antibody-mediated DENV-2 infection of human, FcRII bearing K562 cells *in vitro*. Both peptides were able to inhibit ADE, showing that entry inhibitors are possible candidates for the development of specific treatment for severe DENV infection.

1. Introduction

Dengue is the most important insect-transmitted viral disease and is prevalent in developing tropical and subtropical countries where the main mosquito vectors, *Aedes aegypti* and *Aedes albopictus*, can breed year round. Worldwide, there are an estimated 50–100 million cases of dengue infection per year and 2.5 billion people who live in areas at risk (World Health Organization, 2009). An estimated 500,000 people are hospitalized annually with severe dengue symptoms; dengue hemorrhagic fever/dengue shock syndrome (DHF/DSS), a very large proportion of whom are children (World Health Organization, 2009). Currently there are no specific treatments or vaccines against dengue virus (DENV) and cases are treated using only supportive care.

The four distinct serotypes of dengue virus co-circulate in many areas and give rise to sequential epidemic outbreaks when the number of susceptible individuals in the local human population reaches a critical threshold and weather conditions favor reproduction of the mosquito vectors. Initial infection with one DENV serotype usually generates a protective and long-lasting immune response against re-infection with the same serotype. While antibody cross-reactivity between serotypes is common, cross-serotype protection is only short lived. Low levels of neutralizing antibodies, cross-reactive but non-neutralizing antibodies, or both, from previous infections have been shown to bind virions of other serotypes and target them to Fc receptors on macrophages and certain other cell types, enhancing infection of these cells (Halstead and O'Rourke, 1977). The presence of these cross-reactive and non-neutralizing antibodies has also been shown to correlate with severe disease outcome (DHF/DSS) in several studies (Halstead, 1998; Kliks et al., 1989; Vaughn et al., 2000). This antibody dependent enhancement (ADE) effect may also explain the sequential nature of epidemic outbreaks as well as the severe disease seen in infants being weaned from protective maternal antibodies (Halstead, 1998; Kliks et al., 1988). Concerns regarding incomplete protection and predisposition towards ADE have complicated vaccine development. If ADE is one of the major risk factors for DHF/DSS, and a roadblock for the development and use of vaccines, then the investigation of strategies to block ADE should be considered.

Abbreviations: DENV, dengue virus; DMEM, Dulbecco's modified Eagle's medium; DMSO, dimethylsulfoxide; FBS, fetal bovine serum; FFU, focus forming unit; PBS, phosphate buffered saline; qRT-PCR, quantitative reverse transcriptase polymerase chain reaction.

* Corresponding author at: Department of Biological Sciences, AB7 Room 307, Florida Gulf Coast University, 10501 FGCU Blvd. South, Fort Myers, FL 33965-6565, USA. Tel.: +1 239 590 7439; fax: +1 239 590 7200.
E-mail addresses: cnicholson@fgcu.edu (C.O. Nicholson), jcostin@fgcu.edu (J.M. Costin), dkrowe@eagle.fgcu.edu (D.K. Rowe), Li_Lin@ttsh.com.sg (L. Lin), ekachai@biotec.or.th (E. Jenwitheesuk), ram@compbio.washington.edu (R. Samudrala), sisern@fgcu.edu (S. Isern), smichael@fgcu.edu (S.F. Michael).

0166-3542/$ – see front matter © 2010 Elsevier B.V. All rights reserved.
doi:10.1016/j.antiviral.2010.11.008

As there is no well-accepted animal model that displays the effects of DENV ADE, we used a well-characterized, human cell-based, *in vitro* system for this study. We examined the ability of two distinct DENV entry inhibitors to block ADE in a cell culture system using Fc receptor II (FcRII) bearing human K562 cells. We show that these entry inhibitors are capable of fully blocking the ADE effect and reducing infection to levels equivalent to that found in the absence of anti-DENV serum. These results show promise for the development of specific treatments for DENV infection that might be useful for intervention in the process of ADE, whether induced by waning maternal antibodies, naturally occurring secondary infection, or as a consequence of incomplete or declining vaccine protection.

2. Materials and methods

2.1. Cells and virus

Human FcRII expressing K562 cells (ATCC #CCL-243) were grown in RPMI-1640 medium (HyClone, Logan, UT) containing 10% (v/v) fetal bovine serum (FBS), 2 mM Glutamax, 100 U/ml penicillin G, 100 μg/ml streptomycin, and 0.25 μg/ml amphotericin B at 37 °C with 5% (v/v) CO_2. DENV-2 strain NG-C was obtained from R. Tesh at the University of Texas, Galveston and propagated in the *Macaca mulata* epithelial cell line, LLC-MK2 (ATCC #CCL-7), grown in Dulbecco's modified Eagle's medium (DMEM) with the same supplements and conditions. All cell culture reagents were purchased from Invitrogen (Carlsbad, CA) unless otherwise noted.

2.2. Anti-DENV serum

Human serum was obtained from patients at Tan Tock Seng Hospital, Singapore, approximately two weeks post-recovery. Informed consent was obtained from all study participants, and full institutional review and approval was obtained at Tan Tock Seng Hospital (DSRB B/07/275) and Florida Gulf Coast University (IRB 2007-12) according to US Department of Health and Human Services guidelines. Patients were initially diagnosed by serology or PCR. Post-recovery serum was characterized by ELISA and neutralization assay as described (Schieffelin et al., 2010). Equal volumes from seven highly cross reactive samples were heat inactivated and combined.

2.3. Peptides

DN59 (MAILGDTAWDFGSLGGVFTSIGKALHQVFGAIY) (Hrobowski et al., 2005) and 1OAN1 (FWFTLIKTQAKQPARYRRFC) (Costin et al., 2010.) were synthesized by solid-phase N-α-9-flurenylmethyl-oxycarbonyl chemistry, purified by HPLC, and confirmed by mass spectrometry (Genemed Synthesis, San Antonio, TX or EZBiolab, Carmel, IN). Peptide stock solutions were prepared by dissolving in 20% (v/v) DMSO in water, adjusting with NaOH, and concentrations determined by absorbance at 280 nm.

2.4. Neutralization assays

Virus focus forming unit reduction assays were carried out using LLC-MK2 cells as previously described (Costin et al., 2010; Hrobowski et al., 2005) with the exception that a 1.2% solution of Avicel in complete medium (FMC, Philadelphia, PA) was used in place of agarose. Neutralization assays using quantitative reverse transcriptase PCR (qRT-PCR) were carried out by infecting monolayers of LLC-MK2 in 12 well plates with approximately 4000 focus forming units (FFU) at 37 °C with 5% CO_2. After 1 h, the media was removed and 1 ml of complete culture media was added to each well. Plates were incubated for 72 h at 37 °C with 5% CO_2 and medium was collected and RNA isolated using a QiampViral RNA mini kit (Qiagen, Valencia, CA). qRT-PCR was carried out with primers 10503F and 10599R (Chutinimitkul et al., 2005), using a LightCycler 480 II (Roche, Indianapolis, IN) and a one step LightCycler RNA Master SYBR Green I kit (Roche). Amplification conditions were 61 °C for 30 min, 95 °C for

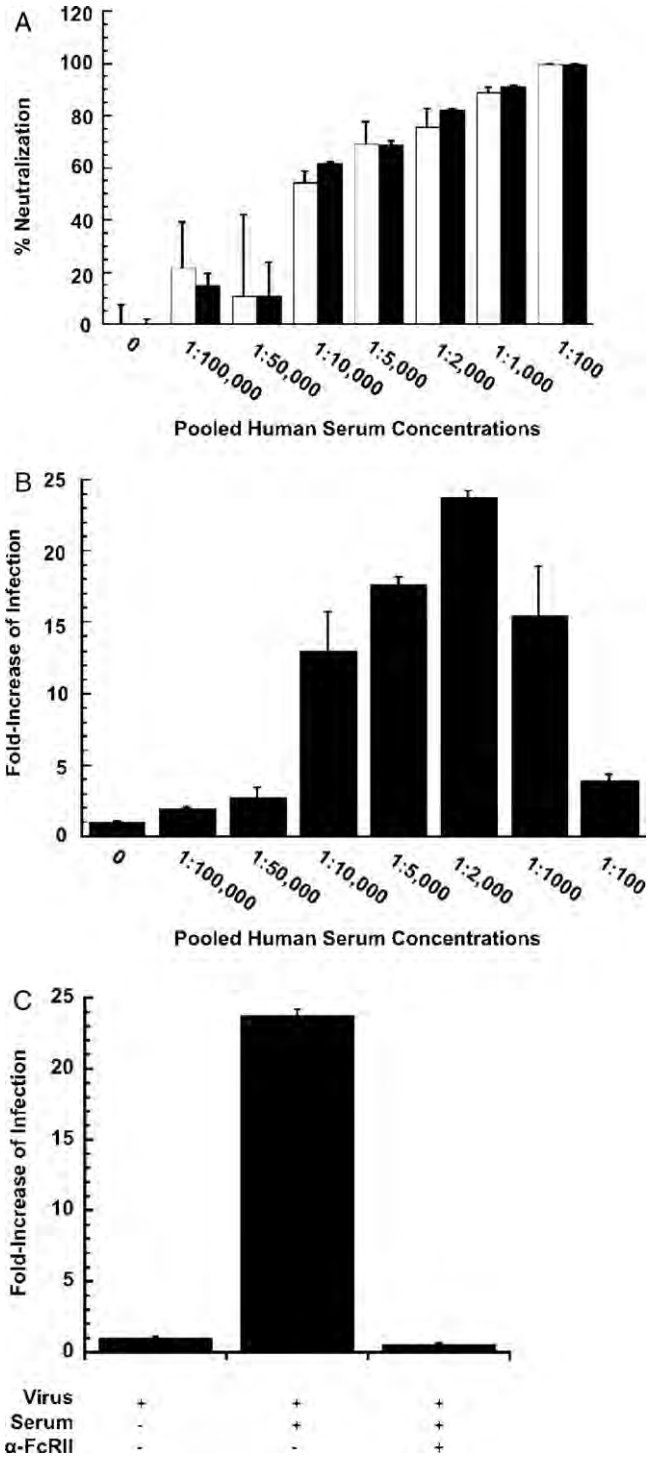

Fig. 1. Pooled anti-DENV serum neutralizes infection in LLC-MK2 epithelial cells. (A) Neutralization was measured either by focus forming unit reduction (white bars), or qRT-PCR (black bars), reaching approximately 80% inhibition at 1:2000 dilution. (B) Pooled anti-DENV serum enhances infection in FcRII expressing K562 cells with a maximum at 1:2000 dilution. (C) Addition of an anti-FcRII Ab blocks the enhancement effect. Graphs show the mean of three independent replicates ±SD.

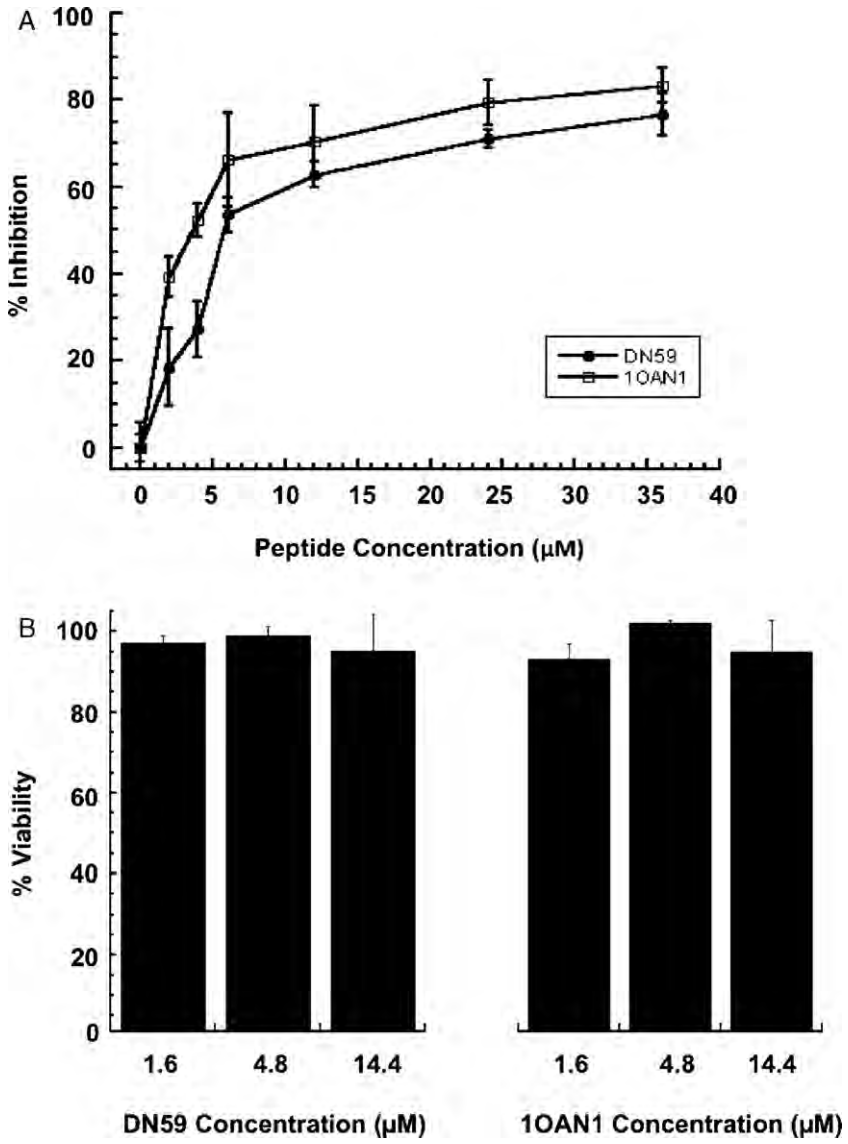

Fig. 2. Entry inhibitors block ADE in Fc bearing cells. (A) Two different DENV entry-inhibitory peptides inhibit infection of FcRII expressing human K562 cells in the presence of the maximally enhancing dilution (1:2000) of anti-DENV serum. (B) Neither peptide shows evidence of cellular toxicity over the concentration range used to inhibit enhancement. Dilution of the peptide inhibitors with virus and medium during infection results in the cells being exposed to the lower concentrations shown in (B). Graphs show the mean of three independent replicates ±SD.

30 s, and 45 cycles of 95 °C for 5 s, 61 °C for 20 s, and 72 °C for 30 s.

2.5. Enhancement and ADE-inhibition assays

Dilutions of pooled serum were first incubated with 4000 FFU of virus for 1 h at 37 °C in 700 μl of serum free RPMI-1640. 200 μl of virus and serum was then incubated with either peptide for an additional 1 h. The addition of antibodies to the virus prior to addition of peptides was done to mimic what would be expected to occur in a hypothetical *in vivo* intervention. The mixtures were added to 80,000 K562 cells in 300 μl of complete growth medium in a 24-well plate and incubated at 37 °C with 5% CO_2 for 72 h. RNA was extracted from cell lysates using the RNeasy Mini kit (Qiagen, Valencia, CA). qRT-PCR was performed as above. ADE-inhibition assays were performed identically using a 1:2000 serum dilution. Control experiments were performed with DMSO and NaOH, as well as in the presence of 1 μg/ml mouse anti-human FcRII (anti-CD32) (Biolegend, San Diego, CA).

2.6. Toxicity assay

The effect of peptides on K562 cells was tested by measuring mitochondrial reductase activity using the TACS™ MTT cell proliferation assay (R&D Systems Inc., Minneapolis, MN) after 72 h of exposure, as per manufacturer's instructions. Peptide concentrations were adjusted by 0.4 to account for the dilution of the peptide/virus mixtures that occurred during the ADE inhibition assays.

3. Results

Pooled human anti-DENV serum was able to neutralize infection in LLC-MK2 epithelial cells, as shown by both a focus forming unit reduction assay and by qRT-PCR (Fig. 1A). This serum was also able to enhance infection in FcRII expressing K562 cells, with a maximum enhancement at 1:2000 dilution (Fig. 1B). This dilution showed an approximately 80% inhibition of infection in LLC-MK2 cells. Addition of an anti-FcRII Ab to the K562 cells blocked enhancement completely (Fig. 1C). Incubation of virus–serum mixtures

with inhibitory peptides showed a dose responsive inhibition of ADE, with a 50% inhibitory concentration of 3 μM for 1OAN1 and 6 μM for DN59 (Fig. 2A). The inhibition of ADE did not reach 100% for either peptide, but reduced the amount of viral genome present to a level equivalent to control infection in the absence of anti-DENV serum. No inhibitory effect was seen in either the LLC-MK2 cells or the K562 cells using buffers containing control amounts of DMSO or NaOH, but without peptides (data not shown). Both peptides were previously shown to be non-toxic in LLC-MK2 cells (Costin et al., 2010; Hrobowski et al., 2005), and neither peptide displayed evidence of toxicity to the K562 cells (Fig. 2B).

4. Discussion

We have shown that two different peptides are able to inhibit ADE-mediated DENV infection of FcRII expressing cells *in vitro*. These two peptides target the DENV surface E glycoprotein, but are distinct in their mechanisms of action. 1OAN1 is a computationally optimized mimic of the first beta sheet strand connecting E protein domains I and II. It interacts with purified, monomeric E protein, alters the surface structure of DENV virions, and has been shown to inhibit DENV entry and block virus:cell binding (Costin et al., 2010). The DN59 inhibitor is a direct mimic of a portion of the E protein pre-membrane stem region (Hrobowski et al., 2005). DENV E stem region peptides similar to DN59 interact with lipid bilayers and bind to post fusion E protein trimers to inhibit the fusion process (Schmidt et al., 2010). It is perhaps surprising that we observed inhibition of ADE, since antibodies are large and could sterically hinder peptide binding. Additionally, both peptides have relatively lower affinities for the E protein, with dissociation constants in the range of 10^{-7} M (Costin et al., 2010; Schmidt et al., 2010), compared to some neutralizing human monoclonal antibodies that bind with dissociation constants in the range of 10^{-9} M (Schieffelin et al., 2010).

The K562 cell line was chosen as a simple and easily interpretable model system for the study of ADE and ADE inhibition as it expresses only the FcRII gamma antibody receptor (Littaua et al., 1990). Other immortalized cell lines or primary macrophage cultures express different combinations of distinct Fc receptors in variable amounts. It remains to be shown if these peptides will block ADE in other cell culture systems. We made no attempt to separate out the possible differences in ADE-mediated entry, ADE-mediated signaling changes, or ADE-mediated upregulation of viral replication that have been noted to occur in some systems (Boonak et al., 2008).

ADE is a phenomenon that is thought to be a major cause of DHF/DSS, and fear of inducing ADE has hampered the development of a DENV vaccine. We show here that entry inhibitors can effectively block ADE *in vitro*. Based on these observations, entry inhibitors like DN59 or 1OAN1 may serve as lead compounds for the development of clinically useful DENV treatments. It may also be important to evaluate other potential DENV treatment strategies for the ability to block ADE.

Acknowledgements

This work was supported by Defense Threat Reduction Agency awards HDTRA1-08-1-0003 and HDTRA1-09-1-0004, and Florida Biodefense Research Consortium contract W911SR-07-C-0084 to SI and SFM.

References

Boonak, K., Slike, B.M., Burgess, T.H., Mason, R.M., Wu, S.J., Sun, P., Porter, K., Rudiman, I.F., Yuwono, D., Puthavathana, P., Marovich, M.A., 2008. Role of dendritic cells in antibody-dependent enhancement of dengue virus infection. J. Virol. 82, 3939–3951.

Chutinimitkul, S., Payungporn, S., Theamboolers, A., Poovorawan, Y., 2005. Dengue typing assay based on real-time PCR using SYBR Green I. J. Virol. Methods 129, 8–15.

Costin, J.M., Jenwitheesuk, E., Lok, S.-M., Hunsperger, E., Conrads, K.A., Fontaine, K.A., Rees, C.R., Rossmann, M.G., Isern, S., Samudrala, R., Michael, S.F., 2010. Structural optimization and de novo design of dengue virus entry inhibitory peptides. PLoS Negl. Trop. Dis. 4 (6), e721, doi:10.1371/journal.pntd.0000721.

Halstead, S.B., 1998. Pathogenesis of dengue: challenges to molecular biology. Science 239, 476–481.

Halstead, S.B., O'Rourke, E.J., 1977. Dengue viruses and mononuclear phagocytes. I. Infection enhancement by non-neutralizing antibody. J. Exp. Med. 146, 201–217.

Hrobowski, Y.M., Garry, R.F., Michael, S.F., 2005. Peptide inhibitors of dengue virus and West Nile virus infectivity. Virol. J. 2, 49, doi:10.1186/1743-422X-2-49.

Kliks, S.C., Nimmanitya, S., Nisalak, A., Burke, D.S., 1988. Evidence that maternal dengue antibodies are important in the development of dengue hemorrhagic fever in infants. Am. J. Trop. Med. Hyg. 38, 411–419.

Kliks, S.C., Nisalak, A., Brandt, W.E., Wahl, L., Burke, D.S., 1989. Antibody-dependent enhancement of dengue virus growth in human monocytes as a risk factor for dengue hemorrhagic fever. Am. J. Trop. Med. Hyg. 40, 444–451.

Littaua, R., Kurane, I., Ennis, F.A., 1990. Human IgG Fc receptor II mediates antibody-dependent enhancement of dengue virus infection. J. Immunol. 144, 3183–3186.

Schieffelin, J.S., Costin, J.M., Nicholson, C.O., Orgeron, N.M., Fontaine, K.A., Isern, S., Michael, S.F., Robinson, J.E., 2010. Neutralizing and non-neutralizing monoclonal antibodies against dengue virus E protein derived from a naturally infected patient. Virol. J. 7, 28, doi:10.1186/1743-422X-7-28.

Schmidt, A.G., Yang, P.L., Harrison, S.C., 2010. Peptide inhibitors of dengue virus entry target a late stage fusion intermediate. PLoS Pathog. 6, 4, doi:10.1371/journal.ppat.1000851.

Vaughn, D.W., Green, S., Nisalak, A., 2000. Dengue viremia titer, antibody response pattern, and virus serotype correlate with disease severity. J. Infect. Dis. 181, 2–9.

World Health Organization, 2009. Fact sheet no. 117. Available from: www.who.int/mediacentre/factsheets/fs117/en/ (accessed 03.06.10).

OPEN ACCESS Freely available online

PLOS ONE

Release of Dengue Virus Genome Induced by a Peptide Inhibitor

Shee-Mei Lok[1,6☯], Joshua M. Costin[2☯], Yancey M. Hrobowski[2,3¤a], Andrew R. Hoffmann[4], Dawne K. Rowe[2], Petra Kukkaro[6], Heather Holdaway[1¤b], Paul Chipman[1¤c], Krystal A. Fontaine[2¤d], Michael R. Holbrook[5¤e], Robert F. Garry[3], Victor Kostyuchenko[6], William C. Wimley[4], Sharon Isern[2], Michael G. Rossmann[1], Scott F. Michael[2]*

1 Department of Biological Sciences, Purdue University, West Lafayette, Indiana, United States of America, **2** Department of Biological Sciences, Florida Gulf Coast University, Fort Myers, Florida, United States of America, **3** Department of Microbiology and Immunology and Graduate Program in Cellular and Molecular Biology, Tulane University Health Sciences Center, New Orleans, Louisiana, United States of America, **4** Department of Biochemistry, Tulane University Health Sciences Center, New Orleans, Louisiana, United States of America, **5** Department of Pathology, University of Texas Medical Branch, Galveston, Texas, United States of America, **6** Emerging Infectious Diseases, Duke–NUS, Department of Biological Sciences, National University of Singapore, Singapore, Singapore

Abstract

Dengue virus infects approximately 100 million people annually, but there is no available therapeutic treatment. The mimetic peptide, DN59, consists of residues corresponding to the membrane interacting, amphipathic stem region of the dengue virus envelope (E) glycoprotein. This peptide is inhibitory to all four serotypes of dengue virus, as well as other flaviviruses. Cryo-electron microscopy image reconstruction of dengue virus particles incubated with DN59 showed that the virus particles were largely empty, concurrent with the formation of holes at the five-fold vertices. The release of RNA from the viral particle following incubation with DN59 was confirmed by increased sensitivity of the RNA genome to exogenous RNase and separation of the genome from the E protein in a tartrate density gradient. DN59 interacted strongly with synthetic lipid vesicles and caused membrane disruptions, but was found to be non-toxic to mammalian and insect cells. Thus DN59 inhibits flavivirus infectivity by interacting directly with virus particles resulting in release of the genomic RNA.

Citation: Lok S-M, Costin JM, Hrobowski YM, Hoffmann AR, Rowe DK, et al. (2012) Release of Dengue Virus Genome Induced by a Peptide Inhibitor. PLoS ONE 7(11): e50995. doi:10.1371/journal.pone.0050995

Editor: Young-Min Lee, Utah State University, United States of America

Received January 29, 2012; **Accepted** October 30, 2012; **Published** November 30, 2012

Funding: The work was supported by Defense Threat Reduction Agency awards HDTRA1-08-1-0003, HDTRA1-09-1-0004, and HDTRA1-10-1-0009 to SI and SFM, by National Institutes of Health Grants R01 AI76331 to MGR, AI64617 to RFG and SFM, GM60000 to WCW, and by NRF fellowship award R-913301-015-281 to SML. The funders had no role in study design, data collection and analysis, decision to publish, or preparation of the manuscript.

Competing Interests: Tulane University has applied for patents covering the peptide described in this work with RFG and SFM as inventors (7,416,733 issued 8/26/2008, 7,854,937 issued 12/21/2010, application 20110130328 filed 8/22/2008). This does not alter the authors' adherence to all the PLOS ONE policies on sharing data and materials.

* E-mail: smichael@fgcu.edu

¤a Current address: Operations and Tactics Division, Center for Naval Analyses, Alexandria, Virginia, United States of America
¤b Current address: Cleveland Center for Membrane and Structural Biology, Case Western Reserve University, Cleveland, Ohio, United States of America
¤c Current address: Department of Biochemistry and Molecular Biology, University of Florida, Gainesville, Florida, United States of America
¤d Current address: Department of Microbiology, University of Washington, Seattle, Washington, United States of America
¤e Current address: NIAID Integrated Research Facility, Ft. Detrick, Frederick, Maryland, United States of America

☯ These authors contributed equally to this work.

Introduction

The four dengue virus serotypes, dengue virus types 1, 2, 3 and 4, are major mosquito-transmitted, human pathogens. Currently there are no available vaccines or therapeutics. Dengue is a positive-sense RNA virus, encapsulated by a lipid membrane [1,2]. The surface of the mature virus particle is composed of 180 envelope (E) glycoprotein molecules and an equal number of membrane (M) protein molecules that assemble at endoplasmic reticulum-derived membranes [1,2]. The ectodomains of the E glycoproteins are arranged in a herringbone pattern on the surface of the lipid membrane that facilitates binding of the virus to host cells [3] and fusion of the virus with the host membrane after receptor-mediated endocytosis [4,5,6]. Each E monomer consists of three domains: DI, DII and DIII [7,8,9,10]. The C-terminal portion of the E protein consists of the stem and membrane anchor regions. The stem region is highly conserved among flaviviruses and is folded into amphipathic helices H1 and H2 that lie underneath the E ectodomain, partially embedded in the lipid envelope (Figure 1A, B) [2].

Ligands that mimic the structure of viral envelope components can sometimes interfere with the normal infection process and, thus, have potential as antiviral agents. For example, the T20 peptide, which is approved for treatment of HIV [11], has a sequence that mimics part of the C-terminal region of the HIV gp41 glycoprotein, and inhibits fusion with host cells [12]. Similarly, DIII of dengue virus E can prevent fusion of virions to host cells [13]. Furthermore, peptides that mimic other regions of E have also been shown to inhibit infection [14,15]. Some of these peptides bind to E and appear to cause changes in the organization of the glycoproteins on the viral surface [15]. Here we report that a peptide mimicking a highly conserved portion of

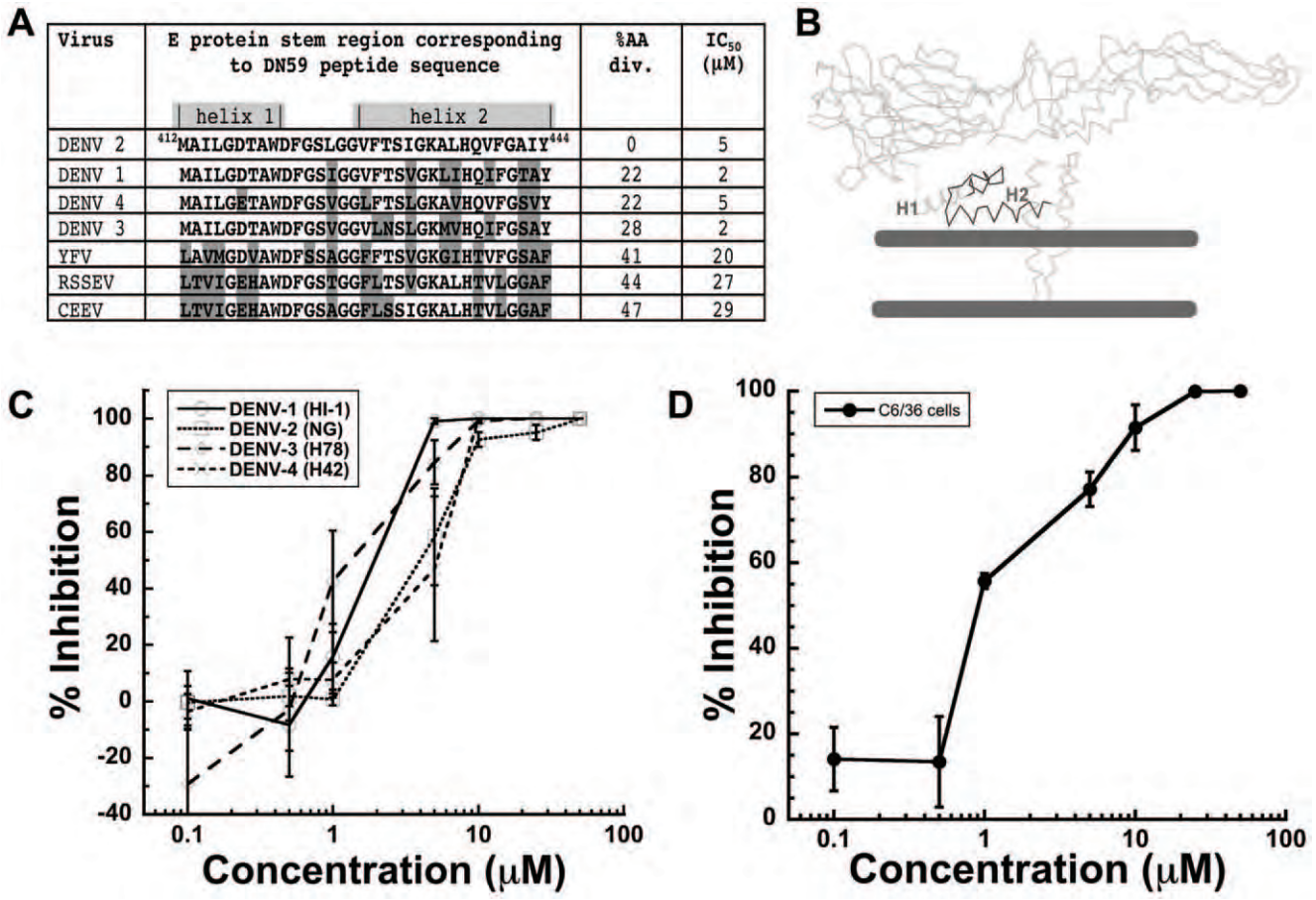

Virus	E protein stem region corresponding to DN59 peptide sequence (helix 1 | helix 2)	%AA div.	IC_{50} (μM)
DENV 2	^{412}MAILGDTAWDFGSLGGVFTSIGKALHQVFGAIY^{444}	0	5
DENV 1	MAILGDTAWDFGSIGGVFTSVGKLIHQIFGTAY	22	2
DENV 4	MAILGETAWDFGSVGGLFTSLGKAVHQVFGSVY	22	5
DENV 3	MAILGDTAWDFGSVGGVLNSLGKMVHQIFGSAY	28	2
YFV	LAVMGDVAWDFSSAGGFFTSVGKGIHTVFGSAF	41	20
RSSEV	LTVIGEHAWDFGSTGGFLTSVGKALHTVLGGAF	44	27
CEEV	LTVIGEHAWDFGSAGGFLSSIGKALHTVLGGAF	47	29

Figure 1. The DN59 peptide inhibits dengue virus infectivity. (A) Sequence comparison of the DN59 amino acid sequence, representing the dengue virus 2 E stem region (residues 412–444), with the stem region of other flaviviruses. YFV - yellow fever virus, RSSEV - Russian spring-summer encephalitis virus, CEEV - Central European encephalitis virus. Non-identical residues are colored in grey. The % amino acid divergence from dengue 2 and IC_{50} values against other flaviviruses are also shown. (B) The C-α backbone of the E protein of dengue 2 as fitted into the 9Å resolution cryoEM map of the mature virus [2]. The region mimicked by DN59 is shown in black outline. Grey bars indicate the lipid bilayer membrane. Part of the stem region helix 2 (H2) interacts with the outer lipid layer of the membrane. (C) FFU reduction assay showing dose response inhibition of infection of dengue virus serotypes 1-4, in mammalian epithelial cells. (D) FFU reduction assay showing dose response inhibition of infection of dengue virus 2 in mosquito cells.
doi:10.1371/journal.pone.0050995.g001

the E protein stem region causes the release of the genome from the virus particle.

Results and Discussion

A 33 amino acid peptide, known as DN59, mimics the dengue virus type 2 E stem region (residues 412 to 444). This peptide was previously shown to inhibit the infectivity of dengue 2 virus and West Nile virus, but activity against other flaviviruses and the mechanism of action were unknown [14]. In Figure 1C, we now show that at concentrations of 2-5 μM, the DN59 peptide reduced the infectivity of all four dengue virus serotypes by 50% (IC_{50}) in a FFU infection assay using mammalian epithelial cells. The infectivity of other flaviviruses (yellow fever virus, Central European encephalitis virus, and Russian spring-summer encephalitis virus) was inhibited at higher DN59 concentrations (Figure S1A).

Cryo-electron (cryoEM) microscopy of dengue virus type 2 particles incubated at 37°C for 30 minutes with 100 μM DN59 in 1% (v/v) DMSO in a 5:1 molar ratio of peptide to E protein on the virus had lost most of their RNA genomes whereas control virus particles in the presence of 1% (v/v) DMSO showed no visible loss of RNA genome (Figure 2A). Additional images showing larger numbers of control and treated particles are shown in Figure S2. The release of RNA presumably accounted for an increase of viscosity of the virus solution as well as a rather electron dense background on the cryoEM micrographs. Although treatment with peptide may disrupt the symmetry of the virus particle, a three-dimensional icosahedral reconstruction of a small number of particles supported the absence of RNA and suggested the formation of holes at the five-fold vertices through which the RNA might exit (Figure 2B and Figure S3).

The release of viral RNA from the particles was consistent with the results of a genome sensitivity assay conducted by exposing peptide-treated virus particles to RNase digestion, followed by quantitative reverse transcription PCR to determine the amount of protected viral RNA. The RNA genomes of untreated particles were protected from RNase digestion, whereas the genomes of particles co-incubated with increasing concentrations of DN59 were susceptible to digestion in a dose-responsive manner (Figure 2C, D). The peptide concentration required to yield 50% degradation of the genome (17 μM) was approximately four-fold higher than the concentration needed to

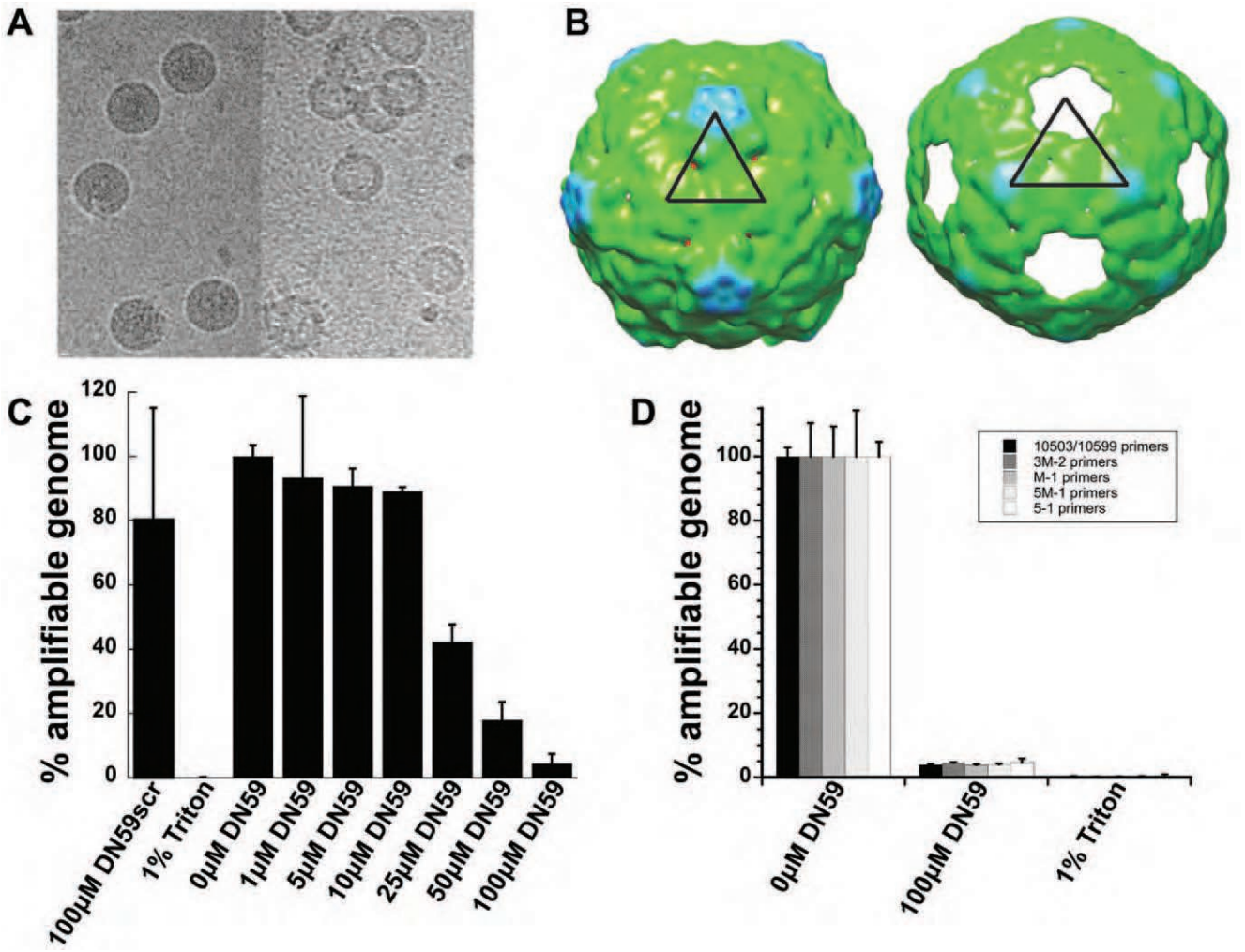

Figure 2. Incubation of mature dengue virus with DN59 peptide results in genome release. (A) CCD images of control dengue virus with 1% (v/v) DMSO (left) and dengue virus incubated with 100 μM DN59 in 1% (v/v) DMSO at 37°C for 30 mins (right). (B) CryoEM image reconstruction of control dengue virus (left) and dengue virus incubated with DN59 (right). Densities are colored according to radius: green (<220Å), cyan (220-230Å), and blue (231-239Å). The icosahedral asymmetric unit is represented by the black triangle. The contour level was chosen as the density that produces a very small hole in the capsid, other than at the five-fold axis. (C) RNase protection assay showing increasing degradation of released viral genome with increasing concentration of DN59. Disruption with detergent (1% triton) resulted in complete degradation. Treatment with a scrambled sequence version of DN59 did not result in significant genome degradation. (D) The RNase protection assay is insensitive to the location of the qRT-PCR primers used to detect the viral genome and indicates that there is no part of the genome that has differential sensitivity to degradation. Bars indicate primer sets targeting different locations in the viral genome.
doi:10.1371/journal.pone.0050995.g002

cause a 50% reduction in infectivity of dengue 2 virus (4.8 μM). This difference might be caused by the use of more than 1,000 times more virus in the genome degradation experiments, or by some treated particles having only partially released genomes after incubation with DN59 (Figure S3A). Although particles with partially released genomes are likely to be non-infectious, their genomes may still have been protected from degradation by RNase. This would cause the IC_{50} for the genome degradation assay to shift upwards in concentration compared to the FFU reduction assay.

The separation of the genome from the virus particle would be expected to irreversibly destroy infectivity. Reversibility was tested directly by treating virus with peptide at a concentration expected to produce approximately 80% inhibition of infectivity, then diluting the virus:peptide mixture 10 fold to a peptide concentration expected to produce negligible inhibition. No reversibility of inhibition was observed in these experiments (Figure 3).

The release of the virus RNA genome was confirmed by centrifuging peptide-treated, untreated, and triton detergent-treated virus particles through a tartrate density gradient, and monitoring the amount of RNA genome and E protein in each fraction. The results showed that the genome and E protein co-migrate in intact virus particles, but migrate to different fractions following peptide or detergent treatment, indicating that the genome and E protein are no longer associated after peptide treatment (Figure 4).

To confirm that there were no other targets for the inhibitory activity of DN59, time of addition and infectivity assays in a different target cell line were conducted. There was no inhibition of infectivity when mammalian target cells were incubated with DN59 and then washed prior to the addition of virus (Figure S1B). Nor was there inhibition of infectivity when DN59 was added after the cells had been infected (Figure S1B). Furthermore, after co-incubation of virus with DN59, infection was inhibited in both

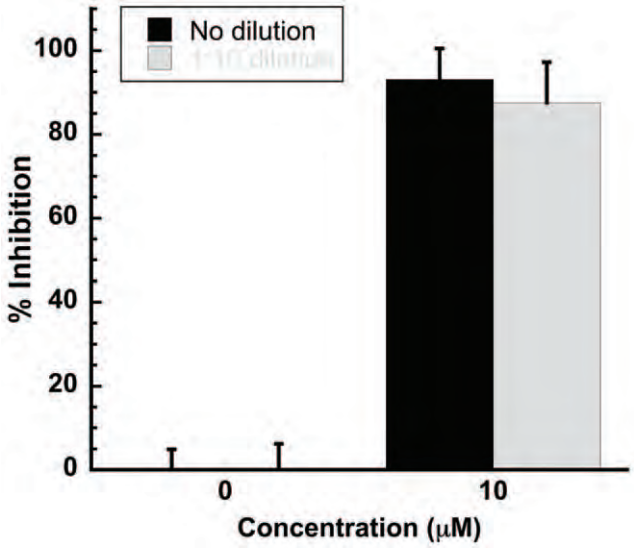

Figure 3. Inhibition of infectivity is not reversible. Dengue virus was incubated with 10 μM DN59, a concentration sufficient to produce approximately 80% inhibition, then either used directly to infect target LLC-MK_2 cells, or diluted 1:10 to 1 μM, a concentration that should produce marginal if any inhibition, then used to infect cells. Virus that was treated with 10 μM DN59, then diluted to 1 μM DN59, showed the same level of inhibition of infectivity as virus that was treated and not diluted.
doi:10.1371/journal.pone.0050995.g003

mammalian epithelial and mosquito cells (Figure 1C, D), showing that changes of the host cell type and corresponding viral entry pathway did not result in changes of the neutralization profile [16,17,18]. Therefore, it can be concluded that DN59 acts directly on the virus particle to release the RNA genome rather than on some other viral or cellular target.

Based on these experiments, DN59 appears to induce formation of holes in the viral membrane. Thus, DN59 might be expected to interact with lipid membranes and form holes or otherwise disrupt membrane bilayer structures. Consistent with this expectation, a concentration-dependent increase in the fluorescence of the tryptophan residue at peptide position nine was observed when peptide was mixed with liposome vesicles composed of either 1-palmitoyl-2-oleoyl-phosphatidylcholine (POPC), or a 9:1 molar ratio of POPC and 1-palmitoyl-2-oleoyl-phosphatidylglycerol (POPG), indicative of strong binding (Figure 5A). Also, addition of DN59 peptide to either POPC or POPC/POPG vesicles containing a fluorescent dye and quencher caused extensive disruption of membrane integrity and leakage of contents to occur at concentrations as low as 2 μM (Figure 5B). These observations confirm that DN59 interacts strongly with liposome vesicles and is capable of disrupting artificial lipid bilayers. The observed peptide-lipid membrane interactions are not merely charge based, as binding and disruption occurred with both zwitterionic POPC vesicles as well as negatively-charged 9:1 POPC/POPG vesicles. Supporting these observations, a recent study of the membrane disruption ability of overlapping peptides from dengue virus type 2 C and E proteins showed that E protein stem derived peptides were highly disruptive to liposomes prepared with a wide variety of lipid compositions [19].

Previously DN59 had been shown to be non-toxic to cultured cells [14]. Similarly, tests using mammalian epithelial and mosquito cells did not show any toxicity at DN59 concentrations as high as 50 μM (Figure 5C). Nor did DN59 induce substantial

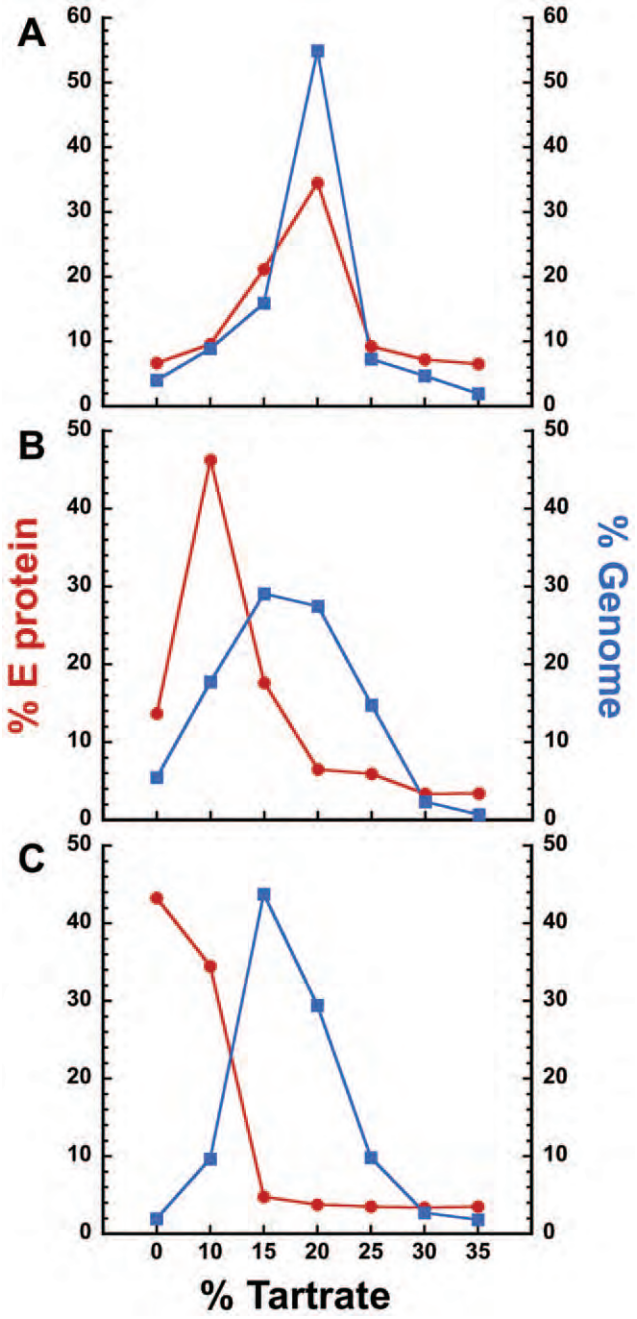

Figure 4. The E protein and genome of virus particles can be separated in a density gradient following treatment with DN59. Dengue virus was untreated (A), treated with 100 μM DN59 (B), or treated with 1% (v/v) triton (C), and centrifuged in a tartrate density gradient. Percent total E protein was measured by ELISA (red circles) and % total genome was measured by qRT-PCR (blue squares) in each fraction. Both peptide treatment and triton detergent treatment result in a separation of E protein and genome in the gradients.
doi:10.1371/journal.pone.0050995.g004

hemolysis of red blood cells (Figure 5D) illustrating that DN59 does not cause general disruption of cellular plasma membranes at concentrations as high as the 100 μM used for cryoEM. Additionally, DN59 does not inhibit the infectivity of other lipid-enveloped viruses, including Sindbis virus (an alphavirus) [14] or the negative-stranded RNA vesicular stomatitis virus (Figure S1C). The lack of apparent disruption of cellular plasma membranes and

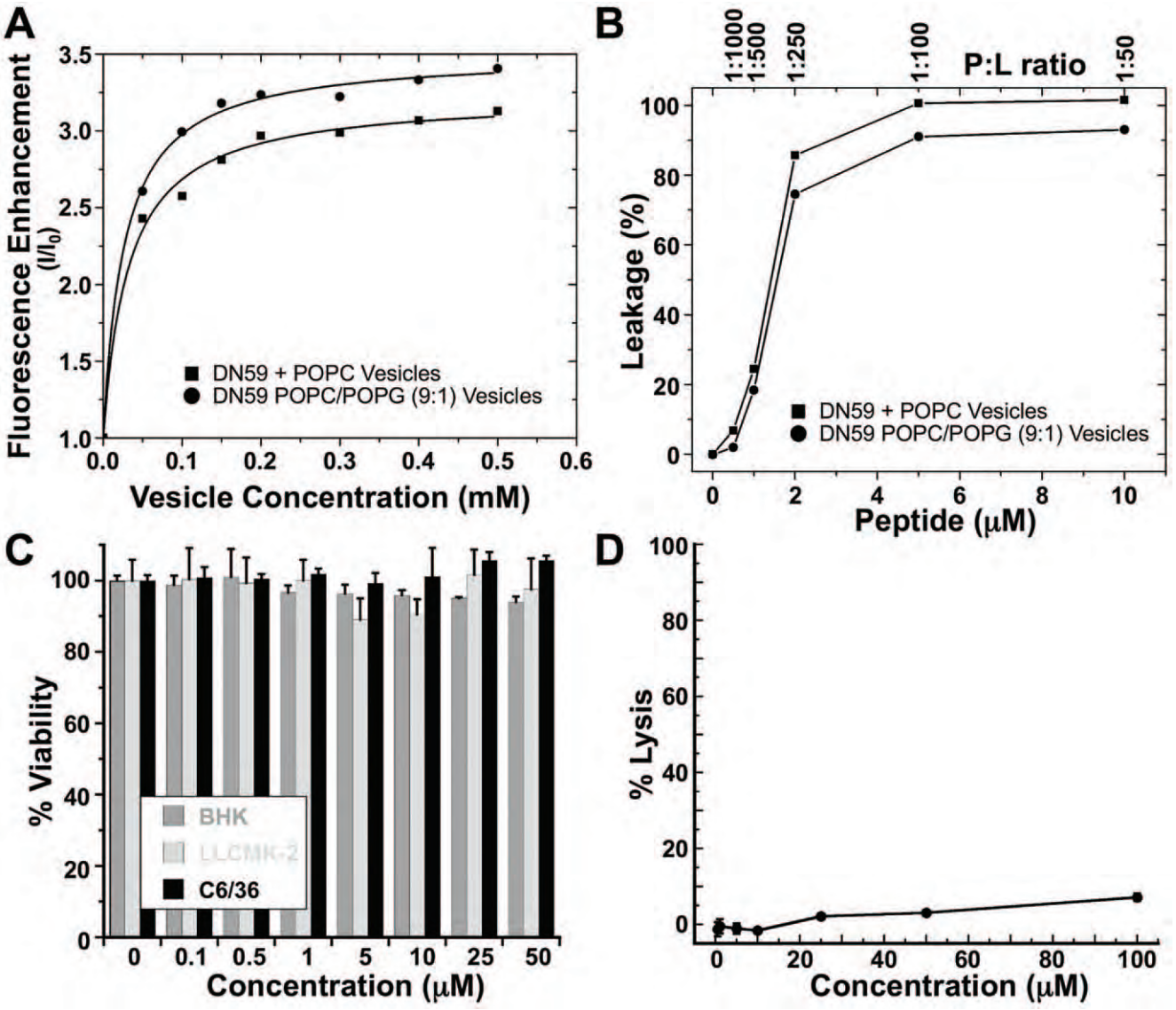

Figure 5. Interaction of DN59 peptide with lipid membranes. (A) DN59 interacts strongly with liposome vesicles. Tryptophan fluorescence-based binding curves for 1 μM DN59 with additions of zwitterionic vesicles made from POPC and anionic vesicles made from POPC and POPG at a 9:1 ratio. The intensities at 335 nm after each titration are shown and the solid lines are the result of curve fitting with a membrane partitioning equation [34]. (B) DN59 disrupts liposome vesicles. Leakage of the dye/quencher pair ANTS/DPX from 0.5 mM vesicles made from POPC or from POPC/POPG (9:1). Peptide was added to vesicles and the sample was incubated for 1 hr prior to the measurement of ANTS intensity. Treatment with 10 μM of the highly lytic bee venom peptide melittin was used to achieve 100% leakage. (C) DN59 is not cytotoxic. A mitochondrial reductase metabolic indicator assay (MTT) was used to test the cellular toxicity of DN59 on BHK-21 cells, LLC-MK_2 cells, and C6/36 cells. There was no significant toxicity of DN59 to cells even at the highest tested concentrations. (D) DN59 is not hemolytic. DN59 was co-incubated with sheep red blood cells and assayed for hemoglobin release. Treatment with 1% (v/v) triton was used to achieve 100% hemolysis.
doi:10.1371/journal.pone.0050995.g005

other viral membranes may be due to lipid composition, protein incorporation, or active repair of cellular membranes. Dengue virus particles bud from internal endoplasmic reticulum membranes of infected cells and so likely have a different composition from the plasma membrane, although the membrane disruption activity of stem region peptides is not strongly influenced by lipid membrane composition [19].

Schmidt et al. [20,21] studied a series of similar dengue E protein stem region peptides whose sequences extensively overlap the sequence of DN59 (residues 412-444 of dengue virus type 2 E protein). Consistent with our earlier work [14], they showed that their most active peptide (residues 419 to 447) inhibits dengue virus infection during an entry step and can bind to synthetic lipid vesicles. Furthermore, they reported that their peptide bound to the post-fusion trimeric form of recombinant dengue surface E protein [5,6] at low pH, but did not bind to the monomeric E protein at neutral pH. They therefore proposed that the peptide neutralizes the virus by first attaching to the viral membrane, and subsequently interacting with the E post-fusion trimers that form when the virus encounters the low pH environment of the endosome, thereby preventing fusion of the virus to the endosomal membrane. Here, however, we have shown that DN59 can induce the formation of holes in the viral membrane, release the genome, and causes the viral particles to become non-infectious even before

interacting with cells. The discrepancy in the mechanism of neutralization detected by our group and Schmidt et al. could possibly be due to the differences in peptide concentration used in these assays. Schmidt et al. showed that 1 μM of the peptide could neutralize 2.5×10^4 infectious virus particles, whereas in our cryoEM studies, the same concentration of DN59 causes RNA release from of 1×10^{10} virus particles. However, direct comparison between these two assays may not be possible. Van der Schaar et al. [22] showed that only a small percentage of the total virus (in the range of 1:2600 to 1:72000) is infectious. Since the neutralization test by Schmidt et al. [20] only shows the number of infectious virus particles, the actual total number of virus particles is not known.

The most likely mechanism by which DN59 or other stem region peptides can penetrate the outer layer of E glycoproteins and gain access to the virus membrane is by way of dynamic "breathing" of the virus particle [23,24,25,26]. The ease with which the virus can breathe will depend on the stability of the virus, which may account in part for the differing inhibitory activities against different flaviviruses (Figure S1A). Once the DN59 peptide has inserted itself between the E ectodomain and the membrane, it likely competes with and displaces the virus E protein stem region (helices H1 and H2) for binding to the lipid membrane and the "underside" of the E protein. Formation of holes in the viral membrane large enough for the escape of the RNA genome may involve structural changes in the surface E and M proteins, or may be due to the action of the peptide alone, similar to what is observed for some anti-microbial peptides [27,28] and what we observed with liposome vesicles. The negative charge on the tightly packaged RNA may also help the RNA to exit the virus particle once the membrane has been destabilized.

Our observations show that DN59, a 33 amino acid peptide mimicking a portion of the dengue virus E protein stem region, functions through an unexpected mechanism that involves disruption of the viral membrane and release of the viral genome.

Materials and Methods

Viruses and Cells

Dengue virus 1 (HI-1), dengue virus 2 (NGC-2), dengue virus 3 (H-78), dengue virus 4 (H-42), and yellow fever virus (17-D) were propagated in LLC-MK_2 cells (American Type Culture Collection (ATCC), Manassas, VA, cat. no. CCL-7) [15]. Russian spring summer encephalitis virus (Sofjin), and Central European encephalitis virus (Hypr) were propagated in BHK-21 cells (ATCC, cat. no. CCL-10). C6/36 cells (ATCC, cat. no. CRL-1660) were maintained in Dulbecco's modified eagle medium (DMEM) with 10% fetal bovine serum (FBS), 100 μM Non-essential amino acids, 2 mM Glutamax, 100 U/ml penicillin G, 100 μg/ml streptomycin and 0.25 μg/ml amphotericin B, at 30°C with 5% CO_2. For the cryo-electron microscopy studies, dengue virus 2 (16681) was grown in C6/36 cells and the tissue culture supernatant was collected on day 3-4, spun at $2,704\times g$ for 10 minutes at 4°C. 8% PEG in NTE (120 mM NaCl, 12 mM Tris, pH 8.0, 1 mM EDTA) was added to the tissue culture supernatant and mixed. The solution was then allowed to sit overnight before the PEG precipitated virus was centrifuged at $14,636\times g$ for 1 hr. The pellet was resuspended in 1 ml NTE buffer, loaded onto a 24% (w/v) sucrose cushion and centrifuged at $175,587\times g$ for 90 min. Pellets were resuspended overnight in NTE before being loaded onto a 10-30% (w/v) potassium sodium tartrate step gradient and centrifuged at $175,587\times g$ for 2 hrs. Purified virus was collected from the 20% potassium-tartrate fraction. The virus solution was then buffer exchanged to NTE buffer using an Amicon Ultra-4 centrifugal filter.

Peptides

Peptide stocks of DN59, the 33 amino acid pre-anchor domain peptide (MAILGDTAWDFGSLGGVFTSIGKALHQVFGAIY) and a randomly scrambled version of the peptide, DN59scr (YFIDTSGAIWGASHLTGVLFDFMGIQGGAVLAK) were purified and then prepared as approximately 1 mM stocks in 20% dimethylsulfoxide (DMSO): 80% H_2O [15]. Concentrations were calculated from side chain absorbance at 280 nm.

Focus Forming Unit (FFU) Reduction Assay

FFU reduction assays were performed as previously described [14]. Approximately 200 FFU of virus were incubated with peptide in serum-free DMEM for 1 hr at room temperature before infecting LLC-MK_2 cell monolayers for 1 hr at 37°C, and overlaying with media containing 0.85% (w/v) Sea-Plaque Agarose (Cambrex Bio Science, Rockland, ME). Infected cells were incubated at 37°C with 5% CO_2 for 2 days (yellow fever virus), 3 days (dengue virus 3 and 4, Russian spring summer encephalitis virus and Central European encephalitis virus) or 5 days (dengue virus 1and 2). Infected cultures were fixed with 10% (v/v) formalin, permeablized with 70% (v/v) ethanol, and foci were detected using mouse monoclonal antibodies against yellow fever virus (Chemicon, Temecula, CA), dengue (E60), or polyclonal anti-Kumlinge virus rED3 antisera, followed by horseradish peroxidase-conjugated goat anti-mouse immunoglobulin (Pierce, Rockford, IL), and developed using AEC chromogen substrate (Dako, Carpinteria, CA) as previously described [15,29].

Virus Inhibition on C6/36 Cells

C6/36 monolayers were infected with approximately 7,600 FFU of dengue virus 2 at 37°C for 1 hr before being aspirated, complete culture media added, and incubated at 37°C and 5% CO_2. After 72 hrs, RNA was isolated from cells using an RNeasy Mini Kit (Qiagen, Valencia, CA). qRT-PCR was performed as previously described [18].

Cryo-electron Microscopy

1 mM DN59 in 10% (v/v) DMSO was mixed with 18 μl of mature dengue virus to give a final DN59 concentration of 100 μM with 1% (v/v) DMSO. The mixture was incubated at 37°C for 30 min, then 4°C for 2 hrs and frozen on holey carbon grids. Dengue virus without peptide and dengue virus incubated with DMSO only controls were also frozen. Images were collected with a Philips CM200 cryo-electron microscope using 200 KV, a magnification of 50,000, an electron dose of 25 e^{-}/A^2, and taken at about 4.3 to 7 μm out-of-focus. Thirty-eight DN59 treated dengue virus particles were selected for three-dimensional (3D) image reconstruction. Initial models for 3D reconstructions were generated using the program starticos in EMAN [30]. This program correlates each image with itself after rotating by 72°, 120° and the starting model is essentially a random model based on combining the three orientations related by icosahedral symmetry. Subsequently, thirty iterations were performed in which the orientation of each of the raw images was determined relative to the current model from the previous cycle using the program SPIDER [31]. The images were split into two groups for resolution estimation, by observing the point at which the Fourier shell coefficient fell below 0.5 [32]. The final resolution was about 40 Å no matter whether N was chosen to be 3, 5, 8, 10 or 12

(Figure S3). Contours were chosen to only just avoid opening a hole in the capsid other than at the five-fold vertices.

RNase Assay and qRT-PCR

Approximately 1.4-2.9×10^4 FFU of dengue virus 2 was incubated with DN59 for 1 hr at room temperature and then digested with micrococcal nuclease (New England BioLabs, Ipswich, MA) for 1 hr at 37°C. RNA was extracted using the Qiagen RNeasy mini kit and qRT-PCR was performed as above using 10503F/10599R [33], 3 M-2F (TCACCAAATCCCACGGTAGAAGCA)/3 M-2R (AGGGCATGTATGGGTTGAGAACCT), M-1F (GAGGCTGGAAGCTAGAAG)/M-1R (GAGATACGGCACCTATGG), 5 M-1F (AAGCAGAACCTCCATTCGGAGACA)/5 M-1R (AAACACTCCTCCCAGGGATCCAAA), and 5-1F (AATCCCACCAACAGCAGGGATACT)/5-1R (CGCCATCACTGTTGGAATCAGCAT) primer sets.

Infectivity Inhibition Reversibility Assay

Similar to the FFU reduction assays, approximately 200 FFU of dengue virus 2 were incubated with 0 or 10 μM DN59 in a total volume of 100 μl serum-free DMEM for 1 hr at room temperature. Immediately before infecting LLC-MK_2 cell monolayers, the virus/peptide mixtures were diluted with serum-free DMEM to 1 ml, reducing the concentration of DN59 to 1 μM.

Tartrate Density Gradient Assay

Approximately 10^6 FFU of dengue virus 2 produced in LLC-MK_2 cells and purified as described above for the cryo-electron microscopy studies, was treated with 100 μM DN59 or 1% (v/v) triton X-100 for 30 min at 37°C. Treated virus was loaded onto a 10-35% (w/v) potassium sodium tartrate step gradient and centrifuged at 175,117×*g* for 2 hrs. Individual fractions were collected and assayed for virus genome and E protein. Genome quantitation was carried out by qRT-PCR as described above for the RNase sensitivity assay using the 10503F/10599R primer set [33]. E protein detection was carried out using modified ELISA. High bind 96-well plates (Costar, Corning, NY) were coated with concavalin A (Vector Laboratories, Burlingame, CA) at 25 mg/ml in 0.01 M HEPES (for 1 hr and washed with PBS containing 0.1% (v/v) Tween-20. Equal aliquots of each gradient fraction were added for 1 hr to allow binding of E to the concavalin A and then washed again. Captured E protein was detected using a human anti-E monoclonal antibody, followed by goat anti-human HRP conjugate. After a final wash, color was developed with tetramethylbenzidine-peroxide (TMB)-H_2O_2 stopped by adding 1% (v/v) phosphoric acid. Optical density was measured at 450 nm.

Lipid Vesicle Binding by Tryptophan Fluorescence

The lipids 1-palmitoyl-2-oleoyl-phosphatidylcholine (POPC) and 1-palmitoyl-2-oleoyl-phosphatidylglycerol (POPG) were purchased from Avanti Polar Lipids (Alabaster, AL). Lipids in chloroform solution were dried under vacuum overnight followed by hydration with phosphate buffered saline (PBS). Ten cycles of freezing and thawing were used to ensure solute entrapment. Unilamellar vesicles of 0.1 μm diameter were made by extrusion of the lipid suspension through 0.1 μm polycarbonate filters [34]. Tryptophan fluorescence spectra were measured on an SLM-Aminco fluorescence spectrophotometer. Samples were mixed in a 10×4 mm quartz cuvette and spectra were collected with excitation at 270 nm and emission from 300-450 nm. Lipid titrations were made from a 50 mM stock solution of vesicles in PBS, with 15 minutes of equilibration after each titration before measurements were made. Binding curves were obtained by taking the intensity at 335 nm for each spectra, minus the intensity of the appropriate peptide-free control sample.

Liposome Vesicle Leakage

The fluorescent dye 8-aminonaphthalene-1,3,6-trisulfonic acid (ANTS) and its obligate quencher p-xylene-bis-pyridinium bromide (DPX) were purchased from Invitrogen (Carlsbad, CA). Vesicles were prepared with ANTS/DPX entrapped inside where DPX quenches ANTS fluorescence [34]. Lipids were hydrated with buffer containing 50 mM ANTS and 12.5 mM DPX followed by extrusion and then gel filtration chromatography using Sephadex G-200 to exchange the external ANTS/DPX solution for buffer. In leakage experiments, 0.5 mM vesicles were mixed with peptide from 0.5 to 10 μM to give peptide to lipid ratios ranging from 1:50 to 1:1000. The increase in ANTS fluorescence after 1 hr incubation with peptide reports on vesicle leakage. A complete leakage control was achieved by the addition of 10 μM of the lytic bee venom peptide melittin.

Cell Toxicity Assays

Cytotoxicity of DN59 was measured by mitochondrial reductase activity using the TACS^{TM} MTT cell proliferation assay (R&D Systems Inc., Minneapolis. MN). DN59 in serum-free DMEM was added to LLC-MK_2, BHK, or C6/36 cells for 1 hr at 37°C, the solution was removed and the cells incubated at 37°C in complete medium with 5% CO_2 for 24 hrs.

Hemoglobin Release Assay

Sheep red blood cells (RBC) (Lampire Biological Products, Pipersville, PA) in anti-coagulant K2-EDTA, were washed and resuspended in PBS to a final concentration of 10% (v/v). Peptide was added to 2% RBC, incubated at 37°C for 1 hr and centrifuged at 13,000 rpm. Supernatants were collected and the absorbance at 560 nm was measured. Results were normalized against treatment with 1% (v/v) triton X-100 as a control for 100% hemolysis.

Vesicular Stomatitis Virus Plaque Reduction Assays

Plaque reduction assays in LLC-MK_2 cells were carried out in a similar manner as above, except that a 1.2% solution of methylcellulose (FMC, Philadelphia, PA) in complete medium was used in place of agarose. Vesicular stomatitis virus eGFP-P was incubated for 24 hrs at 37°C before overlays were aspirated, rinsed with PBS, and plaques were visualized for GFP expression [35].

Supporting Information

Figure S1 Inhibitory effect of DN59 is dependent on its interaction with flavivirus particles. (A) Co-incubation of DN59 with other flaviviruses showed dose response inhibition in a focus-forming unit reduction assay with somewhat higher 50% inhibition concentrations compared to dengue virus. (B) Focus-forming unit reduction assay indicates that DN59 has no inhibitory effect on dengue virus infection when the peptide is added to LLCMK-2 cells and removed prior to the addition of dengue virus, or when DN59 is added to cells that had already been infected. (C) DN59 was co-incubated with the enveloped, negative-stranded RNA, vesicular stomatitis virus (VSV), and infectivity was assayed in a plaque reduction assay. No substantial inhibition of VSV was observed.
(TIF)

Figure S2 Homogeneity of virus particle preparations used for EM imaging. Lower magnification CCD images of control (A) and DN59 treated (B) dengue virus showed that the control virus particles were relatively homogenous and mature. DN59 treated particles clumped and were obscured by an electron dense material.
(TIF)

Figure S3 CryoEM image reconstruction of DN59 treated dengue 2 virus. (A) CryoEM image of DN59 treated particles. The particles appeared empty. (B) Reconstruction and validation of the cryoEM structure. Different starting models (West Nile virus, as well as five reference free models generated using the program starticos [30] with a different number (N) of particles used in the classification of particles with five-fold, three-fold and two-fold projected views) were used to reconstruct untreated control and DN59-treated dengue particles. To permit a direct comparison of the reconstructions produced by these different starting models, the arbitrary contour levels of the control maps were set at two different values. The high contour level was adjusted until the five-fold densities were just visible and the lower contour level was adjusted until holes at the three-fold vertices were just visible. For the DN59-treated dengue virus particles, the contour level was adjusted until the holes at three-fold vertices were just visible. Five out of six starting models for cryoEM image reconstruction of DN59-treated dengue virus had a dominant hole at the five-fold vertices. None of the untreated dengue virus controls had a hole at the five-fold vertices.
(TIF)

Acknowledgments

We thank Y. Xiang (Purdue University) for useful and insightful discussions.

Author Contributions

Conceived and designed the experiments: JMC SML WCW MGR SI RFG SFM. Performed the experiments: SML VK MGR HH PC PK JMC YMH MRH DKR KAF SI ARH. Analyzed the data: JMC SML WCW MGR SI RFG SFM. Wrote the paper: SML JMC WCW MGR SFM.

References

1. Kuhn RJ, Zhang W, Rossmann MG, Pletnev SV, Corver J, et al. (2002) Structure of dengue virus: implications for flavivirus organization, maturation, and fusion. Cell 108: 717–725.
2. Zhang W, Chipman PR, Corver J, Johnson PR, Zhang Y, et al. (2003) Visualization of membrane protein domains by cryo-electron microscopy of dengue virus. Nat Struct Biol 10: 907–912.
3. Pokidysheva E, Zhang Y, Battisti AJ, Bator-Kelly CM, Chipman PR, et al. (2006) Cryo-EM reconstruction of dengue virus in complex with the carbohydrate recognition domain of DC-SIGN. Cell 124: 485–493.
4. Stiasny K, Allison SL, Schalich J, Heinz FX (2002) Membrane interactions of the tick-borne encephalitis virus fusion protein E at low pH. J Virol 76: 3784–3790.
5. Modis Y, Ogata S, Clements D, Harrison SC (2004) Structure of the dengue virus envelope protein after membrane fusion. Nature 427: 313–319.
6. Bressanelli S, Stiasny K, Allison SL, Stura EA, Duquerroy S, et al. (2004) Structure of a flavivirus envelope glycoprotein in its low-pH-induced membrane fusion conformation. EMBO J 23: 728–738.
7. Rey FA, Heinz FX, Mandl C, Kunz C, Harrison SC (1995) The envelope glycoprotein from tick-borne encephalitis virus at 2 Å resolution. Nature 375: 291–298.
8. Modis Y, Ogata S, Clements D, Harrison SC (2003) A ligand-binding pocket in the dengue virus envelope glycoprotein. Proc Natl Acad Sci USA 100: 6986–6991.
9. Zhang Y, Zhang W, Ogata S, Clements D, Strauss JH, et al. (2004) Conformational changes of the flavivirus E glycoprotein. Structure 12: 1607–1618.
10. Modis Y, Ogata S, Clements D, Harrison SC (2005) Variable surface epitopes in the crystal structure of dengue virus type 3 envelope glycoprotein. J Virol 79: 1223–1231.
11. Lalezari JP, Henry K, O'Hearn M, Montaner JSG, Piliero PJ, et al. (2003) Enfuvirtide, an HIV-1 fusion inhibitor, for drug-resistant HIV infection in North and South America. N Engl J Med 348: 2175–2185.
12. Champagne K, Shishido A, Root MJ (2009) Interactions of HIV-1 inhibitory peptide T20 with the gp41 N-HR coiled coil. J Biol Chem 284: 3619–3627.
13. Liao M, Kielian M (2005) Domain III from class II fusion proteins functions as a dominant-negative inhibitor of virus membrane fusion. J Cell Biol 171: 111–120.
14. Hrobowski YM, Garry RF, Michael SF (2005) Peptide inhibitors of dengue virus and West Nile virus infectivity. Virol J 2: 49.
15. Costin JM, Jenwitheesuk E, Lok S-M, Hunsperger E, Conrads KA, et al. (2010) Structural optimization and de novo design of dengue virus entry inhibitory peptides. PLoS Negl Trop Dis 4: e721.
16. Thaisomboonsuk BK, Clayson ET, Pantuwatana S, Vaughn DW, Endy TP (2005) Characterization of dengue-2 virus binding to surfaces of mammalian and insect cells. Am J Trop Med Hyg 72: 375–383.
17. Zaitseva E, Yang S-T, Melikov K, Pourmal S, Chernomordik LV (2010) Dengue virus ensures its fusion in late endosomes using compartment-specific lipids. PLoS Pathog 6: e1001131.
18. Nicholson CO, Costin JM, Rowe DK, Lin L, Jenwitheesuk E, et al. (2011) Viral entry inhibitors block dengue antibody-dependent enhancement *in vitro*. Antiviral Res 89: 71–74.
19. Nemesio H, Palomares-Jerez F, Villalain J (2011) The membrane-active regions of the dengue virus proteins C and E. Biochim Biophys Acta 1808: 2390–2402.
20. Schmidt AG, Yang PL, Harrison SC (2010) Peptide inhibitors of dengue-virus entry target a late-stage fusion intermediate. PLoS Pathog 6: e1000851.
21. Schmidt AG, Yang PL, Harrison SC (2010) Peptide inhibitors of flavivirus entry derived from the E protein stem. J Virol 84: 12549–12554.
22. van der Schaar HM, Rust MJ, Waarts BL, van der Ende-Metselaar H, Kuhn RJ, et al. (2007) Characterization of the early events in dengue virus cell entry by biochemical assays and single-virus tracking. J Virol 81: 12019–12028.
23. Bothner B, Dong XF, Bibbs L, Johnson JE, Siuzdak G (1998) Evidence of viral capsid dynamics using limited proteolysis and mass spectrometry. J Biol Chem 273: 673–676.
24. Lewis JK, Bothner B, Smith TJ, Siuzdak G (1998) Antiviral agent blocks breathing of the common cold virus. Proc Natl Acad Sci USA 95: 6774–6778.
25. Johnson JE (2003) Virus particle dynamics. Adv Protein Chem 64: 197–218.
26. Lok SM, Kostyuchenko V, Nybakken GE, Holdaway HA, Battisti AJ, et al. (2008) Binding of a neutralizing antibody to dengue virus alters the arrangement of surface glycoproteins. Nat Struct Mol Biol 15: 312–317.
27. Cruciani RA, Barker JL, Durell SR, Raghunathan G, Guy HR, et al. (1992) Magainin 2, a natural antibiotic from frog skin, forms ion channels in lipid bilayer membranes. Eur J Pharmacol 226: 287–296.
28. Matsuzaki K, Murase O, Fujii N, Miyajima K (1995) Translocation of a channel-forming antimicrobial peptide, magainin 2, across lipid bilayers by forming a pore. Biochemistry 34: 6521–6526.
29. Tigabu B, Juelich T, Bertrand J, Holbrook MR (2009) Clinical evaluation of highly pathogenic tick-borne flavivirus infection in the mouse model. J Med Virol 81: 1261–1269.
30. Ludtke SJ, Baldwin PR, Chiu W (1999) EMAN: semiautomated software for high-resolution single-particle reconstructions. J Struct Biol 128: 82–97.
31. Shaikh TR, Gao H, Baxter WT, Asturias FJ, Boisset N, et al. (2008) SPIDER image processing for single-particle reconstruction of biological macromolecules from electron micrographs. Nat Protoc 3: 1941–1974.
32. van Heel M, Schatz M (2005) Fourier shell correlation threshold criteria. J Struct Biol 151: 250–262.
33. Chutinimitkul S, Payungporn S, Theamboolers A, Poovorawan Y (2005) Dengue typing assay based on real-time PCR using SYBR Green I. J Virol Methods 129: 8–15.
34. White SH, Wimley WC, Ladokhin AS, Hristova K (1998) Protein folding in membranes: determining energetics of peptide-bilayer interactions. Methods Enzymol 295: 62–87.
35. Schott D, Cureton DK, Whelan SP, Hunter C (2005) An antiviral role for the RNA interference machinery in *Caenorhabditis elegans*. Proc Natl Acad Sci USA 102: 18420–18424.

JVI Accepts, published online ahead of print on 17 October 2012
J. Virol. doi:10.1128/JVI.02273-12

Title

Mechanistic study of broadly neutralizing human monoclonal antibodies against dengue virus that target the fusion loop

Running Title

Human dengue antibodies that inhibit fusion

Authors

Joshua M. Costin[1]†, Elena Zaitseva[2]†, Kristen M. Kahle[3], Cindo O. Nicholson[1], Dawne K. Rowe[1], Amanda S. Graham[1], Lindsey E. Bazzone[4], Greg Hogancamp[1], Marielys Figueroa Sierra[1], Rachel H. Fong [3], Sung-Tae Yang[2], Li Lin[5], James E. Robinson[4], Benjamin J. Doranz[3], Leonid V. Chernomordik[2], Scott F. Michael[1], John S. Schieffelin[4], and Sharon Isern[1]#

Affiliation

[1]Department of Biological Sciences, Florida Gulf Coast University, Fort Myers, FL 33965 USA; [2]Section on Membrane Biology, Laboratory of Cellular and Molecular Biophysics, Eunice Kennedy Shriver National Institute of Child Health and Human Development, National Institutes of Health, Bethesda, MD, 20892 USA; [3]Integral Molecular, Inc., Philadelphia, PA 19104 USA; [4]Section of Pediatric Infectious Disease, Department of Pediatrics, Tulane University School of Medicine, New Orleans, LA, 70112 USA; and [5]Communicable Disease Center, Tan Tock Seng Hospital, Singapore 308433

#Corresponding author sisern@fgcu.edu

†Authors contributed equally to the work.

Present Address

C.O.N.: Department of Molecular Genetics and Microbiology, Duke University Medical Center, Durham, NC 27710 USA

D.K.R.: University of Georgia College of Veterinary Medicine, Athens, GA 30602 USA

M.F.S.: Florida State University College of Medicine, Tallahassee, FL 32304 USA

S.-T.Y.: Department of Molecular Physiology and Biological Physics, University of Virginia, Charlottesville, VA 22908 USA

L.L.: Department of Medicine, Alexandra Hospital, Singapore 159964

Abstract Word Count = 227

Text Word Count = 10,095

Abstract

There are no available vaccines for dengue, the most important mosquito-transmitted viral disease. Mechanistic studies with anti-dengue virus (DENV) human monoclonal antibodies (hMAbs) provide a rational approach to identify and characterize neutralizing epitopes on DENV structural proteins that can serve to inform vaccine strategies. Here we report a class of hMAbs that is likely to be an important determinant in the human humoral response to DENV infection. In this study, we identified and characterized three broadly neutralizing anti-DENV hMAbs 4.8A, D11C, and 1.6D. These antibodies were isolated from three different convalescent patients with distinct histories of DENV infections, yet demonstrated remarkable similarities. All three hMAbs recognized the E glycoprotein with high affinity, neutralized all four serotypes of DENV, and mediated antibody-dependent enhancement of infection in Fc receptor-bearing cells at sub-neutralizing concentrations. Neutralization activity of these hMAbs correlated with a strong inhibition of virus-liposome and intracellular fusion, not virus-cell binding. We mapped epitopes of these antibodies to the highly conserved fusion loop region of E domain II. Mutations at fusion loop residues W101, L107, and/or G109 significantly reduced the binding of the hMAbs to E protein. The results show that hMAbs directed against the highly conserved E protein fusion loop block viral entry downstream of virus-cell binding by inhibiting E protein-mediated fusion. Characterization of hMAbs targeting this region may provide new insights into DENV vaccine and therapeutic strategies.

Introduction

62 Dengue imposes one of the largest socioeconomic burdens of any mosquito-borne
63 human disease in the world, yet there is currently no available vaccine or specific
64 treatment. Worldwide, there are an estimated 50 to 100 million cases of dengue infection
65 per year and 2.5 billion people living in dengue endemic regions are at risk of infection (49,
66 83). An estimated 500,000 people, many of them children, are hospitalized annually with
67 severe dengue symptoms including dengue hemorrhagic fever/dengue shock syndrome
68 (DHF/DSS) (26, 83). Of note, after an extended absence, dengue has recently re-emerged in
69 South Florida (5, 25). Local transmission has also recently been reported in Southern
70 France and Croatia (44, 66).

71 The four distinct serotypes of dengue virus (DENV) co-circulate in many areas of the
72 world and give rise to sequential epidemic outbreaks when the number of susceptible
73 individuals in the local population reaches a critical threshold and weather conditions
74 favor reproduction of the mosquito vectors *Aedes aegypti* and *Aedes albopictus*. Initial
75 infection with one DENV serotype usually generates a protective and long-lasting immune
76 response against re-infection with the same serotype. While antibody cross-reactivity
77 between serotypes is common, cross-serotype protection is only short lived (64). Low
78 levels of neutralizing antibodies, cross-reactive but non-neutralizing antibodies, or both,
79 from previous infections bind virions of other serotypes and target them to Fc receptors on
80 macrophages and certain other cell types, enhancing infection of these cells (31). The
81 presence of these cross-reactive and non-neutralizing antibodies also correlated with
82 severe disease outcome (DHF/DSS) in several studies (30, 42, 78). Higher levels of viremia
83 are associated with the development of DHF (78, 79). This antibody-dependent

84 enhancement (ADE) effect may also explain the sequential nature of epidemic outbreaks, as
85 well as the severe disease seen in infants as maternal antibodies wane (30, 42, 69).
86 Like other members of the flavivirus genus, DENV has a lipid envelope and a
87 positive-stranded RNA genome that codes for a single large polyprotein. This polyprotein
88 is cleaved into separate segments to form the structural proteins capsid (C), premembrane
89 (prM/M), and envelope (E), and enzymatic components required for viral replication and
90 transmission (6). The external E glycoprotein participates in cell recognition and cell entry
91 and is physically arranged in a herringbone pattern as a series of 90 homodimers on the
92 outer surface of the mature virus particle (43). On immature particles, the prM protein lies
93 over the E protein and serves to protect the virus particle from undergoing premature
94 fusion or inactivation within the secretory pathway of the host cell. PrM is subsequently
95 cleaved by a host protease to release the ectodomain and allow for viral maturation (85).
96 The E protein consists of three structural domains (D), DI, DII and DIII (50, 59). At one end
97 of the molecule is the fusion loop within DII and at the other end is DIII, which is involved
98 in host cell binding (15). Upon infection and entry of DENV into the acidic environment of
99 the endosome, the E proteins undergo a conformational change and re-assemble into 60
100 trimers with their fusion loops forming the tip of a trimeric spike oriented to insert into the
101 endosomal membrane within the target cell. Subsequent reconfiguration of the E protein
102 trimers results in fusion of the viral membrane and target cell endosomal membrane to
103 facilitate release of viral contents into the cytoplasm (33, 36, 87).
104 The nature of the human antibody response against DENV is likely to play a
105 dominant role in defining the outcome of infection. A preponderance of antibodies that
106 recognize neutralizing epitopes will lead to virus clearance and reduced symptoms, while

an abundance of antibodies that recognize enhancing epitopes will lead to more severe disease. Multiple questions remain about the nature of the antibody balance, including which epitopes are most important for neutralization versus enhancement and whether these are distinct or overlapping epitopes.

Studies with serum from convalescent DENV patients have yielded conflicting information regarding the human antibody response and the epitopes that these antibodies target. Interestingly, while one of the predominant epitopes recognized by human serum antibodies appears to include the fusion loop and adjacent regions (45, 47), one study reported that these fusion loop antibodies are non-neutralizing (45). He et al. tested the ability of patient sera to block binding of DENV-2 to Vero cells and reported that neutralization occurred primarily by blocking cell attachment, suggestive of a major role for antibodies targeting DIII (35). In contrast, Wahala et al. subsequently reported that human antibodies directed towards epitopes other than DIII (presumably DI/II) are primarily responsible for neutralization (81).

Monoclonal antibodies have been used to further elucidate important epitopes. However, to date, most anti-DENV monoclonal antibodies are of murine origin (mMAbs) generated from mice (15, 29, 70). MMAbs may not accurately represent the human antibody response against DENV, as mice do not experience human disease other than a transitory viremia and produce an antibody response with a more limited diversity and typically lower affinity antibodies than humans.

Recent studies with human monoclonal anti-DENV antibodies (hMAbs) have highlighted both similarities and major differences between the behavior of serum from convalescent DENV patients and purified hMAbs. In Schieffelin et al. three antibodies that

targeted the E protein were isolated from a single donor (65). All three antibodies were cross-reactive with at least two DENV serotypes, one was neutralizing, and all were able to enhance DENV infection. Dejnirattisai et al. reported that in a panel of hMAbs from seven donors, the majority of the antibody response was against prM and was very poorly neutralizing, but highly enhancing (19). Beltramello et al. described a wide variety of hMAbs from five DENV patients (4). These included hMAbs against prM as well as E. However, in contrast to the findings of Dejnirattisai, et al., half of the prM hMAbs reported by Beltramello et al. showed substantial neutralization activity (4). Among the hMAbs recognizing E, Beltramello et al. described antibodies targeting DI/II and DIII. The DIII hMAbs were very highly neutralizing, and included serotype specific and cross-reactive examples. The neutralization activity of the DI/II hMAbs was more diverse and included non-neutralizing, serotype specific neutralizing, and cross-neutralizing examples. Two of the cross-neutralizing DI/II hMAbs were mapped to the fusion loop using WNV E protein mutants.

De Alwis et al. 2011 reported that after primary infection most hMAbs were cross-reactive and weakly neutralizing, and that many bound to prM (17). Using a modified screening procedure, they were able to detect rare DIII hMAbs that were serotype-specific and strongly neutralizing. Recently, de Alwis et al. 2012 reported that the majority of antibodies in human sera bound to intact virions, not monomeric E (18). They found that though abundant in human sera, cross-reactive antibodies did not contribute to neutralization and that type-specific antibodies were responsible for potent neutralization. These findings were confirmed with 3 hMAbs that were isolated by first screening for antibodies that bound to intact virions and then screened for a subset of antibodies that

were potently neutralizing. They generated escape mutants and mapped the mutations to the quaternary epitopes containing contacts on two different E proteins in hinge region between DI and II.

These studies with hMAbs emphasize the complexity of the human antibody response against DENV and highlight the importance of further examination of the roles of different epitopes in prM, E protein DI/II (either the fusion loop or the hinge region) and in DIII, and the mechanisms by which different antibodies neutralize DENV infection. For instance, an affected stage of viral entry – virus binding to cell surface vs. fusion between viral envelope and endosomal membrane, has never been identified for any neutralizing hMAb.

In this work, we specifically screened for broadly cross-reactive and neutralizing hMAbs from three patients with distinct histories of DENV infection, and we identified three similar hMAbs that mapped to the conserved epitope containing the E protein DII fusion loop. These hMAbs were broadly reactive, high affinity, and conformationally sensitive. With some exceptions they showed broad, but intermediate neutralization activity against all four DENV serotypes, and also enhanced all four serotypes. Using a novel assay, we confirmed that these hMAbs inhibited intracellular virus fusion during entry, rather than cell binding, and provide a mechanistic characterization of these hMAbs.

Materials and Methods

Cells, viruses, and recombinant E proteins

The *Macaca mulatta* kidney epithelial cell line LLC-MK_2 (American Type Culture Collection (ATCC), Manassas VA), used in neutralization assays and to propagate DENV, and

176 the human embryonic kidney cell line, HEK-293T (ATCC), used for cloning and expression
177 of hMAbs were grown in Dulbecco's modified eagle medium (DMEM) containing 10% (v/v)
178 fetal bovine serum (FBS), 2 mM Glutamax, 100 U/ml penicillin G, 100 µg/ml streptomycin
179 and 0.25 µg/ml amphotericin B, at 37°C with 5% (v/v) CO_2. K-562 human hematopoietic
180 cells (ATCC), used for virus enhancement assays, were grown in RPMI-1640, 10% (v/v)
181 FBS, 2 mM Glutamax, 100 U/ml penicillin G, 100 µg/ml streptomycin and 0.25 µg/ml
182 amphotericin B, at 37°C with 5% (v/v) CO_2. The *Macaca mulatta* kidney epithelial cell line
183 MA104 (ATCC) used in intracellular fusion and pre-fusion assays were grown in Advanced
184 DMEM medium (ADMEM) supplemented with 10% fetal bovine serum, 25 mM HEPES, 292
185 µg/ml L-glutamine, 100 U/ml penicillin G, 100 µg/ml streptomycin, at 37°C with 5% (v/v)
186 CO_2. Human embryonic kidney cell line HEK-293 (ATCC) used in epitope mapping to
187 express prM/E mutants were grown in DMEM supplemented with 10% (v/v) FBS, 10 mM
188 Hepes, 100 U/ml penicillin G, 100 µg/ml streptomycin, 1 mM sodium pyruvate, 2 mM L-
189 glutamine (Mediatech), and 1X non-essential amino acids mixture (BioWhittaker, Lonza
190 Walkersville, Inc. Walkersville, MD) at 37°C with 5% (v/v) CO_2.

191 DENV-1 strain HI-1, DENV-2 strain NG-2, DENV-3 strain H-78, and DENV-4 strain H-
192 42 were obtained from R. Tesh at the World Health Organization Arbovirus Reference
193 Laboratory at the University of Texas at Galveston. Viruses were propagated in LLC-MK_2 as
194 previously described (65). LLC-MK_2 cells were inoculated with DENV stock at 70% to 80%
195 confluency, cultured in DMEM and 10% (v/v) fetal bovine serum (FBS). Following the
196 appropriate incubation period for the various DENV strains, cell culture supernatant was
197 collected and used in neutralization and enhancement assays or the culture media was
198 switched to Protein Free Hybridoma Medium (Gibco, Carlsbad, CA) prior to use in antibody

detection ELISA assays. Infected adherent cells as well as supernatant fluids were collected and treated with 1% (v/v) Triton X-100 to solubilize and inactivate virus as described previously and both were aliquoted and stored at -20°C for use in ELISA assays (65).

Purified DENV-2 strain NG-2 virions used in SDS-PAGE were prepared from large-scale cultures of infected LLC-MK_2 cells as follows. Virus particles in cell culture supernatant were precipitated in 8% (w/v) polyethylene glycol 8000 (PEG) in an SLA-3000 rotor at 9,300 rpm for 51 min at 4°C, pelleted in a 24% (w/v) sucrose cushion using an SW-41 ti rotor at 32,000 rpm for 90 min at 4°C, equilibrium banded using a 10-35% potassium sodium tartrate step density gradient in a SW-41 ti rotor at 32,000 rpm for 2 hr at 4°C, and dialyzed and concentrated using an Amicon Ultra-4 centrifugal filter unit (Millipore, Billerica, MA) in NTE buffer (120 mM NaCl, 12 mM Tris, 1 mM EDTA, pH 8.0).

Recombinant DENV-1, 2, 3, and 4 sE containing the N-terminal 80% of E protein expressed in *Drosophila melanogaster* strain Schneider 2 cells and purified by affinity chromatography were obtained from Hawaii Biotech Inc. (Aiea, HI) (16, 50). Recombinant DENV-2 N-terminal E protein containing domains I and II (sDI/II), and DENV-2 E protein domain III (sDIII) expressed in *Escherichia coli* were obtained from Meridian Life Science (Saco, ME).

Patient samples

The collection and use of human blood samples for this project was reviewed and approved by the institutional review boards of Florida Gulf Coast University, Tulane University School of Medicine, and Tan Tock Seng Hospital. Informed written consent was obtained for all patients. Three patients were identified as having recovered from DENV infection. Patient 7B had acquired DENV while traveling in Myanmar. Blood was drawn

from this patient two years post-hospitalization as previously described (65). Patient DA003 was hospitalized in Singapore and had blood drawn approximately 4 weeks post-recovery. As DENV IgG antibodies were detected in addition to IgM antibodies, the patient was diagnosed with secondary dengue infection with low disease severity since no hemo-concentration or bleeding were present. Patient 8C contracted DENV in Jamaica and had blood drawn approximately three months post-recovery. The patient had fever for 12 days, headache, retro-orbital pain, and blood in sputum on day 10. No information on the type of DENV antibodies present was available from this patient. For all patients, blood was drawn after informed written consent was obtained, and PBMCs were isolated by Ficoll-Hypaque gradient centrifugation and viably frozen in liquid nitrogen. The patient sera were tested by ELISA and neutralization assays to positively determine infection with DENV.

Epstein-Barr virus transformation

The production of hMAbs by Epstein-Barr virus (EBV) transformation of B cells has previously been described (61, 62, 65, 84). Using this method, transformed clonal B cell lines were produced for hMAbs 4.8A (65) and D11C. Briefly, cryopreserved PBMCs were thawed, placed in culture, and inoculated with EBV (B95-8 strain). Cells were resuspended in RPMI containing 20% (v/v) FBS, Primacin (InVivoGen, San Diego, CA) and 2 μg/ml CpG 2006 (Midland Certified Reagent Co., Midland, TX) and plated at 10^4 cells per well in 96-well tissue culture plates. These plates had been previously seeded with approximately 50,000 irradiated mature macrophages per well derived from PBMCs of healthy blood donors that served as feeder cultures to promote outgrowth of transformed B cells. Antibody-positive wells containing viable cells were sub-cultured at several dilutions and re-screened by ELISA. Cell lines that continued to grow and produce antibody during

several low cell density passages were finally cloned at limiting dilution. Definitively cloned cell lines were expanded to grow as suspension cultures in stationary 490 cm^2 roller bottle cultures (Corning, Corning, NY) from which cell culture fluid was harvested weekly. HMAbs were purified from one to two liters of culture supernatant by protein A affinity chromatography. The IgG subclass and light chain type of each antibody was determined by reactivity with mMAbs to the four heavy chain subclasses (Southern Biotech, Birmingham, AL) and polyclonal goat antibodies to kappa and lambda chains by ELISA using established methods.

Cloning and expression of human monoclonal antibodies

To generate hMAbs, transient stimulation of memory B-cells was used as an alternative approach to EBV transformation (55). HMAb 1.6D was isolated using this method. Cryopreserved PBMCs were thawed and washed as above and then resuspended in RPMI containing 20% (v/v) FBS, Primacin, 2.5 µg/ml R848, a toll-like receptor 7 (TLR) and TLR8 agonist (InvivoGen, San Diego, CA) and 50 U/ml recombinant human interleukin-2 (Roche Diagnostics Corporation, Indianapolis, IN). After incubating for three days at 37°C and 5% (v/v) CO_2, cells were recounted and plated at 500 to 10^4 cells per well in 96-well tissue culture plates containing feeder cells.

To generate molecular clones of hMAbs, we constructed linear full-length Ig heavy- and light-chain gene expression cassettes as described (46). Molecular clones were constructed for hMAbs 1.6D, from stimulated PBMCs, and D11C, from the transformed B-cell line. Briefly, RNA extracted from hMAb positive B cells was reverse transcribed and cloned into gene expression cassettes. Purified PCR products of the paired Ig heavy and light chain gene expression cassettes were co-transfected into 80–90% confluent HEK-

293T cells grown in 48-well tissue culture plates (300 ng of each chain per well) using Fugene Transfection Reagent (Roche Diagnostics Corporation, Indianapolis, IN) following manufacturer's instructions. Transfection supernatants were tested for hMAb production against all four DENV serotypes by Concanavalin A (ConA) ELISA. Positive cultures were seeded into 96-well plates in DMEM with 10% (v/v) FBS and 20 μg/ml Blastocidin S (InvivoGen), to ensure formation of stable hMAb-producing cell lines. Cultures were cloned by serial subculture at progressively lower cell densities in 96-well plates, with repeated antibody screening at each step. Molecular clones were constructed for hMAbs 1.6D, from stimulated PBMCs, and D11C, from the transformed B-cell line.

Antibody detection with enzyme-linked immunosorbent assay

B cell cultures were screened for antibody production using ELISA as described previously (61, 65). Briefly, 96-well plates (Costar, Corning, Corning, NY) were coated with ConA at 25 μg/ml in 0.01 M HEPES (Gibco, Carlsbad, CA) for 1 hr. The wells were washed (PBS containing 0.1% (v/v) Tween-20) and Triton X-100-solubilized DENV produced in serum free medium was incubated for 1 hr. All steps in this ELISA were performed at room temperature. After a wash step, unreacted ConA binding sites in the wells were blocked with RPMI Medium 1640 and 10% (v/v) FBS for 30 min. Samples from B cell cultures were transferred to assay plates and incubated for 1 hr. The wells were again washed and incubated with peroxidase-conjugated goat anti-human IgG-gamma (Zymed, San Francisco, CA) or peroxidase-conjugated affinity purified anti-mouse IgG (Rockland, Gilbertsville, PA) diluted 1:2000 in PBS containing 0.5% (v/v) Tween-20, 10% (w/v) whey (BiPro, Le Sueur, MN), and 10% (v/v) FBS for 1 hr. After a final wash step, color was developed with

tetramethylbenzidine-peroxide (TMB)-H_2O_2 as substrate for peroxidase. The reaction was stopped after 4 min by adding 1% (v/v) phosphoric acid and color was read as optical density (OD) at 450 nm.

Confocal microscopy

DENV-infected cells were immunostained with hMAbs and imaged using confocal microscopy. LLC-MK_2 cells were grown on No. 1.5 Gold Seal cover glass coverslips (Erie Scientific Company, Portsmouth, NH) placed in each well of a 6-well plate overnight to 80% confluency. Wells containing coverslips were infected with DENV in serum free media at a multiplicity of infection (MOI) of 0.002 for 1 hr at 37°C, aspirated, fresh culture media added, and incubated 3 days at 37°C. Infected cultures were fixed with 10% (w/v) formalin overnight at 4°C, permeabilized with 70% (v/v) ethanol for 20 min, and rinsed with PBS prior to immunostaining. Virus proteins were detected using 1µg/ml hMAb 4.8A, D11C, or 1.6D (American Type Culture Collection, Manassas, VA) overnight at 4°C, followed by 2µg/ml goat anti-human Alexa Fluor 488 (Invitrogen Corporation, Carlsbad, CA) for 4 hr at RT. Cells were then counterstained with 2 µg/ml Hoechst (Cambrex, Walkersville, MD) for 10 min at room temperature and washed with PBS. Coverslips were mounted on Fisherbrand Superfrost microscope slides (Fisher Scientific, Pittsburgh, PA) using Fluormount-G (Southern Biotech, Birmingham, AL) and visualized on an Olympus FV1000 Confocal Microscope System.

Western blotting

Purified DENV-2, DENV-2 sE, produced as described (16, 50) (Hawaii Biotech Inc., Aiea, HI), DENV-2 E sDI/II, and DENV-2 E sDIII (Meridian Life Science, Saco, ME) were

subjected to SDS-PAGE using 4-15% (w/v) or 15% (w/v) Tris-HCl polyacrylamide preparative gels, for purified DENV-2 and soluble recombinant proteins, respectively (Bio-Rad, Hercules CA). Unless otherwise specified, samples were electrophoresed under non-reducing conditions in 25 mM Tris, 192 mM glycine, 3.5 mM SDS (Sigma-Aldrich, St. Louis, MO) and loaded in a buffer containing 0.7% (w/v) SDS. Reduced samples were loaded in a buffer containing 0.005% (w/v) SDS and 40 mM DTT. Precision Plus protein Kaleidoscope ladder was used as a standard (Bio-Rad, Hercules, CA). Proteins were transferred to Amersham Hybond-LFP PVDF membranes (GE Healthcare, Piscataway NJ) in 25 mM Tris, 192 mM glycine, and 20% (v/v) methanol (Fisher, Pittsburgh PA), and membrane strips were blocked in 3% (w/v) BSA (Sigma-Aldrich, St. Louis, MO), 0.1% (v/v) Tween-20 in PBS and then probed overnight at 4°C with 5 µg/ml of hMAbs 4.8A, D11C, and 1.6D, mMAbs 3H5.1 (Millipore, Billerica MA) specific for DENV-2 E DIII, 4G2 specific for DENV E DI/II, or 30% (v/v) cell culture supernatant mMAb D2-C2 specific for DENV-2, -4 capsid protein (57) diluted in blocking buffer. Membrane strips were then incubated with Alexa Fluor 488 conjugated goat anti-human or anti-mouse antibodies (Invitrogen, Carlsbad, CA) diluted in 0.1% (v/v) Tween-20 in PBS for 4 hr at room temperature, and rinsed in 0.1% (v/v) Tween-20 in PBS prior to scanning with a Typhoon TRIO Variable Mode Imager (GE Healthcare, Piscataway NJ). Photomultiplier tube (PMT) voltage settings used for detecting antibody binding on blot strips ranged from 220 V to 562 V depending on the primary antibody-secondary antibody combination. Increasing the PMT voltage increases the signal level, but not the signal-to-noise ratio. The PMT voltage values used for visualizing the individual blots are indicated in the figure legends.

Biolayer interferometry binding assay

Real-time binding assays between purified hMAbs and DENV-1, 2, 3 and 4 sE proteins (Hawaii Biotech Inc.), were performed using biolayer interferometry with an Octet QK system (Fortebio, Menlo Park, CA) as previously described but with human IgG high-binding sensors instead of streptavidin sensors (14, 65). Briefly, hMAbs 4.8A, D11C, and 1.6D were coupled to kinetics grade anti-human IgG Fc capture (AHC) biosensors (Fortebio, Menlo Park, CA). HMAb binding concentrations that gave a signal between 0.8 and 1.2 nm binding to the sensor surfaces within 200 seconds were used for sE binding studies. Unbound hMAbs were removed from the surface of the sensors by incubation in kinetics buffer containing 1 mM phosphate, 15 mM NaCl, 0.002% (v/v) Tween-20, 0.005% (w/v) sodium azide, 0.1 mg/ml (w/v) BSA, pH7.4 in PBS. Probes coupled to hMAbs were allowed to bind to sE at several different concentrations, and binding kinetics were calculated using the Octet QK software package, which fit the observed binding curves to a 1:1 binding model to calculate the association rate constants. DENV-1, 2, 3, and 4 sE proteins were allowed to dissociate by incubation of the sensors in kinetics buffer. Dissociation kinetics were calculated using the Octet QK software package, which fit the observed dissociation curves to a 1:1 model to calculate the dissociation rate constants. Association and dissociation rate constants were calculated using at least two different concentrations of sE. Equilibrium dissociation constants were calculated as the kinetic dissociation rate constant divided by the kinetic association rate constant.

Focus-forming-unit reduction neutralization assay

LLC-MK_2 target cells were seeded at a density of approximately 500,000 cells in each

well of a 12-well plate 24 hr prior to DENV inoculation. Approximately 100 focus forming units (ffu) of DENV were incubated with dilutions of heat inactivated patient serum or purified hMAb (0.4, 2, 4, 20, and 40 µg/ml final) in serum-free DMEM for 1 hr at room temperature. DENV mixtures were allowed to infect confluent target cell monolayers for 1 hr at 37°C, with rocking every 15 min, after which time the inoculum was aspirated and overlaid with fresh MEM/10% (v/v) FBS containing 1.2% (w/v) microcrystalline cellulose (Avicel, FMC, Newark, DE). Infected cells were then incubated at 37°C with 5% (v/v) CO_2 for two (DENV-4) or three (DENV-1, -2, and -3) days. Cells were fixed and foci were visualized as for confocal microscopy above, except a horseradish peroxidase-conjugated goat anti-mouse immunoglobulin (Pierce, Rockford, IL) was used as the detection antibody and developed using 3,3'-diaminobenzidine tetrahydrochloride (Sigma-Aldrich, St. Louis, MO). IC_{50} values in µg/ml were determined graphically from the % neutralization plots. A sigmoidal curve fit program was not used since several of the DENV serotype/antibody combinations did not reach 100% inhibition and thus fit poorly to sigmoidal curves, skewing the calculations. Results are expressed as pooled data from two independent experiments with three replicates each.

Antibody-dependent enhancement assay

Antibody-dependent enhancement assays were performed as previously described (53). Briefly, 250 ffu of DENV was incubated with various concentrations of hMAbs for 1 hr at 37°C. Each DENV-antibody mixture was added to 300 µl of K562 cells, cell density = 2.7 x 10^5/ml, and incubated for 3 days at 37°C, 5% (v/v) CO_2. The final hMAb concentrations were 0.04, 0.4, 2, 4, 20, and 40 µg/ml. Afterwards, cells were collected and total RNA isolated using an RNeasy Mini-kit (Qiagen, Valencia CA) following the manufacturers

protocol. A quantitative RT-PCR was performed on isolated RNA using a universal DENV primer pair (10). Amplification conditions were 95°C for 5 sec, 61°C for 20 sec, and 72°C for 30 sec.

Virus-liposome fusion assay

Fusogenic activity of dengue virions towards liposomes was characterized using a novel high-throughput plate-reader assay, a version of an assay described in (86). Viral particles were labeled with fluorescent lipid DiD (Vybrant cell-labeling kit, Molecular Probes, Eugene, OR) in a self-quenching concentration, as described in (86). Large unilamellar liposomes of 100 nm diameter were formed by extrusion technique from the 1:1 (mol/mol) mixture of 1,2-dioleoyl-*sn*-glycero-3-phosphocholine (PC) and 1,2-dioleoyl-sn-glycero-3-phospho-(1'-rac-glycerol) (PG) (Avanti Polar Lipids, Alabaster, AL). DiD-labeled viral particles (~10^5 infectious units) in PBS without calcium and magnesium, pH 7.5 were incubated with different concentrations of the antibodies for 1 hr at room temperature in total volume of 50 µl. Virions pre-incubated with antibodies were then mixed in wells of 96-well plates (3 wells for each condition) with acidified liposome-containing buffer (final concentration of PC and PG 30 µM, pH 5.5). After 10 min co-incubation of virions and liposomes at acidic pH, fluorescence was recorded at excitation and emission wavelengths of 630 and 665 nm. At the end of each recording (10 min incubation at 22°C), Triton X-100 was added to a final concentration of 0.1% (v/v) to fully dequench DiD. The efficiency of fusion is presented as the difference between fluorescence intensities measured after 10 min co-incubation of labeled virions with liposomes at pH 5.5 and at pH 7.5, normalized to the difference between fluorescence intensities measured for

406 fully dequenched DiD and at pH 7.5. In control experiments, we used dengue virions
407 inactivated by an application of a histidine-modifying reagent diethylpyrocarbonate
408 (DEPC) (Sigma, St. Louis, MO) (2 mM, 15 min, room temperature).
409
410 **Virus-intracellular fusion and pre-cellular fusion assays**
411 DENV-2 virions were labeled by DiD as described above. Virus-endosome fusion
412 events were detected as an increase in cell fluorescence upon DiD dilution (86). MA104
413 cells (ATCC) (~10^3 cells/well) were grown overnight in the 96-well microtiter plates
414 (Ibidi,Verona, WI). Cells were then incubated for 30 min at 11°C followed by 5 min at 37°C
415 with 10^4 DiD-labeled infectious DENV-2 particles that had been pre-incubated with hMAbs
416 in 100 µl of serum-free ADMEM for 1 hr at room temperature. Unbound DENV-2 and
417 hMAbs were removed by washing twice with 400 µl of serum-free ADMEM, and cells were
418 incubated for an additional 25 min at 37°C. For each well, we captured images of 5
419 randomly chosen fields of view using a Zeiss Observer Z1 (oil immersion objective, 40x)
420 (Carl Zeiss Microscopy, LLC, Thornwood, NY) and generated maximum intensity z-
421 projections based on 15 z-slices of 0.5 µm each for the subsequent analysis. The projections
422 of the cells were analyzed using ImageJ software to subtract the background and threshold
423 using Triangle algorithm. For each condition, we averaged fluorescence intensities in 15
424 fields (5 fields for each of 3 wells). The data are presented as the mean and the standard
425 deviation of the mean for the averaged intensities (n=3) normalized to the averaged
426 intensities measured for the cells incubated with DENV-2 in the absence of hMAbs.
427 After taking the images for the above analysis, we examined the effects of the hMAbs
428 on the total number of cell-associated virions using a novel assay that measured

dequenching of DiD incorporated into unfused viral envelopes. MA104 cells incubated without DENV-2, or with DENV-2 and 10 µg/ml of heparan sulfate, or with DENV-2 and 100 µg/ml of hMAbs 4.8A, D11C or 1.6D were lysed by a 15 min incubation with 0.1% (v/v) triton X-100 at 37°C. The lysates were cleared by a 5 min centrifugation at 14,000xg and 80 µl of each supernatant were mixed with 1920 µl of a 20 mM Hepes, 150 mM NaCl, pH 7.5 buffer. Using a Fluoromax 4 Horiba Jobin Yvon spectrophotometer (Horiba Scientific, Edison, NJ), we measured the emission fluorescence at 665 nm using an excitation wavelength of 600 nm. The data are presented as the mean and the standard deviation of the mean of three independent experiments normalized to the fluorescence intensity measured for DENV-2 infected cells in the absence of hMAbs.

Antibody binding competition enzyme-linked immunosorbent assay

HMAbs 4.8A, D11C, and 1.6D were tested for cross-competition with each other to determine whether they recognized overlapping or non-overlapping sites on DENV-1 E protein using an enzyme-linked immunosorbent assay (13, 60, 65). Solubilized dengue E protein in detergent-treated, serum free culture fluid was immobilized in Con A coated wells. The plates were washed and blocked for 30 minutes at room temperature. Purified hMAbs or dilution buffer was incubated in the wells for 30 minutes at room temperature. Biotinylated hMAbs were then added to the wells at dilutions that gave less than maximal binding and incubated for one hour at room temperature. Bound biotinylated hMAb was detected with horseradish peroxidase streptavidin (Vector, Burlingame, CA). After a wash step, color was developed with TMB-H_2O_2 as substrate for peroxidase. The reaction was

stopped after 4 min by adding 1% (v/v) phosphoric acid and color was read as optical density (OD) at 450 nm.

Antibody binding competition biolayer interferometry assay

Real-time competition assays between purified hMAb 1.6D and purified DENV-2 sE were performed using biolayer interferometry with an Octet QK system (Fortebio, Menlo Park, CA). To determine whether the hMAbs recognized overlapping or non-overlapping sites, we analyzed hMAb 1.6D for competition with itself as well as with mMAbs 4G2 and 3H5.1. Anti-HIV hMAb 1.7B was used as a negative control. Twenty-five µg/ml of hMAb 1.6D diluted in kinetics buffer containing 1 mM phosphate, 15 mM NaCl, 0.002% (v/v) Tween-20, 0.005% (w/v) sodium azide, 0.1 mg/ml (w/v) BSA, pH7.4 in PBS was coupled to anti-human IgG Fc capture (AHC) biosensors (Fortebio, Menlo Park, CA). Unbound hMAb 1.6D was removed from the surface of the sensors by incubation in kinetics buffer. sE was pre-incubated with hMAb or mMAbs at a 1:1 molar ratio. HMAb 1.6D coupled AHC sensors were then incubated with 50 nM sE, either pre-bound to antibodies or in kinetics buffer only. Association of sE with the hMAb 1.6D coupled sensor was measured by light interference.

Epitope mapping using prM/E mutants

Mutations were introduced into the prM/E polyprotein of DENV-3 (strain CH53489) by PCR using a Diversity Mutagenesis kit (Clontech Laboratories, Inc., Mountain View, CA), sequenced, and selected to test for hMAb reactivity from a larger library of mutations. Expression plasmids encoding each mutant were transfected into HEK-293 cells, fixed in

4% (v/v) paraformaldehyde (Electron Microscopy Sciences, Hatfield, PA) 18 hr post-transfection, and permeabilized for 45 min with 0.1% (w/v) saponin (Sigma-Aldrich) in PBS plus calcium and magnesium (PBS++). Cells were stained for 1 hr with hMAbs 4.8A, D11C, 1.6D (0.11 µg/ml in 10% NGS (Sigma)/0.1% (w/v) saponin), a human polyclonal serum (1:1000), or the anti-DENV E mMAb 1A1D-2, (1:10,000 mouse ascites fluid, kindly provided by John Roehrig, CDC) (63). Cells were washed three times with PBS++/0.1% (w/v) saponin followed by the addition of 0.4 µg/ml HRP-conjugated secondary antibody (Jackson ImmunoResearch Laboratories, West Grove, PA) for 1 hr. Following washes, Femto Substrate (Pierce) was added to each well and luminescence values were measured after 5 min (Wallac Victor 2, PerkinElmer, Waltham, MA). All incubations were performed at room temperature. Antibody reactivities against each mutant E protein clone were calculated relative to wild-type E protein reactivity by subtracting the signal from mock-transfected controls and normalizing to the signal from wild-type E-transfected controls. Mutations within critical clones were identified as critical to the hMAb epitope if they did not support reactivity of the test hMAb, but supported reactivity of human polyclonal serum and the conformation-dependent mMAb 1A1D-2. The critical residue within critical clones that contained more than one mutation was identified by assessing other clones containing each of those mutations.

Results

Broadly reactive anti-dengue antibodies were isolated from three different patients

With the goal of understanding the human antibody response in naturally occurring DENV infections, we isolated hMAbs from peripheral blood B cells obtained from patients

with distinct histories of DENV infection. These three patients, 7B, 8C, and DA003, contracted DENV in geographically distinct regions, Myanmar, Jamaica, and Singapore, respectively. Cryopreserved peripheral blood mononuclear cell (PBMC) samples were collected at different times post-recovery (approximately two years for 7B, three months for 8C, and four weeks for DA003). Patient DA003 was diagnosed with secondary dengue infection. All three patients were confirmed seropositive to DENV antigens as shown in Fig. 1A and reported previously for patient 7B (65). From each patient, several hMAbs were produced either by Epstein Barr Virus (EBV) transformation of B cells (7B and DA003) (65) or by memory B-cell stimulation, followed by molecular cloning (8C) (46, 55). To screen for hMAbs binding to glycosylated DENV proteins, we used a previously described ELISA in which Triton X-100 solubilized-DENV proteins were captured in concanavalin A (conA) coated wells of ELISA plates (65). This selection procedure likely biased identification towards cross-reactive hMAbs recognizing the E and prM proteins. Initial selection was done using DENV-2 (7B) or DENV-1 and 3 (8C and DA003). Based on ELISA reactivity to E proteins from all four DENV serotypes (and for neutralizing activity, see section below), we selected 4.8A, D11C, and 1.6D from patients 7B, DA003, and 8C, respectively. The broad reactivity is illustrated in Fig. 1B for hMAbs D11C and 1.6D, and in Schieffelin et al. for hMAb 4.8A (65). Since we used a number of different methods to isolate these antibodies, we cannot determine what percentage of the total repertoire these antibodies represent. However, since we isolated these antibodies from three out of three patients with different infection histories, we can conclude that they are not uncommon. The three hMAbs were composed of IgG1 heavy chains and kappa light chains.

519 We further showed that the hMAbs 4.8A, D11C and 1.6D could bind to DENV
520 antigens expressed in DENV-1, 2, 3 or 4 infected monkey epithelial LLC-MK_2 cells, using
521 immunofluorescence assays (Fig. 1C). All three hMAbs exhibited a characteristic crescent-
522 shaped perinuclear staining against all four DENV serotypes, under fluorescence confocal
523 microscopy. No staining was observed in uninfected cells. The low virus multiplicity of
524 infection (MOI = 0.002) used allowed for a clear distinction of staining between virus-
525 infected versus non-infected cells.
526
527 **Recognition of DENV E protein by human monoclonal anti-dengue antibodies**
528 To confirm that the hMAbs recognize DENV E protein, we prepared Western blots
529 using gradient purified DENV-2 particles under reducing and non-reducing conditions and
530 probed the blot strips with equal amounts (5 μg/ml) of hMAbs 4.8A, D11C, and 1.6D. As
531 shown in Fig. 2A, all three hMAbs recognized a 52-kDa band consistent with the size of
532 DENV-2 E protein, in non-reduced samples. No other bands were observed. The 52-kDa
533 band was not present in reduced samples, indicating that all three hMAbs bound to
534 epitopes dependent on disulfide bonds. As a control, an anti-DENV capsid mMAb D2-C2
535 (57) recognized bands consistent with the size of DENV-2 capsid protein in both reduced
536 and non-reduced samples. To confirm that the hMAbs bound specifically to E protein, we
537 also prepared Western blots under non-reducing conditions using recombinant DENV-2
538 soluble E protein (sE), which contains the ectodomain of the E protein, and reacted blot
539 strips with hMAbs 4.8A, D11C, and 1.6D along with mMAbs 4G2 (22, 37) and 3H5.1 (71) as
540 controls. As shown in Fig. 2B, a band consistent with the size of sE was observed for all

hMAbs that was identical to the size of the bands recognized by the two control mMAbs specific for DENV E protein.

To determine how tightly hMAbs 4.8A, D11C, and 1.6D bound to sE, we performed biolayer interferometry binding assays with hMAbs coupled to IgG binding sensors. After removing unbound hMAbs, we incubated with different concentrations of DENV-1, 2, 3 or 4 sE. Binding of the sE proteins to the hMAbs on the surface of the probes was measured by the change in interference from light reflected from the surface of the probe. After binding, the probes were placed in a solution without sE protein to similarly measure sE-hMAb dissociation. Antibody on- and off-rates and equilibrium dissociation constants were calculated assuming a 1:1 binding ratio. As expected from patient serum and the hMAb ELISA results, all three of the hMAbs bound to all four serotypes of DENV equally well with equilibrium dissociation constants (K_Ds) in the 10^{-9} to 10^{-10} M range (Table 1).

Broadly neutralizing activity of human monoclonal anti-dengue antibodies

We analyzed neutralizing antibodies in patient sera using focus-forming-unit reduction neutralization assays in monkey epithelial LLC-MK_2 cells in which serial dilutions of patient sera were incubated with DENV-1, 2, 3 or 4. Sera from patients 8C and DA003 neutralized all four serotypes (Fig. 3A). Serum from patient 7B was previously reported to strongly neutralize DENV-1 and 3 and weakly neutralize DENV-2 and 4 (65). To characterize the neutralizing activities of the hMAbs derived from the subjects, we performed neutralization assays with each hMAb (Fig. 3B-D). All three hMAbs neutralized DENV-1 through 4 to some extent in a dose-dependent manner. Some of the hMAbs were stronger neutralizers than others whereas some neutralized specific serotypes more

564 strongly than others. For example, the IC_{50} of hMAbs D11C and 1.6D was 1 μg/ml or below
565 (Fig. 3C and D) whereas hMAb 4.8A did not reach 50% inhibition of infectivity against
566 DENV-2 or DENV-4 over the hMAb concentrations tested (Fig. 3B). The observed
567 neutralization activity of hMAb 4.8A was consistent with patient 7B serum activity (65).
568 Additionally, D11C neutralized DENV-1, 2 and 4 more strongly than DENV-3 (Fig. 3C).
569 HMAb 1.6D neutralized DENV-1 through 4 with similar activity (Fig. 3D).
570 To determine the neutralization potential of the hMAbs against other flaviviruses,
571 we performed neutralization assays using yellow fever virus (YF-17D) and YF-17D
572 pseudotyped with West Nile E glycoprotein (Fig. 3B-D). The hMAbs neutralized WNV to
573 some extent, but did not appreciably neutralize yellow fever virus.
574
575 **Antibody-dependent enhancement mediated by human monoclonal anti-dengue**
576 **antibodies**
577 At certain concentrations and with the proper Fc domain, all anti-DENV antibodies
578 have the potential to mediate antibody-dependent enhancement in Fc receptor-bearing
579 cells *in vitro*. For neutralizing antibodies, this enhancement effect decreases as antibody
580 concentration increases due to the antibody's ability to completely coat the virus and
581 effectively neutralize it. However, for non-neutralizing antibodies, the enhancement
582 potential remains high even at high antibody concentrations (65). To determine the
583 antibody-dependent enhancement potential of the three hMAbs, we incubated each of the
584 four DENV serotypes with increasing concentrations of hMAbs 4.8A, D11C and 1.6D and
585 infected the Fc receptor II-bearing human macrophage-like cell line K562. Subsequent
586 viral replication was measured by DENV-specific qRT-PCR. In the absence of antibodies

587 that could serve to mediate DENV infection, K562 cells were more permissive to DENV-2
588 infection than to DENV-1, 3 and 4. As a result, normalized enhancements were typically
589 lower for DENV-2 than the other 3 serotypes. As presented in Fig. 4A-D, each antibody
590 displayed a similar general trend, with a peak enhancement of infection at antibody
591 concentrations of 0.4 to 2-4 μg/ml, followed by neutralization, resulting in reduced
592 infection at increasing antibody concentrations.
593
594 **Neutralizing activity of human monoclonal anti-dengue antibodies correlates with**
595 **inhibition of fusion, not binding**
596 Antibodies directed against virus surface proteins are predicted to inhibit an early
597 entry step into target cells. DENV enters through receptor-mediated endocytosis, where
598 the E glycoprotein binds to a cellular receptor on the plasma membrane followed by
599 endocytosis and fusion of the viral and cellular membranes in the low pH environment of
600 endocytic vesicles, allowing the viral genome to enter target cells. To determine the details
601 of the mechanism of neutralization, we explored the effects of our antibodies on different
602 stages of viral entry.
603 To investigate whether hMAbs could inhibit DENV-2 fusion, we used an assay that
604 measures fusogenic activity of DENV particles towards liposomes (11, 86). DENV-2
605 particles labeled with a self-quenching concentration of a fluorescent lipid DiD were pre-
606 treated with hMAbs prior to co-incubation with liposomes at acidic pH. Lipid mixing
607 between labeled viral and unlabeled liposomal membranes was monitored as an increase
608 in fluorescence reflecting DiD dilution. As expected, no increase in the fluorescence, and
609 thus no lipid mixing, was observed for virions inactivated by a histidine-modifying reagent

610 diethylpyrocarbonate (86). In contrast to the negative control anti-HIV gp120 hMAb EH21,
611 all three anti-DENV E hMAbs strongly inhibited virus-liposome fusion in a dose-dependent
612 manner (Fig. 5A). The relative fusion-inhibiting activity of the hMAbs, with 1.6D being the
613 most potent and 4.8A being the least potent, corresponded to their relative neutralization
614 activity (Fig. 3B-D).

615 Since virus-liposome fusion relies on random collisions between virions and
616 liposomes rather than on E-mediated virion-liposome binding, the ability of hMAbs 4.8A,
617 D11C and 1.6D to inhibit fusion between virions and liposomes suggested that viral entry
618 *in vivo* might also be inhibited at the fusion stage of the entry. To test this hypothesis, we
619 directly examined the effects of the antibodies on intracellular fusion of DENV-2 and on the
620 pre-fusion stages of viral entry into rhesus macaque kidney epithelial cells (MA104). For
621 DENV-2 labeled with DiD at a self-quenching concentration, fusion events along the
622 endocytic pathway dilute DiD and, thus, lead to an increase in fluorescence signal (1, 77,
623 86). We quantified the efficiency of intracellular fusion by measuring cell fluorescence with
624 a novel microtiterplate version of the assay described in (86). Virions were pre-incubated
625 with the antibodies and then applied to the cells at 11°C for 30 minutes to permit binding
626 while holding the virions in a temperature-arrested state. The temperature was then raised
627 to 37°C to allow uptake and fusion of the virions. After the first 5 minutes of incubation at
628 37°C, we removed unbound virions and antibodies by rinsing, and after 25 additional
629 minutes assayed intracellular fusion by fluorescence microscopy (Fig. 5B). Fusion of DiD-
630 labeled virus within endosomes leads to dequenching of DiD and appearance of brightly
631 fluorescent intracellular structures. Cells were counterstained with DAPI to visualize the
632 nuclei. All three anti-DENV hMAbs inhibited intracellular fusion in a dose-dependent

manner (Fig. 5C) corresponding to their relative inhibiting activity in viral neutralization and virus-liposome fusion assays (1.6D being the most potent and 4.8A being the least potent, Fig. 3B-D, 5A). In contrast, a control anti-HIV gp120 hMAb EH21 did not inhibit intracellular fusion. These results suggest that 4.8A, D11C, and 1.6D directly interfere with the structural transitions required for the virus to fuse to the endosomal membrane.

For virions to reach endosomes and fuse, they must first bind to the cell surface and undergo internalization. In order to test whether our hMAbs inhibited virus-cell binding, the total number of virions associated with cells must be evaluated, including (i) cell surface-bound virions, (ii) internalized but yet unfused virions, and, finally, (iii) fused virions. Note that when we measured fusion after a 30 minute incubation at 37°C, fused virions would represent only a small fraction of all cell-associated virions (77) and only fused virions would be dequenched. After measuring the intracellular fusion efficiency, we lysed the cells and fully dequenched the DiD probe in all unfused virions using Triton X-100 to disrupt the viral membranes. The level of unquenched DiD fluorescence was therefore proportional to the total number of cell-associated virions and, thus, can be used to evaluate the effects of different reagents on virus-cell binding (Fig. 5D). As expected, heparan sulfate (10 μg/ml), which inhibits DENV binding to cells (7), dramatically lowered the numbers of cell associated virions, and consequently, the DiD fluorescence of cell lysates. Pre-incubation of virions with high concentrations of our hMAbs (100 μg/ml, sufficient to profoundly inhibit intracellular fusion) had no effect on cell lysate DiD fluorescence intensity indicating that these antibodies do not appreciably affect virus:cell binding. These findings demonstrate that hMAbs 4.8A, D11C, and 1.6D block viral infection downstream of virus-cell binding at the stage of virus-endosome fusion.

Interestingly, hMAb 4.8A did not completely suppress DENV-2 fusion even at very high concentrations, correlating with the observed neutralization activity of this hMAb against DENV-2. The inability of some antibodies to completely neutralize infection and fusion has been previously reported (11, 20, 76, 80) suggesting that even at saturation these antibodies only partially neutralize fusogenic activity of each E protein. Alternatively, the epitopes at some of the viral surface E proteins may be inaccessible, reflecting a heterogeneity of virions and/or E protein chemical environments. For all three hMAbs, inhibition of lipid mixing required somewhat higher concentrations of hMAbs than virus neutralization. This can reflect different conditions: (in neutralization assay we used 10^2 infectious units vs. $10^5$and 10^4infectious units in liposome and intracellular fusion assays, respectively). This difference may also indicate that for DENV, as for several other viruses (8, 12), early stages of viral fusion (detected as lipid mixing in our assay) require fewer functional fusion proteins and, thus, are more difficult to inhibit than an opening of a fusion pore large enough to release viral RNA, a prerequisite of viral infection. As a result, at neutralizing concentrations of the antibodies, virions may still have enough of functional (="not antibody bound") fusion proteins to mediate lipid mixing.

Taken together, our results show that hMAbs 4.8A, D11C, and 1.6D neutralize infection by inhibiting E protein-mediated membrane fusion rather than pre-fusion stages of viral entry.

Targeting of distinct but overlapping fusion loop epitopes

To determine which E protein domain(s) hMAbs 4.8A, D11C, and 1.6D interacted with, we subjected recombinant DENV-2 E protein sDI/II and sDIII to SDS-PAGE under non-

679 reducing conditions and probed with equal amounts of hMAbs 4.8A, D11C, and 1.6D and
680 control mMAbs 3H5.1 (specific for DENV-2 E DIII) or 4G2 (specific for DENV E DII fusion
681 loop). As illustrated in Fig. 6A, hMAbs 4.8A, D11C, and 1.6D interacted specifically with
682 sDI/II and not with sDIII.
683 To determine whether hMAbs 4.8A, D11C and 1.6D bound to overlapping epitopes
684 on E protein, we used an ELISA binding-competition assay as previously reported (65).
685 Unlabeled hMAbs 4.8A, D11C, 1.6D, EH21 (an anti-HIV-1 gp120 antibody), or mMAb 4G2
686 (that binds to the DENV fusion loop) were incubated with DENV-1 antigen bound in ConA-
687 coated plates. Biotinylated antibodies were then added to wells containing pre-bound
688 unlabeled antibodies. If the labeled and unlabeled antibodies bound to the same or
689 overlapping epitope, then the labeled antibody would not bind, resulting in a low signal
690 upon development with streptavidin-conjugated enzyme. As shown in Fig. 6B, biotinylated
691 hMAbs 4.8A, D11C, and 1.6D were unable to bind to wells containing any of their unlabeled
692 counterparts. In addition, mMAb 4G2, which binds to the fusion loop, was unable to bind in
693 the presence of hMAbs 4.8A, D11C, or 1.6D. These results suggest that the three hMAbs
694 and 4G2, share an overlapping epitope. Of note, when wells pre-incubated with unlabeled
695 mMAb 4G2 were incubated with labeled hMAbs, the hMAbs were able to displace mMAb
696 4G2 to some extent. This result could suggest that the hMAbs and mMAb 4G2 bind to
697 different epitopes. However, the results could also arise if hMAbs 4.8A, D11C, and 1.6D bind
698 to the same E protein epitope as mMAb 4G2 but with higher affinities (as is further
699 suggested in experiments described below). As a validation of the competition assay, the
700 negative control hMAb EH21 did not compete for binding with either the hMAbs or mMAb
701 4G2.

To further investigate the relative binding affinity of hMAbs to their epitopes, we chose hMAb 1.6D for additional studies in an antibody binding-competition biolayer interferometry assay. HMAb 1.6D was coupled to human IgG binding sensors. After removing unbound hMAb 1.6D, we applied DENV-2 sE that had been pre-incubated at a 1:1 molar ratio with hMAb 1.6D, mMAbs 4G2 or 3H5.1, or media only, to the sensors. As before, binding of the sE protein to the hMAbs on the surface of the probes was measured by the change in interference from light reflected from the surface of the probe. The magnitude of the signal was indicative of the thickness of the antibody-sE complexes. It was anticipated that if an antibody effectively competed for binding to the hMAb 1.6D epitope, sE pre-complexed with that particular antibody would not be able to bind to the hMAb 1.6D-coated sensor. In contrast, if a particular antibody bound to a different epitope on sE, the sE-antibody complex would be able to bind to the hMAb 1.6D-coated sensor. Fig. 6C illustrates the individual binding curves. As expected, DENV-2 sE bound to the hMAb 1.6D-coated sensor, generating a signal proportional to the thickness of the antibody on the sensor plus the sE protein. When sE was pre-complexed with hMAb 1.6D prior to addition (sE + 1.6D), sE binding to hMAb 1.6D captured on the sensor was profoundly reduced, indicating that hMAb 1.6D can compete very effectively with itself for binding. When mMAb 3H5.1, which binds to DIII, was pre-complexed with sE, the sE-3H5.1 complex bound to the hMAb 1.6D coated sensor, resulting in an increased signal due to the increased thickness of the probe-coupled complex, which consisted of the sE plus two antibodies. As a control, when an irrelevant anti-HIV hMAb (1.7B) was added to sE, the binding signal was equivalent to sE alone. When mMAb 4G2 was pre-complexed with sE, sE bound to the hMAb 1.6D-coated sensor, however the thickness of the complex was indicative of only sE

binding to the sensor with no additional antibody. This result is likely due to effective competition of the hMAb 1.6D with the mMAb 4G2 binding epitope, consistent with competition by ELISA (Fig. 6B). The antibody binding competition biolayer interferometry assay further established that hMAbs bound to epitopes on the E protein fusion loop and suggested that these hMAbs may have higher affinities than similar mMAbs.

To more precisely define the epitopes for hMAbs 4.8A, D11C, and 1.6D, we screened a library of DENV-3 E point mutants to identify mutations that reduce hMAb binding. Three residues, W101, L107, and G109, were identified that when mutated, significantly reduced 4.8A, D11C, or 1.6D binding compared to wild-type E protein (Fig. 7A). These residues were located directly within the fusion loop (residues 98 to 109) and mapped in close proximity on a structure of the E protein (Fig. 7B). Each E protein mutant reacted to a human polyclonal serum and the conformation-dependent mMAb 1A1D-2 that targets a different epitope (48), confirming that each clone was expressed and was not simply globally misfolded. HMAb 4.8A binding was reduced by mutations at any of the three positions, while D11C and 1.6D binding were reduced by mutations at only W101 or G109. These data suggest that 4.8A, D11C, and 1.6D have overlapping but distinct epitopes in the fusion loop, consistent with their ability to compete with each other and with a fusion loop mMAb.

Discussion

This study focused on the portion of the human antibody response that is broadly neutralizing and potentially protective against all DENV serotypes. Several other classes of DENV neutralizing hMAbs are primarily serotype-specific, including hMAbs that target E protein DIII (4, 17, 19), and hMAbs that recognize quaternary epitopes between two E

748 proteins (18, 73). We established the mechanism of action of broadly neutralizing
749 antibodies produced in three human dengue patients. Though the hMAbs were isolated
750 from patients from different countries, diverse ethnic backgrounds, different infecting
751 viruses, and at different times post-recovery, similar broadly neutralizing hMAbs were
752 produced, suggesting that the target of these hMAbs is a common epitope that plays an
753 important role in DENV infectivity. With the goal of determining the mechanism of
754 neutralization, using a novel assay, we uncoupled DENV binding to target cells from fusion
755 and found that the neutralization activity of the hMAbs correlated with inhibition of fusion
756 rather than virus-cell binding. We further mapped the binding of the hMAbs to the highly
757 conserved fusion loop region in DII of the E glycoprotein.

758 A common theme among different structural classes of enveloped virus fusion
759 proteins is the existence of an internal or N-terminal hydrophobic fusion loop or fusion
760 peptide. Neutralizing antibodies directed against these fusion regions have been well
761 described in other virus systems, including closely related flaviviruses (9), more distantly
762 related alphaviruses (32), and unrelated orthomyxoviruses (34), among others. Our
763 results are consistent with a recent study that identified two other broadly neutralizing
764 hMAbs from a single patient that target DENV DI/II and whose binding to WNV DI/II was
765 ablated when residues in the fusion loop were altered suggesting that these antibodies may
766 also bind to the DENV fusion loop (4). Importantly, reports focusing on polyclonal
767 antibody fractions from DENV patient-derived serum have shown that the predominant
768 fraction of the broadly neutralizing activity targets DI/II and specifically the fusion loop,
769 consistent with our hMAb results (45, 47, 81). Broadly neutralizing chimpanzee and
770 mMAbs targeting the DENV fusion loop have been described previously (22, 23, 37). Our

771 finding that hMAbs recognizing the fusion loop inhibit the fusion stage of DENV entry into
772 mammalian cells is consistent with earlier reports that a chimpanzee MAb against the
773 fusion loop inhibits fusion between mosquito cells mediated by cell-surface bound dengue
774 virions (24). The hMAbs reported here can individually block the binding of a mMAb
775 recognizing the fusion loop, confirming that they share an overlapping epitope. However,
776 mMAb pre-bound to E could not block binding by the hMAbs, indicating that the particular
777 mMAb used either has a lower affinity than the hMAbs or that hMAbs bind to the fusion
778 loop differently, in a manner that allows the hMAbs to displace the mMAb.
779 The DENV fusion loop is highly conserved, so it is not clear why hMAb 4.8A inhibited
780 DENV-2 and 4 less strongly than DENV-1 and 3, nor why hMAb D11C inhibited DENV-3 less
781 strongly. Additionally, other flaviviruses with nearly identical fusion loop sequences are
782 not inhibited effectively, with hMAbs 4.8A, D11C, and 1.6D achieving only an intermediate
783 level of neutralization against WNV, and very poor neutralization against YFV. It is possible
784 that the fusion loop region may be oriented differently or have altered accessibility in
785 different viruses (20). These hMAbs bind to E under native conditions, but do not bind
786 denatured and reduced E protein (Fig. 2A), suggesting that disulfide bridges are preserving
787 a structural conformation of the epitopes. Additional non-conserved, fusion loop-adjacent
788 residues may also contribute to antibody binding. Such residues could have a cumulative
789 effect on binding energetics that is not detected when individual residues are mutated in
790 isolation. These potential additional contact residues might be on the same E protein, or
791 part of an adjacent E protein on the virus surface. Binding to recombinant sE monomers
792 and dissociated E protein in ELISAs and Western blots is not identical to binding the E
793 proteins as they are arranged on the surface of a virion. E protein dimers are located in

794 distinct symmetry positions on assembled viruses, and steric hindrance may alter the
795 binding of antibodies to these positions similar to observations with binding to WNV (54).
796 Both antibody-virus binding (20) and virus-cell binding (86) can be ineffective at
797 4°C, the temperature that is often used in binding assays (74, 77). Thus, while our virus-
798 cell binding assay based on measuring DiD fluorescence can be used to quantify binding at
799 different temperatures, we measured the efficiency of virus binding at physiological
800 temperature. Note that, as for other virus-cell binding assays (see for instance, (74, 82)),
801 our assay does not distinguish between potential non-productive, non-specific binding to
802 the cell surface and specific, productive binding between virions and a yet unidentified
803 specific cell surface receptors for DENV, the identity of which is under debate (reviewed in
804 (38)). We therefore questioned whether our hMAbs might neutralize virus by inhibiting
805 specific virus-receptor binding. We estimated that to be undetectable within the error of
806 our data, any putative specific binding would represent only a small fraction of total
807 binding. Additionally, the hMAbs would need to inhibit only this specific binding but not
808 the non-specific one and only this specific binding would allow productive viral entry and
809 infection. While we cannot exclude the possibility that our hMAbs block viral entry and
810 infection by blocking unknown specific virus-receptor binding yet causing no changes in
811 the total virus-cell binding, we consider the conclusion that hMAbs block the entry at the
812 fusion stage rather than at the virus-cell binding stage to be the most likely interpretation
813 of our data. The liposome fusion assay results also support this conclusion.
814 Broadly neutralizing hMAbs can potentially be used in the development of
815 therapeutic treatments. Most previous work in this area has focused on the use of mMAbs
816 (70). The present study has shown that, for binding to E, an anti-DENV hMAb can

outcompete a mMAb with a similar epitope. This observation is not surprising since human antibodies tend to have longer variable regions than mouse antibodies (40, 67). HMAbs are also much less likely to provoke an immune response when used therapeutically in patients, which can even be directed against the antigenically distinct variable regions in humanized mMAbs where the heavy and light chain constant regions have been replaced with human sequences (39). A recent study using a mouse model of lethal DENV infection showed that hMAbs protected mice after exposure to DENV, highlighting the important role that hMAbs can play in the development of DENV therapeutics (4).

While the neutralization activities reported here are lower than those of some recently described hMAbs (4, 17, 19), it is difficult to compare neutralization potency between assay systems in different laboratories as the potency can vary depending on the specific assay used, the serotype and strain of virus, the target cell line, and the incubation conditions of the assay (63, 75). Despite difficulties comparing methodology, neutralization potency alone offers an incomplete view of the human antibody response. Given our study and the work of others, there appears to be a wide spectrum of hMAb responses directed against the DENV surface proteins ranging from potently neutralizing, serotype specific antibodies to non-neutralizing, cross-reactive antibodies, and many hMAbs falling in between these two extremes (4, 17-19, 65). Using vesicular stomatitis virus mMAbs, Bachmann et al. demonstrated that *in vivo* protection was independent of immunoglobulin subclass, avidity, and *in vitro* neutralization activity, and that above a minimal avidity threshold ($> 2 \times 10^7\ M^{-1}$), protection depended simply on a minimum serum concentration (2). For therapeutic or protective purposes, whether it would be

preferable to have multiple serotype-specific, highly neutralizing anti-DENV hMAbs or a single cross-reactive and moderately neutralizing hMAb is currently unknown.

We have not characterized the extent to which the virus preparations we used for our neutralization assays contain mature, immature or partially mature particles. Thus, we do not know if hMAbs 4.8A, D11C and 1.6D neutralize infectivity by preferentially binding to completely mature, partially mature, or completely immature virions. A previous study suggested a structural basis for the preferential binding of fusion loop antibodies to the partially exposed fusion loop region on immature flaviviruses (9), but differences between the mMAb used in that study, which bound to the bc loop in addition to the fusion loop, and our hMAbs make it difficult to speculate on the role of mature versus immature virion structure in our results.

One of the most striking outcomes of other recent studies of hMAbs against DENV is the discovery that the response is dominated by broadly reactive, but non-neutralizing antibodies directed against prM and E, that serve only to enhance DENV infection in macrophages and other Fc receptor-bearing cells (4, 17, 19, 65). The majority, if not all, of DENV vaccine candidates approaching or in clinical trials contain full-length DENV prM and E proteins (3, 21, 27, 28, 41, 52, 56, 58, 68, 72). Full-length DENV prM and E proteins, whether expressed as part of an attenuated DENV strain or expressed in another manner, may induce a broadly reactive and primarily non-neutralizing antibody response. Although both neutralizing and non-neutralizing antibodies can enhance infection, large numbers of broadly reactive non-neutralizing antibodies could shift the response in favor of enhancement, which may result in an increased risk of severe disease in vaccine recipients. However, if immunogens can be developed that present the fusion loop in the proper

863 context, a broadly reactive neutralizing response might be possible for a DENV vaccine.
864 The enhancing activity induced by such an immunogen might be reduced compared to full-
865 length prM and E.
866
867 **Acknowledgments**
868 This work was supported by the Defense Threat Reduction Agency under award
869 numbers HDTRA1-08-1-0003, HDTRA1-09-1-0004, and HDTRA1-10-1-0009, and the
870 National Science Foundation under grant number CBET-0923030 to S.I. and S.F.M.; the
871 Intramural Research Program of the Eunice Kennedy Shriver National Institute of Child
872 Health and Human Development, National Institutes of Health (NIH) and by a National
873 Institute of Allergy and Infectious Diseases (NIAID), NIH Intramural Biodefense Research
874 grant and the Intramural AIDS Targeted Antiviral Program to L.V.C.; by NIAID contract
875 HHSN272200900055C to B.J.D.; and by NIH Centers of Biomedical Research Excellence
876 award P20RR021970-06 to J.S.S. and J.E.R.
877 J.M.C., E.Z., J.E.R., B.J.D., L.V.C., S.F.M., J.S.S., and S.I. conceived and designed
878 experiments. J.M.C., E.Z., K.M.K., C.O.N., D.K.R., A.S.G., L.E.B., G.H., M.F.S., R.H.F., S.-T.Y., J.S.S.,
879 and S.I. performed the experiments. L.L. contributed reagents, materials, and analysis tools.
880 J.M.C., E.Z., K.M.K., B.J.D., L.V.C., S.F.M., J.S.S., and S.I. analyzed the data. S.F.M. and S.I. wrote
881 the paper.
882 B.J.D. is a shareholder in Integral Molecular, Inc.
883
884 **References**
885

1. **Ayala-Nunez, N. V., J. Wilschut, and J. M. Smit.** 2011. Monitoring virus entry into living cells using DiD-labeled dengue virus particles. Methods **55:**137-143.
2. **Bachmann, M. F., U. Kalinke, A. Althage, G. Freer, C. Burkhart, H. Roost, M. Aguet, H. Hengartner, and R. M. Zinkernagel.** 1997. The role of antibody concentration and avidity in antiviral protection. Science **276:**2024-2027.
3. **Beckett, C. G., J. Tjaden, T. Burgess, J. R. Danko, C. Tamminga, M. Simmons, S. J. Wu, P. Sun, T. Kochel, K. Raviprakash, C. G. Hayes, and K. R. Porter.** 2011. Evaluation of a prototype dengue-1 DNA vaccine in a Phase 1 clinical trial. Vaccine **29:**960-968.
4. **Beltramello, M., K. L. Williams, C. P. Simmons, A. Macagno, L. Simonelli, N. T. Quyen, S. Sukupolvi-Petty, E. Navarro-Sanchez, P. R. Young, A. M. de Silva, F. A. Rey, L. Varani, S. S. Whitehead, M. S. Diamond, E. Harris, A. Lanzavecchia, and F. Sallusto.** 2010. The human immune response to Dengue virus is dominated by highly cross-reactive antibodies endowed with neutralizing and enhancing activity. Cell host & microbe **8:**271-283.
5. **CDC.** 2010. Locally acquired Dengue--Key West, Florida, 2009-2010. MMWR. Morbidity and mortality weekly report **59:**577-581.
6. **Chang, G.-J. J.** 1997. Molecular biology of dengue viruses, p. 175-198. *In* D. J. Gubler and G. Kuno (ed.), Dengue and Dengue Hemorrhagic Fever. CABI, Wallingford, UK.
7. **Chen, Y., T. Maguire, R. E. Hileman, J. R. Fromm, J. D. Esko, R. J. Linhardt, and R. M. Marks.** 1997. Dengue virus infectivity depends on envelope protein binding to target cell heparan sulfate. Nature medicine **3:**866-871.

8. **Chernomordik, L. V., and M. M. Kozlov.** 2003. Protein-lipid interplay in fusion and fission of biological membranes. Annual review of biochemistry **72:**175-207.

9. **Cherrier, M. V., B. Kaufmann, G. E. Nybakken, S. M. Lok, J. T. Warren, B. R. Chen, C. A. Nelson, V. A. Kostyuchenko, H. A. Holdaway, P. R. Chipman, R. J. Kuhn, M. S. Diamond, M. G. Rossmann, and D. H. Fremont.** 2009. Structural basis for the preferential recognition of immature flaviviruses by a fusion-loop antibody. The EMBO journal **28:**3269-3276.

10. **Chutinimitkul, S., S. Payungporn, A. Theamboonlers, and Y. Poovorawan.** 2005. Dengue typing assay based on real-time PCR using SYBR Green I. Journal of virological methods **129:**8-15.

11. **Cockburn, J. J., M. E. Navarro Sanchez, A. P. Goncalvez, E. Zaitseva, E. A. Stura, C. M. Kikuti, S. Duquerroy, P. Dussart, L. V. Chernomordik, C. J. Lai, and F. A. Rey.** 2012. Structural insights into the neutralization mechanism of a higher primate antibody against dengue virus. The EMBO journal **31:**767-779.

12. **Cohen, F. S., and G. B. Melikyan.** 2004. The energetics of membrane fusion from binding, through hemifusion, pore formation, and pore enlargement. The Journal of membrane biology **199:**1-14.

13. **Cole, K. S., M. Alvarez, D. H. Elliott, H. Lam, E. Martin, T. Chau, K. Micken, J. L. Rowles, J. E. Clements, M. Murphey-Corb, R. C. Montelaro, and J. E. Robinson.** 2001. Characterization of neutralization epitopes of simian immunodeficiency virus (SIV) recognized by rhesus monoclonal antibodies derived from monkeys infected with an attenuated SIV strain. Virology **290:**59-73.

930 14. **Costin, J. M., E. Jenwitheesuk, S. M. Lok, E. Hunsperger, K. A. Conrads, K. A.**
931 **Fontaine, C. R. Rees, M. G. Rossmann, S. Isern, R. Samudrala, and S. F. Michael.**
932 2010. Structural optimization and de novo design of dengue virus entry inhibitory
933 peptides. PLoS neglected tropical diseases **4:**e721.
934 15. **Crill, W. D., and J. T. Roehrig.** 2001. Monoclonal antibodies that bind to domain III
935 of dengue virus E glycoprotein are the most efficient blockers of virus adsorption to
936 Vero cells. Journal of virology **75:**7769-7773.
937 16. **Cuzzubbo, A. J., T. P. Endy, A. Nisalak, S. Kalayanarooj, D. W. Vaughn, S. A. Ogata,**
938 **D. E. Clements, and P. L. Devine.** 2001. Use of recombinant envelope proteins for
939 serological diagnosis of Dengue virus infection in an immunochromatographic assay.
940 Clinical and diagnostic laboratory immunology **8:**1150-1155.
941 17. **de Alwis, R., M. Beltramello, W. B. Messer, S. Sukupolvi-Petty, W. M. Wahala, A.**
942 **Kraus, N. P. Olivarez, Q. Pham, J. D. Brien, W. Y. Tsai, W. K. Wang, S. Halstead, S.**
943 **Kliks, M. S. Diamond, R. Baric, A. Lanzavecchia, F. Sallusto, and A. M. de Silva.**
944 2011. In-depth analysis of the antibody response of individuals exposed to primary
945 dengue virus infection. PLoS neglected tropical diseases **5:**e1188.
946 18. **de Alwis, R., S. A. Smith, N. P. Olivarez, W. B. Messer, J. P. Huynh, W. M. Wahala,**
947 **L. J. White, M. S. Diamond, R. S. Baric, J. E. Crowe, Jr., and A. M. de Silva.** 2012.
948 Identification of human neutralizing antibodies that bind to complex epitopes on
949 dengue virions. Proceedings of the National Academy of Sciences of the United
950 States of America **109:**7439-7444.
951 19. **Dejnirattisai, W., A. Jumnainsong, N. Onsirisakul, P. Fitton, S. Vasanawathana,**
952 **W. Limpitikul, C. Puttikhunt, C. Edwards, T. Duangchinda, S. Supasa, K.**

Chawansuntati, P. Malasit, J. Mongkolsapaya, and G. Screaton. 2010. Cross-reacting antibodies enhance dengue virus infection in humans. Science **328:**745-748.

20. **Dowd, K. A., C. A. Jost, A. P. Durbin, S. S. Whitehead, and T. C. Pierson.** 2011. A dynamic landscape for antibody binding modulates antibody-mediated neutralization of West Nile virus. PLoS pathogens **7:**e1002111.

21. **Durbin, A. P., and S. S. Whitehead.** 2010. Dengue vaccine candidates in development. Current topics in microbiology and immunology **338:**129-143.

22. **Gentry, M. K., E. A. Henchal, J. M. McCown, W. E. Brandt, and J. M. Dalrymple.** 1982. Identification of distinct antigenic determinants on dengue-2 virus using monoclonal antibodies. The American journal of tropical medicine and hygiene **31:**548-555.

23. **Goncalvez, A. P., R. E. Engle, M. St Claire, R. H. Purcell, and C. J. Lai.** 2007. Monoclonal antibody-mediated enhancement of dengue virus infection in vitro and in vivo and strategies for prevention. Proceedings of the National Academy of Sciences of the United States of America **104:**9422-9427.

24. **Goncalvez, A. P., R. H. Purcell, and C. J. Lai.** 2004. Epitope determinants of a chimpanzee Fab antibody that efficiently cross-neutralizes dengue type 1 and type 2 viruses map to inside and in close proximity to fusion loop of the dengue type 2 virus envelope glycoprotein. Journal of virology **78:**12919-12928.

25. **Graham, A. S., C. A. Pruszynski, L. J. Hribar, D. J. DeMay, A. N. Tambasco, A. E. Hartley, E. M. Fussell, S. F. Michael, and S. Isern.** 2011. Mosquito-associated dengue virus, Key West, Florida, USA, 2010. Emerging infectious diseases **17:**2074-2075.

976 26. **Gubler, D. J.** 2002. Epidemic dengue/dengue hemorrhagic fever as a public health,
977 social and economic problem in the 21st century. Trends in microbiology **10:**100-
978 103.
979 27. **Guirakhoo, F., S. Kitchener, D. Morrison, R. Forrat, K. McCarthy, R. Nichols, S.**
980 **Yoksan, X. Duan, T. H. Ermak, N. Kanesa-Thasan, P. Bedford, J. Lang, M. J.**
981 **Quentin-Millet, and T. P. Monath.** 2006. Live attenuated chimeric yellow fever
982 dengue type 2 (ChimeriVax-DEN2) vaccine: Phase I clinical trial for safety and
983 immunogenicity: effect of yellow fever pre-immunity in induction of cross
984 neutralizing antibody responses to all 4 dengue serotypes. Human vaccines **2:**60-67.
985 28. **Guy, B., M. Saville, and J. Lang.** 2010. Development of Sanofi Pasteur tetravalent
986 dengue vaccine. Human vaccines **6**.
987 29. **Halstead, S. B.** 2003. Neutralization and antibody-dependent enhancement of
988 dengue viruses. Advances in virus research **60:**421-467.
989 30. **Halstead, S. B.** 1988. Pathogenesis of dengue: challenges to molecular biology.
990 Science **239:**476-481.
991 31. **Halstead, S. B., and E. J. O'Rourke.** 1977. Dengue viruses and mononuclear
992 phagocytes. I. Infection enhancement by non-neutralizing antibody. The Journal of
993 experimental medicine **146:**201-217.
994 32. **Hammar, L., S. Markarian, L. Haag, H. Lankinen, A. Salmi, and R. H. Cheng.** 2003.
995 Prefusion rearrangements resulting in fusion Peptide exposure in Semliki forest
996 virus. The Journal of biological chemistry **278:**7189-7198.
997 33. **Harrison, S. C.** 2008. Viral membrane fusion. Nature structural & molecular biology
998 **15:**690-698.

34. **Hashem, A. M., G. Van Domselaar, C. Li, J. Wang, Y. M. She, T. D. Cyr, J. Sui, R. He, W. A. Marasco, and X. Li.** 2010. Universal antibodies against the highly conserved influenza fusion peptide cross-neutralize several subtypes of influenza A virus. Biochemical and biophysical research communications **403:**247-251.

35. **He, R. T., B. L. Innis, A. Nisalak, W. Usawattanakul, S. Wang, S. Kalayanarooj, and R. Anderson.** 1995. Antibodies that block virus attachment to Vero cells are a major component of the human neutralizing antibody response against dengue virus type 2. Journal of medical virology **45:**451-461.

36. **Heinz, F. X., and S. L. Allison.** 2003. Flavivirus structure and membrane fusion. Advances in virus research **59:**63-97.

37. **Henchal, E. A., J. M. McCown, D. S. Burke, M. C. Seguin, and W. E. Brandt.** 1985. Epitopic analysis of antigenic determinants on the surface of dengue-2 virions using monoclonal antibodies. The American journal of tropical medicine and hygiene **34:**162-169.

38. **Hidari, K. I., and T. Suzuki.** 2011. Dengue virus receptor. Tropical medicine and health **39:**37-43.

39. **Hwang, W. Y., and J. Foote.** 2005. Immunogenicity of engineered antibodies. Methods **36:**3-10.

40. **Johnson, G., and T. T. Wu.** 1998. Preferred CDRH3 lengths for antibodies with defined specificities. International immunology **10:**1801-1805.

41. **Kitchener, S., M. Nissen, P. Nasveld, R. Forrat, S. Yoksan, J. Lang, and J. F. Saluzzo.** 2006. Immunogenicity and safety of two live-attenuated tetravalent dengue vaccine formulations in healthy Australian adults. Vaccine **24:**1238-1241.

1022 42. **Kliks, S. C., S. Nimmanitya, A. Nisalak, and D. S. Burke.** 1988. Evidence that
1023 maternal dengue antibodies are important in the development of dengue
1024 hemorrhagic fever in infants. The American journal of tropical medicine and hygiene
1025 **38:**411-419.
1026 43. **Kuhn, R. J., W. Zhang, M. G. Rossmann, S. V. Pletnev, J. Corver, E. Lenches, C. T.**
1027 **Jones, S. Mukhopadhyay, P. R. Chipman, E. G. Strauss, T. S. Baker, and J. H.**
1028 **Strauss.** 2002. Structure of dengue virus: implications for flavivirus organization,
1029 maturation, and fusion. Cell **108:**717-725.
1030 44. **La Ruche, G., Y. Souares, A. Armengaud, F. Peloux-Petiot, P. Delaunay, P.**
1031 **Despres, A. Lenglet, F. Jourdain, I. Leparc-Goffart, F. Charlet, L. Ollier, K.**
1032 **Mantey, T. Mollet, J. P. Fournier, R. Torrents, K. Leitmeyer, P. Hilairet, H. Zeller,**
1033 **W. Van Bortel, D. Dejour-Salamanca, M. Grandadam, and M. Gastellu-**
1034 **Etchegorry.** 2010. First two autochthonous dengue virus infections in metropolitan
1035 France, September 2010. Euro Surveill **15:**19676.
1036 45. **Lai, C. Y., W. Y. Tsai, S. R. Lin, C. L. Kao, H. P. Hu, C. C. King, H. C. Wu, G. J. Chang,**
1037 **and W. K. Wang.** 2008. Antibodies to envelope glycoprotein of dengue virus during
1038 the natural course of infection are predominantly cross-reactive and recognize
1039 epitopes containing highly conserved residues at the fusion loop of domain II.
1040 Journal of virology **82:**6631-6643.
1041 46. **Liao, H. X., M. C. Levesque, A. Nagel, A. Dixon, R. Zhang, E. Walter, R. Parks, J.**
1042 **Whitesides, D. J. Marshall, K. K. Hwang, Y. Yang, X. Chen, F. Gao, S. Munshaw, T.**
1043 **B. Kepler, T. Denny, M. A. Moody, and B. F. Haynes.** 2009. High-throughput

isolation of immunoglobulin genes from single human B cells and expression as monoclonal antibodies. Journal of virological methods **158:**171-179.

47. **Lin, H. E., W. Y. Tsai, I. J. Liu, P. C. Li, M. Y. Liao, J. J. Tsai, Y. C. Wu, C. Y. Lai, C. H. Lu, J. H. Huang, G. J. Chang, H. C. Wu, and W. K. Wang.** 2012. Analysis of epitopes on dengue virus envelope protein recognized by monoclonal antibodies and polyclonal human sera by a high throughput assay. PLoS neglected tropical diseases **6:**e1447.

48. **Lok, S. M., V. Kostyuchenko, G. E. Nybakken, H. A. Holdaway, A. J. Battisti, S. Sukupolvi-Petty, D. Sedlak, D. H. Fremont, P. R. Chipman, J. T. Roehrig, M. S. Diamond, R. J. Kuhn, and M. G. Rossmann.** 2008. Binding of a neutralizing antibody to dengue virus alters the arrangement of surface glycoproteins. Nature structural & molecular biology **15:**312-317.

49. **Mackenzie, J. S., D. J. Gubler, and L. R. Petersen.** 2004. Emerging flaviviruses: the spread and resurgence of Japanese encephalitis, West Nile and dengue viruses. Nature medicine **10:**S98-109.

50. **Modis, Y., S. Ogata, D. Clements, and S. C. Harrison.** 2003. A ligand-binding pocket in the dengue virus envelope glycoprotein. Proceedings of the National Academy of Sciences of the United States of America **100:**6986-6991.

51. **Modis, Y., S. Ogata, D. Clements, and S. C. Harrison.** 2005. Variable surface epitopes in the crystal structure of dengue virus type 3 envelope glycoprotein. Journal of virology **79:**1223-1231.

1065 52. **Morrison, D., T. J. Legg, C. W. Billings, R. Forrat, S. Yoksan, and J. Lang.** 2010. A
1066 novel tetravalent dengue vaccine is well tolerated and immunogenic against all 4
1067 serotypes in flavivirus-naive adults. The Journal of infectious diseases **201:**370-377.
1068 53. **Nicholson, C. O., J. M. Costin, D. K. Rowe, L. Lin, E. Jenwitheesuk, R. Samudrala, S.**
1069 **Isern, and S. F. Michael.** 2011. Viral entry inhibitors block dengue antibody-
1070 dependent enhancement in vitro. Antiviral research **89:**71-74.
1071 54. **Pierson, T. C., Q. Xu, S. Nelson, T. Oliphant, G. E. Nybakken, D. H. Fremont, and**
1072 **M. S. Diamond.** 2007. The stoichiometry of antibody-mediated neutralization and
1073 enhancement of West Nile virus infection. Cell host & microbe **1:**135-145.
1074 55. **Pinna, D., D. Corti, D. Jarrossay, F. Sallusto, and A. Lanzavecchia.** 2009. Clonal
1075 dissection of the human memory B-cell repertoire following infection and
1076 vaccination. European journal of immunology **39:**1260-1270.
1077 56. **Poo, J., F. Galan, R. Forrat, B. Zambrano, J. Lang, and G. H. Dayan.** 2010. Live-
1078 attenuated Tetravalent Dengue Vaccine in Dengue-naive Children, Adolescents, and
1079 Adults in Mexico City: Randomized Controlled Phase 1 Trial of Safety and
1080 Immunogenicity. The Pediatric infectious disease journal.
1081 57. **Puttikhunt, C., P. Ong-Ajchaowlerd, T. Prommool, S. Sangiambut, J. Netsawang,**
1082 **T. Limjindaporn, P. Malasit, and W. Kasinrerk.** 2009. Production and
1083 characterization of anti-dengue capsid antibodies suggesting the N terminus region
1084 covering the first 20 amino acids of dengue virus capsid protein is predominantly
1085 immunogenic in mice. Archives of virology **154:**1211-1221.
1086 58. **Raviprakash, K., D. Wang, D. Ewing, D. H. Holman, K. Block, J.**
1087 **Woraratanadharm, L. Chen, C. Hayes, J. Y. Dong, and K. Porter.** 2008. A

tetravalent dengue vaccine based on a complex adenovirus vector provides significant protection in rhesus monkeys against all four serotypes of dengue virus. Journal of virology **82:**6927-6934.

59. **Rey, F. A., F. X. Heinz, C. Mandl, C. Kunz, and S. C. Harrison.** 1995. The envelope glycoprotein from tick-borne encephalitis virus at 2 A resolution. Nature **375:**291-298.

60. **Robinson, J. E., K. S. Cole, D. H. Elliott, H. Lam, A. M. Amedee, R. Means, R. C. Desrosiers, J. Clements, R. C. Montelaro, and M. Murphey-Corb.** 1998. Production and characterization of SIV envelope-specific rhesus monoclonal antibodies from a macaque asymptomatically infected with a live SIV vaccine. AIDS research and human retroviruses **14:**1253-1262.

61. **Robinson, J. E., D. Holton, J. Liu, H. McMurdo, A. Murciano, and R. Gohd.** 1990. A novel enzyme-linked immunosorbent assay (ELISA) for the detection of antibodies to HIV-1 envelope glycoproteins based on immobilization of viral glycoproteins in microtiter wells coated with concanavalin A. Journal of immunological methods **132:**63-71.

62. **Robinson, J. E., D. Holton, S. Pacheco-Morell, J. Liu, and H. McMurdo.** 1990. Identification of conserved and variant epitopes of human immunodeficiency virus type 1 (HIV-1) gp120 by human monoclonal antibodies produced by EBV-transformed cell lines. AIDS research and human retroviruses **6:**567-579.

63. **Roehrig, J. T., J. Hombach, and A. D. Barrett.** 2008. Guidelines for Plaque-Reduction Neutralization Testing of Human Antibodies to Dengue Viruses. Viral immunology **21:**123-132.

1111 64. **Sabin, A. B.** 1952. Research on dengue during World War II. The American journal
1112 of tropical medicine and hygiene **1:**30-50.
1113 65. **Schieffelin, J. S., J. M. Costin, C. O. Nicholson, N. M. Orgeron, K. A. Fontaine, S.**
1114 **Isern, S. F. Michael, and J. E. Robinson.** 2010. Neutralizing and non-neutralizing
1115 monoclonal antibodies against dengue virus E protein derived from a naturally
1116 infected patient. Virology journal **7:**28.
1117 66. **Schmidt-Chanasit, J., M. Haditsch, I. Schoneberg, S. Gunther, K. Stark, and C.**
1118 **Frank.** 2010. Dengue virus infection in a traveller returning from Croatia to
1119 Germany. Euro Surveill **15**.
1120 67. **Schroeder, H. W., Jr.** 2006. Similarity and divergence in the development and
1121 expression of the mouse and human antibody repertoires. Developmental and
1122 comparative immunology **30:**119-135.
1123 68. **Simasathien, S., S. J. Thomas, V. Watanaveeradej, A. Nisalak, C. Barberousse, B.**
1124 **L. Innis, W. Sun, J. R. Putnak, K. H. Eckels, Y. Hutagalung, R. V. Gibbons, C. Zhang,**
1125 **R. De La Barrera, R. G. Jarman, W. Chawachalasai, and M. P. Mammen, Jr.** 2008.
1126 Safety and immunogenicity of a tetravalent live-attenuated dengue vaccine in
1127 flavivirus naive children. The American journal of tropical medicine and hygiene
1128 **78:**426-433.
1129 69. **Simmons, C. P., T. N. Chau, T. T. Thuy, N. M. Tuan, D. M. Hoang, N. T. Thien, B.**
1130 **Lien le, N. T. Quy, N. T. Hieu, T. T. Hien, C. McElnea, P. Young, S. Whitehead, N. T.**
1131 **Hung, and J. Farrar.** 2007. Maternal antibody and viral factors in the pathogenesis
1132 of dengue virus in infants. The Journal of infectious diseases **196:**416-424.

70. **Sukupolvi-Petty, S., S. K. Austin, M. Engle, J. D. Brien, K. A. Dowd, K. L. Williams, S. Johnson, R. Rico-Hesse, E. Harris, T. C. Pierson, D. H. Fremont, and M. S. Diamond.** 2010. Structure and function analysis of therapeutic monoclonal antibodies against dengue virus type 2. Journal of virology **84:**9227-9239.

71. **Sukupolvi-Petty, S., S. K. Austin, W. E. Purtha, T. Oliphant, G. E. Nybakken, J. J. Schlesinger, J. T. Roehrig, G. D. Gromowski, A. D. Barrett, D. H. Fremont, and M. S. Diamond.** 2007. Type- and subcomplex-specific neutralizing antibodies against domain III of dengue virus type 2 envelope protein recognize adjacent epitopes. Journal of virology **81:**12816-12826.

72. **Sun, W., D. Cunningham, S. S. Wasserman, J. Perry, J. R. Putnak, K. H. Eckels, D. W. Vaughn, S. J. Thomas, N. Kanesa-Thasan, B. L. Innis, and R. Edelman.** 2009. Phase 2 clinical trial of three formulations of tetravalent live-attenuated dengue vaccine in flavivirus-naive adults. Human vaccines **5:**33-40.

73. **Teoh, E. P., P. Kukkaro, E. W. Teo, A. P. Lim, T. T. Tan, A. Yip, W. Schul, M. Aung, V. A. Kostyuchenko, Y. S. Leo, S. H. Chan, K. G. Smith, A. H. Chan, G. Zou, E. E. Ooi, D. M. Kemeny, G. K. Tan, J. K. Ng, M. L. Ng, S. Alonso, D. Fisher, P. Y. Shi, B. J. Hanson, S. M. Lok, and P. A. MacAry.** 2012. The structural basis for serotype-specific neutralization of dengue virus by a human antibody. Science translational medicine **4:**139ra183.

74. **Thaisomboonsuk, B. K., E. T. Clayson, S. Pantuwatana, D. W. Vaughn, and T. P. Endy.** 2005. Characterization of dengue-2 virus binding to surfaces of mammalian and insect cells. The American journal of tropical medicine and hygiene **72:**375-383.

1155 75. **Thomas, S. J., A. Nisalak, K. B. Anderson, D. H. Libraty, S. Kalayanarooj, D. W.**
1156 **Vaughn, R. Putnak, R. V. Gibbons, R. Jarman, and T. P. Endy.** 2009. Dengue
1157 plaque reduction neutralization test (PRNT) in primary and secondary dengue virus
1158 infections: How alterations in assay conditions impact performance. The American
1159 journal of tropical medicine and hygiene **81:**825-833.
1160 76. **Thompson, B. S., B. Moesker, J. M. Smit, J. Wilschut, M. S. Diamond, and D. H.**
1161 **Fremont.** 2009. A therapeutic antibody against west nile virus neutralizes infection
1162 by blocking fusion within endosomes. PLoS pathogens **5:**e1000453.
1163 77. **van der Schaar, H. M., M. J. Rust, B. L. Waarts, H. van der Ende-Metselaar, R. J.**
1164 **Kuhn, J. Wilschut, X. Zhuang, and J. M. Smit.** 2007. Characterization of the early
1165 events in dengue virus cell entry by biochemical assays and single-virus tracking.
1166 Journal of virology **81:**12019-12028.
1167 78. **Vaughn, D. W., S. Green, S. Kalayanarooj, B. L. Innis, S. Nimmannitya, S.**
1168 **Suntayakorn, T. P. Endy, B. Raengsakulrach, A. L. Rothman, F. A. Ennis, and A.**
1169 **Nisalak.** 2000. Dengue viremia titer, antibody response pattern, and virus serotype
1170 correlate with disease severity. The Journal of infectious diseases **181:**2-9.
1171 79. **Vaughn, D. W., S. Green, S. Kalayanarooj, B. L. Innis, S. Nimmannitya, S.**
1172 **Suntayakorn, A. L. Rothman, F. A. Ennis, and A. Nisalak.** 1997. Dengue in the
1173 early febrile phase: viremia and antibody responses. The Journal of infectious
1174 diseases **176:**322-330.
1175 80. **Vogt, M. R., B. Moesker, J. Goudsmit, M. Jongeneelen, S. K. Austin, T. Oliphant, S.**
1176 **Nelson, T. C. Pierson, J. Wilschut, M. Throsby, and M. S. Diamond.** 2009. Human

monoclonal antibodies against West Nile virus induced by natural infection neutralize at a postattachment step. Journal of virology **83:**6494-6507.

81. **Wahala, W. M., A. A. Kraus, L. B. Haymore, M. A. Accavitti-Loper, and A. M. de Silva.** 2009. Dengue virus neutralization by human immune sera: role of envelope protein domain III-reactive antibody. Virology **392:**103-113.

82. **Watterson, D., B. Kobe, and P. R. Young.** 2012. Residues in domain III of the dengue virus envelope glycoprotein involved in cell-surface glycosaminoglycan binding. The Journal of general virology **93:**72-82.

83. **WHO.** 2012. Dengue and severe dengue, Fact sheet no. 117. Available: http://www.who.int/mediacentre/factsheets/fs117/en/.

84. **Xiang, S. H., N. Doka, R. K. Choudhary, J. Sodroski, and J. E. Robinson.** 2002. Characterization of CD4-induced epitopes on the HIV type 1 gp120 envelope glycoprotein recognized by neutralizing human monoclonal antibodies. AIDS research and human retroviruses **18:**1207-1217.

85. **Yu, I. M., W. Zhang, H. A. Holdaway, L. Li, V. A. Kostyuchenko, P. R. Chipman, R. J. Kuhn, M. G. Rossmann, and J. Chen.** 2008. Structure of the immature dengue virus at low pH primes proteolytic maturation. Science **319:**1834-1837.

86. **Zaitseva, E., S. T. Yang, K. Melikov, S. Pourmal, and L. V. Chernomordik.** 2010. Dengue virus ensures its fusion in late endosomes using compartment-specific lipids. PLoS pathogens **6:**e1001131.

87. **Zhang, W., P. R. Chipman, J. Corver, P. R. Johnson, Y. Zhang, S. Mukhopadhyay, T. S. Baker, J. H. Strauss, M. G. Rossmann, and R. J. Kuhn.** 2003. Visualization of

membrane protein domains by cryo-electron microscopy of dengue virus. Nature structural biology **10:**907-912.

Figure Legends

FIG. 1. Broadly reactive patient-derived monoclonal antibodies. (A) DENV-1, 2, 3, and 4 glycosylated antigens were captured on ConA coated plates and probed with dilutions of patient 8C and DA003 sera. Data points show the mean of one experiment with three replicates. Error bars show standard deviation. **(B)** DENV-1, 2, 3, and 4 glycosylated antigens were captured on ConA coated plates and probed with dilutions of hMAbs D11C and 1.6D. Representative data shows the mean of one experiment with three replicates. Error bars show standard deviation. **(C)** LLC-MK_2 cells infected with DENV-1, 2, 3, and 4 at an MOI of 0.002 were probed with hMAbs 4.8A, D11C, and 1.6D and imaged by confocal microscopy. The nuclei were counterstained with Hoechst.

FIG. 2. Recognition of the E protein. (A) Western blots were prepared with gradient purified DENV-2 particles and blot strips were probed with hMAbs 4.8A, D11C, and 1.6D, or anti-DENV capsid mMAb D2-C2 (57) under reducing and non-reducing conditions. Binding of hMAbs to DENV-2 proteins on the blot strips was detected at PMT 400 V. **(B)** Western blots were prepared with DENV-2 sE and blot strips were probed with hMAbs 4.8A, D11C, 1.6D, and control mMAbs 4G2 and 3H5.1 under non-reducing conditions. Binding of hMAbs and mMAbs to DENV-2 sE on the blot strips was detected at PMT 220 V.

FIG. 3. Broad neutralizing activity. Focus-forming-unit reduction neutralization assays were performed by incubating DENV-1, 2, 3, and 4 with **(A)** serial dilutions of sera from patient 8C and DA003, **(B)** hMAb 4.8A, **(C)** hMAb D11C, and **(D)** hMAb 1.6D prior to infecting monolayers of LLC-MK_2 cells. IC_{50} values in µg/ml were determined graphically and were as follows: for hMAb 4.8A with DENV-1 2.1 ± 1.1, DENV-2 >40, DENV-3 2.4± 0.1, DENV-4 >40; for hMAb D11C with DENV-1 1.5 ± 0.1, DENV-2 1.0 ± 0.4, DENV-3 10.2 ± 0.8, DENV-4 1.6 ± 0.6; and for hMAb 1.6D with DENV-1 1.5 ± 1.1, DENV-2 0.2 ± 0.0, DENV-3 0.5 ± 0.1, DENV-4 2.7 ± 0.8. Pooled data points show the mean of at least two independent experiments with three replicates each. Error bars indicate standard deviation.

FIG. 4. Antibody-dependent enhancement. Enhanced infection of Fc receptor-bearing K562 cells was measured by DENV-specific qRT-PCR following infection with **(A)** DENV-1, **(B)** DENV-2, **(C)** DENV-3, and **(D)** DENV-4 in the presence of hMAbs 4.8A, D11C, and 1.6D. Each data point is the mean of three replicates. Error bars indicate standard deviation.

FIG. 5. Mechanism of neutralization. (A) Low pH activated virus-liposome fusion was measured using fluorescently labeled DENV-2 incubated with hMAbs 4.8A, D11C, and 1.6D. Fluorescence signal was normalized to signal generated in the absence of hMAbs to calculate percent liposome fusion. **(B)** Intracellular fusion of DiD labeled DENV-2 within endosomes leads to dequenching of DiD. Confluent monolayers of MA104 cells were infected with equivalent amounts of DENV-2 pre-incubated with or without 100 µg/ml hMAbs as indicated. Intracellular structures at the site of fusion events fluoresce red. Cells

1245 were counterstained with DAPI to visualize nuclei. **(C)** Intracellular fusion levels were
1246 quantified after incubation of DENV-2 with different concentrations of hMAbs. EH21 is an
1247 irrelevant anti-HIV hMAb. Fluorescence levels were normalized to virus only controls. **(D)**
1248 Total fluorescence of all bound DENV-2 was quantified by fully dequenching the cells.
1249 DENV-2 was incubated with 100 μg/ml of each hMAb. Fluorescence levels were normalized
1250 to virus only controls. Heparan sulfate at 10 μg/ml, a known inhibitor of DENV binding,
1251 was used as a positive control for binding inhibition. For **(A)**, **(C)**, and **(D)** each data point
1252 is the mean of three replicates. Error bars indicate standard deviation.
1253
1254 **FIG. 6. Coarse-level epitope mapping. (A)** Western blots were prepared with DENV-2
1255 sDI/II and sDIII blot strips were probed with 5 μg/ml of hMAbs 4.8A, D11C, 1.6D, and
1256 control mMAbs 4G2 and 3H5.1 under non-reducing conditions. Binding of antibodies to
1257 sDI/II on blot strips was detected at PMT 475 V or 562 V for hMAbs and mMAbs,
1258 respectively, whereas binding of both hMAbs and mMAbs to sDIII on blot strips was
1259 detected at PMT 420 V. **(B)** A competition ELISA was used to determine whether hMAbs
1260 4.8A, D11C, and 1.6D and mMAb 4G2 recognized overlapping epitopes on DENV-1 E protein.
1261 HMAb EH21 against HIV-1 ENV was used as a negative control. Unlabeled antibodies
1262 (shown on the x-axis) were added to DENV-1 E protein-coated wells. Upon removal of
1263 unbound antibodies, wells were probed with biotinylated antibodies (shown in plot
1264 legend). **(C)** Antibody binding competition was measured using biolayer interferometry.
1265 Biosensor probes were coupled to hMAb 1.6D and subsequently incubated with either
1266 DENV-2 sE alone or sE complexed with hMAbs 1.6D or control anti-HIV 1.7B or with
1267 mMAbs 4G2 or 3H5.1.

1268

1269 **FIG. 7. Molecular-level epitope mapping. (A)** Cells expressing DENV E mutants were
1270 fixed and immunostained with the indicated antibodies. Clones with reactivity ≤25%
1271 relative to WT DENV-3 E were identified as critical for hMAb binding. The reactivities of
1272 mutant clones containing each critical residue with hMAbs 4.8A, D11C, 1.6D, and the
1273 control mMAb 1A1D-2 and human polyclonal serum (hPAb) are shown. Results were
1274 repeated three times and standard deviations of quadruplicate wells are shown. **(B)** Critical
1275 residues for hMAbs 4.8A (W101, L107, and G109), D11C (W101 and G109), and 1.6D
1276 (W101 and G109) were visualized on a structure of DENV-3 E protein (Protein Data Bank
1277 accession code 1uzg; (51)). DI, DII, and DIII are depicted in red, yellow, and blue,
1278 respectively, and the fusion loop (residues 98-109) is circled.

1279

1280 **Tables**

1281 **Table 1.** Equilibrium dissociation constants (K_D) of hMAbs 4.8A, D11C, 1.6D bound to
1282 DENV-1, 2 3, and 4 sE (M ± SD).

1283

1284 **Table 1**

1285

Equilibrium Dissociation Constants of hMAbs bound to DENV sE

(M ± SD)	4.8A	D11C	1.6D
DENV-1 sE	1.2×10^{-9} ± 1.6×10^{-9}	1.4×10^{-10} ± 1.2×10^{-10}	1.5×10^{-10} ± 5.0×10^{-11}
DENV-2 sE	1.3×10^{-9} ± 1.1×10^{-9}	1.2×10^{-10} ± 9.4×10^{-11}	3.5×10^{-10} ± 4.5×10^{-10}
DENV-3 sE	7.4×10^{-10}	6.2×10^{-10}	1.8×10^{-10}

	± 7.7 x 10^{-10}	± 3.2 x 10^{-10}	± 8.0 x 10^{-11}
DENV-4 sE	7.6 x 10^{-10} ± 5.4 x 10^{-10}	2.9 x 10^{-10} ± 1.5 x 10^{-10}	2.4 x 10^{-10} ± 5.6 x 10^{-11}

1286

1287

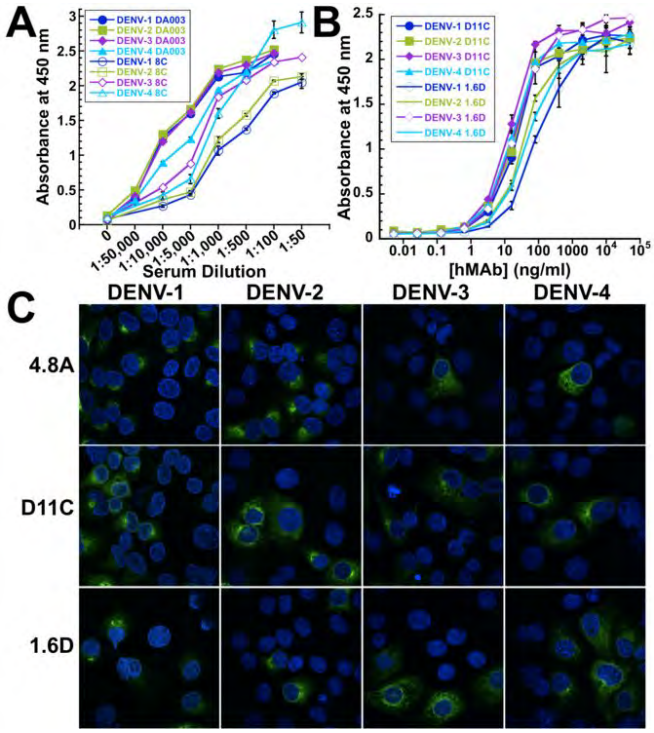

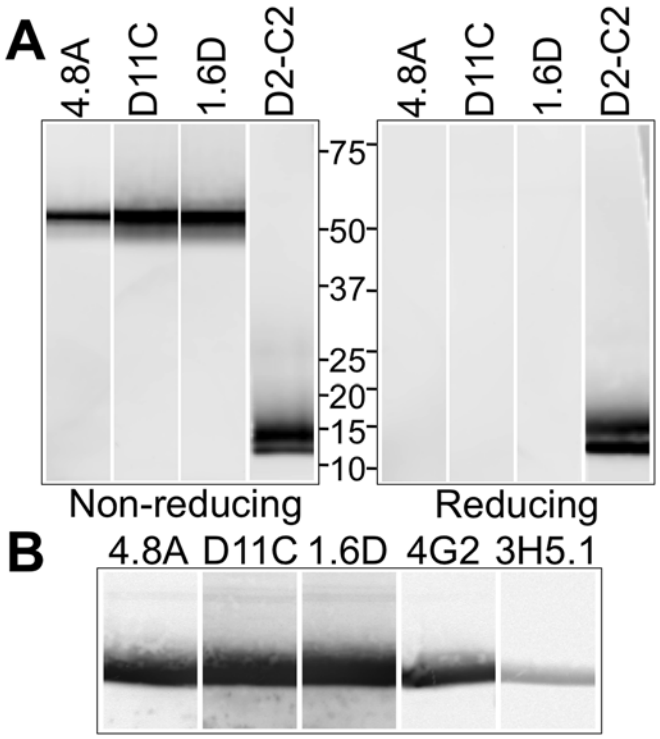

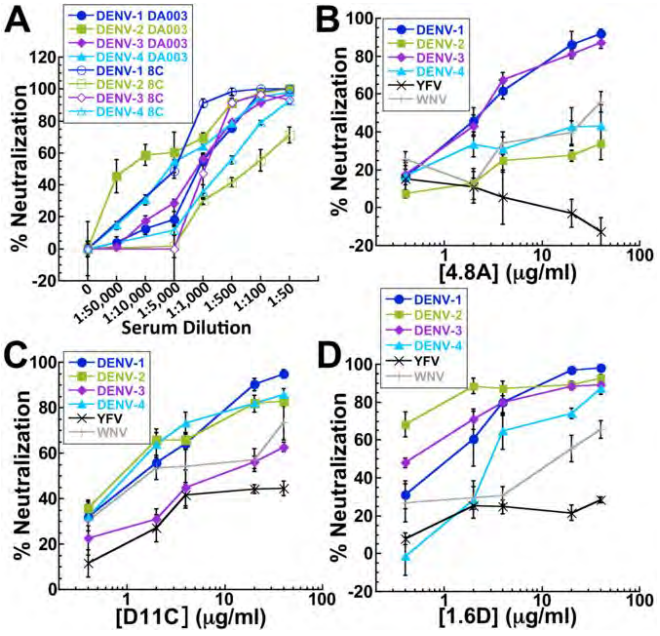

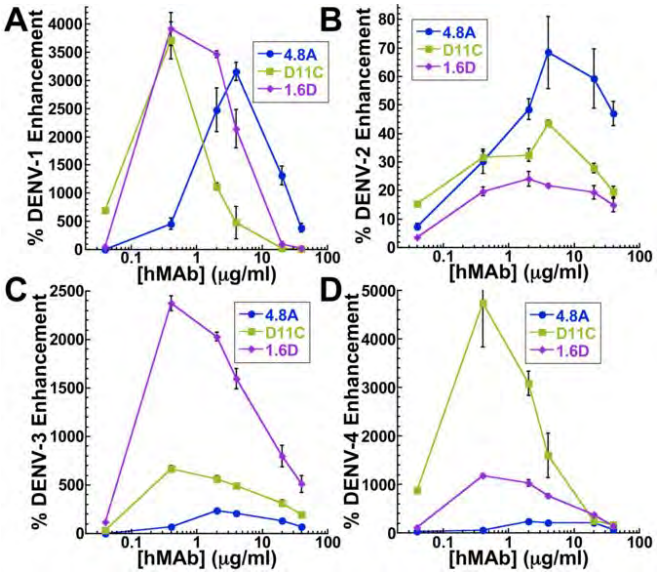

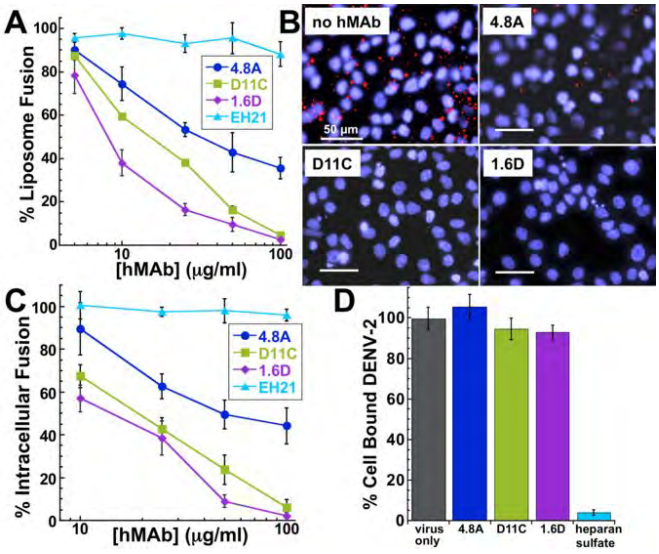

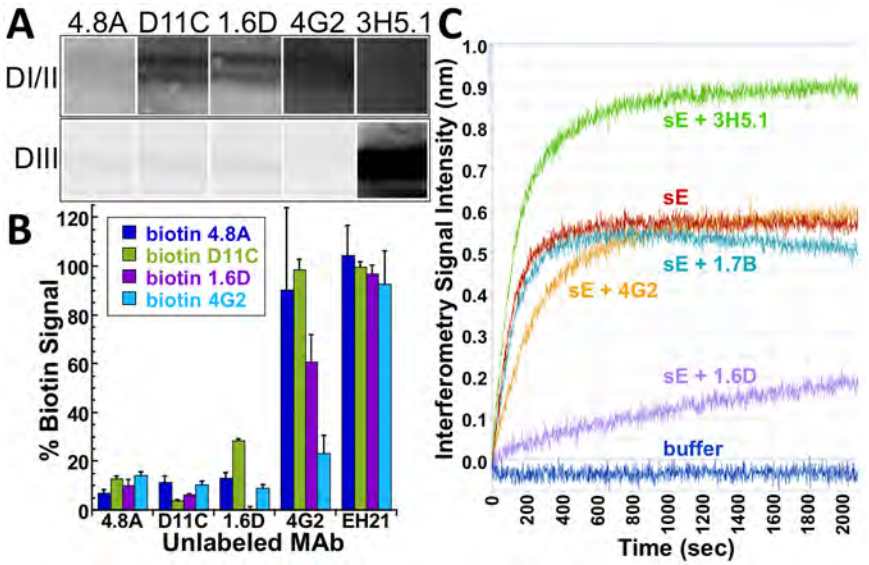

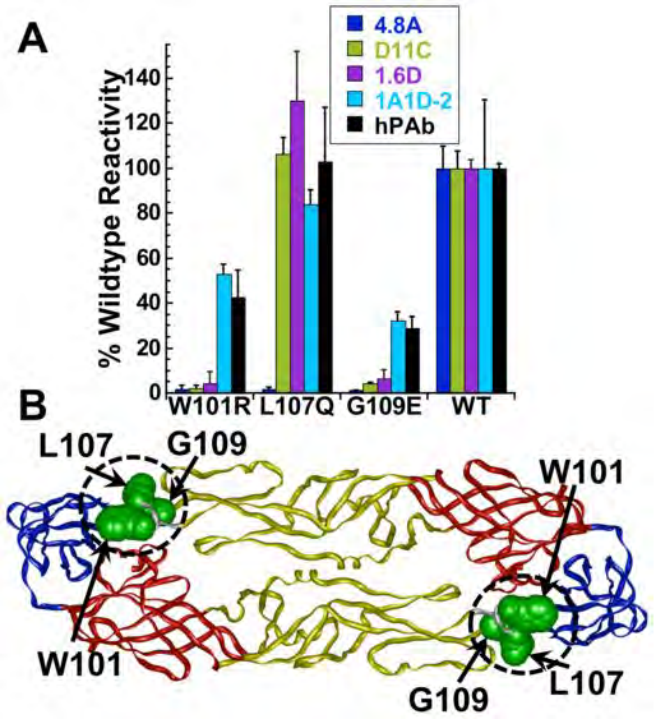

DEPARTMENT OF DEFENSE

DEFENSE THREAT REDUCTION
AGENCY
8725 JOHN J. KINGMAN ROAD
STOP 6201
FORT BELVOIR, VA 22060
ATTN: H. MEEKS

DEFENSE TECHNICAL
INFORMATION CENTER
8725 JOHN J. KINGMAN ROAD,
SUITE 0944
FT. BELVOIR, VA 22060-6201
ATTN: DTIC/OCA

DEPARTMENT OF DEFENSE CONTRACTORS

QUANTERION SOLUTIONS, INC.
1680 TEXAS STREET, SE
KIRTLAND AFB, NM 87117-5669
ATTN: DTRIAC